AGU100 ADVANCING EARTH AND SPACE SCIENCE

Reviews of Geophysics

REVIEW ARTICLE
10.1029/2018RG000615

Key Points:
- We define aerosol mixing state and connect it to the physicochemical properties of aerosol particles
- We discuss existing measurements and models to understand chemical and physicochemical mixing state
- We explain the connection between aerosol mixing state and climate-relevant aerosol properties

Correspondence to:
N. Riemer and A. P. Ault,
nriemer@illinois.edu;
aulta@umich.edu

Citation:
Riemer, N., Ault, A. P., West, M., Craig, R. L., & Curtis, J. H. (2019). Aerosol mixing state: Measurements, modeling, and impacts. *Reviews of Geophysics*, *57*, 187–249. https://doi.org/10.1029/2018RG000615

Received 2 JUL 2018
Accepted 14 MAR 2019
Accepted article online 21 MAR 2019
Published online 21 MAY 2019



# Aerosol Mixing State: Measurements, Modeling, and Impacts

**N. Riemer[1], A. P. Ault[2,3], M. West[4], R. L. Craig[3,5], and J. H. Curtis[1]**

[1]Department of Atmospheric Sciences, University of Illinois at Urbana-Champaign, Urbana, IL, USA, [2]Department of Environmental Health Sciences, University of Michigan, Ann Arbor, MI, USA, [3]Department of Chemistry, University of Michigan, Ann Arbor, MI, USA, [4]Department of Mechanical Science and Engineering, University of Illinois at Urbana-Champaign, Urbana, IL, USA, [5]Department of Chemistry, The College of Wooster, Wooster, OH, USA

**Abstract** Atmospheric aerosols are complex mixtures of different chemical species, and individual particles exist in many different shapes and morphologies. Together, these characteristics contribute to the aerosol mixing state. This review provides an overview of measurement techniques to probe aerosol mixing state, discusses how aerosol mixing state is represented in atmospheric models at different scales, and synthesizes our knowledge of aerosol mixing state's impact on climate-relevant properties, such as cloud condensation and ice nucleating particle concentrations, and aerosol optical properties. We present these findings within a framework that defines aerosol mixing state along with appropriate mixing state metrics to quantify it. Future research directions are identified, with a focus on the need for integrating mixing state measurements and modeling.

## 1. Introduction

An aerosol is a population of solid or liquid particles suspended in a gas. The atmospheric aerosol plays an important role in a number of key processes related to atmospheric chemistry and physics. Aerosol particles directly scatter and absorb solar radiation (Ravishankara et al., 2015), which impacts the large-scale dynamics of the atmosphere and climate (Bellouin et al., 2005). Particles also serve as the nuclei for cloud droplets and ice crystals (Andreae & Rosenfeld, 2008; DeMott et al., 2016, 2010; Farmer et al., 2015), thereby indirectly impact radiative transfer (Penner et al., 2004). They also provide surfaces and reaction sites for heterogeneous chemistry to occur (George et al., 2015), which impacts both aerosol properties and gas phase concentrations (Abbatt et al., 2012). These macroscale impacts are determined by the distribution of properties across the population of particles that make up the atmospheric aerosol. Important properties of particles within the atmospheric aerosol include per-particle composition, per-particle morphology, and the spatial distribution of chemical species within individual particles. To complicate matters, the chemical and physical properties of particles with the atmospheric aerosol are dynamic and constantly evolving during their atmospheric lifetimes. Characterizing this diversity of particle chemical compositions and physical properties within the particle population of the atmospheric aerosol poses a tremendous challenge for both experimental methods and model development; however, it is necessary to quantify the atmospheric aerosol's impact on the Earth's system.

Individual particles within an aerosol are complex mixtures of different chemical species (Junge, 1952; Murphy & Thomson, 1997; Prather et al., 2008). To illustrate this complexity, a single 100-nm particle is composed of millions of molecules and can contain hundreds to thousands of distinct chemical species within an attoliter ($10^{-18}$ L) volume. These species include both primary species (present in the condensed phase at the time of emission) and secondary species (formed in the atmosphere). Examples of primary particles with complex compositions include individual combustion particles that are mixtures of elemental carbon (also known as black carbon, BC, or soot), organic carbon, and metals from unburnt lubricating oils (Toner et al., 2006) and sea spray aerosol particles that contain sodium chloride and organic carbon from biological material (Barger & Garrett, 1970; Prather et al., 2013). Secondary species include nitrate from $NO_x$ oxidation, sulfate from $SO_2$ oxidation (Seinfeld & Pandis, 2016), and secondary organic aerosol (SOA) formed from the oxidation of volatile organic compounds (VOCs) to low volatility species (Hallquist et al., 2009). Importantly, within an aerosol each individual particle typically contains different mixtures of primary and secondary species, even over a narrow particle size range. The relative abundance of particles from different primary

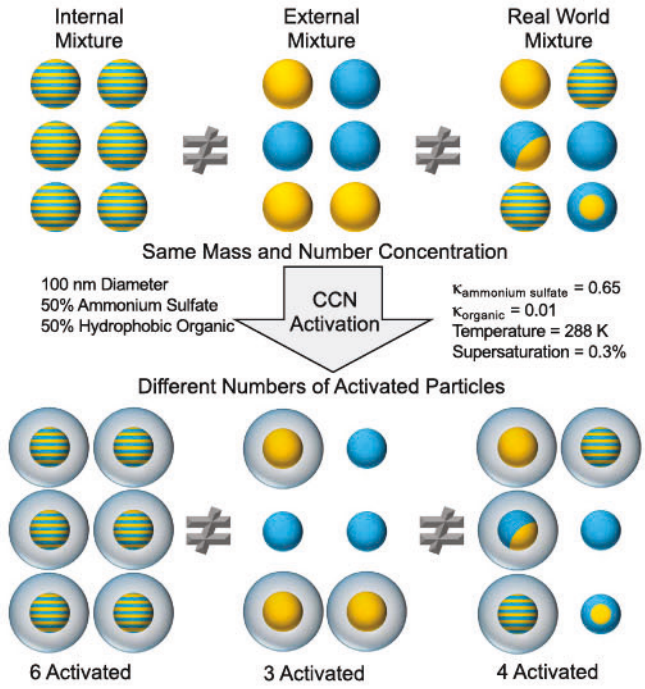


**Figure 1.** Illustrative example of the impact that aerosol mixing state can have on cloud droplet formation, specifically the ability of particles to act as cloud condensation nuclei (CCN). For each of the three example populations (internal mixture, external mixture, and real-world mixture), the six particles summed together consist of 50% ammonium sulfate (gold) and 50% hydrophobic organic material (blue), with blue and yellow stripes representing a 50%/50% mixture of the two components evenly distributed within a particle. For this example, a hypothetical size of 100 nm places the particles in the size range where chemical composition impacts CCN activity. The top distributions show individual particle composition and morphology (e.g., core-shell), while the bottom distributions show which particles in the distribution would activate act as CCN and activate at 288 K and 0.3% supersaturation, assuming that ammonium sulfate has $\kappa = 0.65$ and the hydrophobic organic species has $\kappa = 0.01$.

sources that are aged by different secondary processes also changes, both temporally and with respect to particle size. The variability within the atmospheric aerosol of composition at the single-particle level has been documented by field measurements globally for decades (Ault et al., 2010; Bondy et al., 2018; Casuccio et al., 2004; Dall'Osto et al., 2010; Gard et al., 1998; Middlebrook et al., 2003; Murphy et al., 1998a; Pratt & Prather, 2010; Reinard et al., 2007; Sullivan et al., 2007a) but effectively accounting for that complexity within global models remains challenging (Bauer et al., 2013; Fierce et al., 2017).

The first introduction of the concept of aerosol mixing state was by Winkler (1973), as a way to account for differences in chemical composition across an aerosol. According to his definition "internal mixing" is present when the population of particles within an aerosol consist of the same mixture of chemical species, while "external mixing" is present when all particles in an aerosol consist of pure chemical species and have distinct compositions. In reality purely internal or external aerosol mixing states are rare in the atmosphere (Bondy et al., 2018; Healy et al., 2014; O'Brien et al., 2015). Winkler (1973) went on to point out that the "same net composition of an aerosol can be caused by an infinite variety of different internal distributions of the various compounds." Note that the term "mixing state," as originally defined, refers to a property of the overall particle population within an aerosol, not to the property of an individual particle. Thus, it is helpful to define some initial terms that will be explored more rigorously below. Aerosol mixing state is defined as the distribution of properties across a population of particles within an aerosol. Traditionally, discussions of mixing state have focused on chemical mixing state, which is defined as the distribution of chemical species across individual particles within the particle population of an aerosol. The addition of physical properties adds a layer of complexity referred to as the physicochemical mixing state (Ault & Axson, 2017), which can be needed to fully connect to climate-relevant optical or cloud nucleating properties, but is more challenging to represent and quantify.

Considering the role of aerosol particles as cloud condensation nuclei (CCN), as ice nucleating particles (INPs), and as scatterers and absorbers of electromagnetic radiation, it is clear that aerosol mixing state is of great interest since all of these impacts depend on properties such as per-particle composition and particle morphology. The connection between mixing state and climate-relevant properties is illustrated in Figure 1, for the example of CCN activity. In this example, each population contains equal bulk mass fractions of ammonium sulfate (yellow) and a hydrophobic organic species (blue) of the same size (100 nm), but the distribution of species varies between and within particles. On the left is an example of a completely internal mixture, where both species are homogeneously mixed within each particle, indicated by the blue and yellow striped particles. The middle shows an external mixture, where each particle consists of either solely ammonium sulfate or the hydrophobic organic species. The population on the right shows an example that is in between the external and the internal mixture while also highlighting that the species can be arranged differently within the particle (e.g., homogeneous, core shell, or partially engulfed). This "real-world" example represents the kind of complexity typical of the ambient atmosphere. The variation in mixing state between these hypothetical examples result in differing numbers of particles activating as CCN and forming cloud droplets: three for the external mixture, six for the internal mixture, and four for the real-world mixture. Thus, despite each population having the exact same mass of ammonium sulfate and the hydrophobic organic species, as well as the same particle size, differences in CCN activation are observed when comparing the populations. Similar arguments can be made for the ability of aerosol particles to act as INPs and for aerosol optical properties.

The continuous evolution of mixing state for an aerosol in the atmosphere is shown conceptually in Figure 2 and is the result of a number of processes. As an air parcel containing an internally mixed, background aerosol is advected over an urban area (1), the population becomes more externally mixed as primary particle

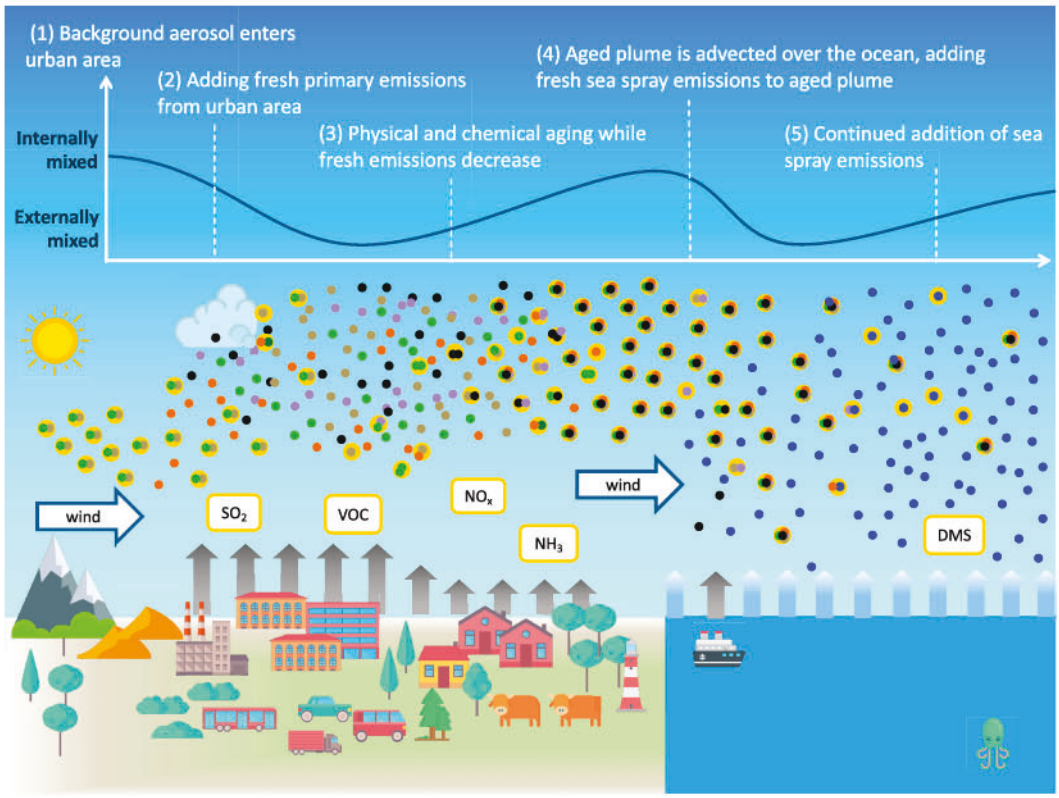


**Figure 2.** Evolution of aerosol mixing state of an aerosol that is transported in the atmosphere. The line graph at the top illustrates how aerosol mixing state changes qualitatively between a more or less internally mixed state and how different aerosol processes contribute to that change. Adding new types of aerosol particles makes the population more externally mixed (steps 2 and 4), while aerosol aging processes (step 3) or the addition of one dominate particle type (step 5) moves the population toward a more internally mixed state. DMS = dimethyl sulfide.

emissions from many different sources (e.g., vehicle combustion and power plants) enter the air parcel (2). Simultaneously, many processes occur that make the population more homogeneous and move it toward a more internally mixed state (3). These include the formation of secondary aerosol material in cloud-free air or within cloud droplets, coagulation among different particles, and heterogeneous reactions on the surface of or within the particles. After the parcel moves over the ocean and sea spray aerosol (as well as ship) emissions are added, the population becomes more externally mixed yet again because new particle types are added to the population (4). Further away from the continent, as the population becomes more and more dominated by sea spray aerosol, the mixing state moves toward a more internal mixture (5). The degree that the chemical mixing state is an external or internal mixture can be quantified more precisely by the mixing state parameter, which will be explained in section 5.1.

Along with a wide variety of chemical mixing states based on variation in per-particle compositions, different physical properties can vary across the particle population of an aerosol (Ault & Axson, 2017), leading to a complex physicochemical mixing state. For example, while aqueous salt particles are well approximated by spheres, soot particles are emitted as fractal-like aggregates (Moffet & Prather, 2009; Wentzel et al., 2003), mineral dust particles are irregularly shaped (Kalashnikova & Sokolik, 2002; Moffet et al., 2008), and chemically mixed particles can have various arrangements of their constituent species (China et al., 2013; Li et al., 2016; Moffet et al., 2016). Similar to chemical composition, particle physical structure can also undergo changes during a particle's lifetime in the atmosphere. Soot aggregates tend to compact as secondary aerosol species condense on them (Zhang et al., 2008) or as water evaporates from them (Mikhailov et al., 2001). Coagulation events can lead to partially encapsulated particles (China et al., 2015). Thus, as with chemical mixing state, physicochemical mixing state is dynamic and constantly evolving.

There is no single instrument that can perfectly characterize all aspects of aerosol mixing state, but over the past two decades, sophisticated techniques have been developed that allow us to probe various

physicochemical properties of particles and understand their contribution to the mixing state of an aerosol in increasing detail (Ault & Axson, 2017; Laskin et al., 2016; Prather et al., 2008; Pratt & Prather, 2012a). Concurrently, atmospheric models have become sufficiently complex to incorporate aspects of aerosol mixing state in their predictions (Riemer & West, 2013; Riemer et al., 2010). This review compares and contrasts the different approaches regarding measuring and modeling aerosol mixing state and synthesizes our knowledge of how important these details are to understand aerosol impacts on climate.

When defining the scope of this review, it is not feasible to fully explore all aspects of aerosol composition and physical properties that connect to mixing state. Thus, we list some pertinent reviews with further details on specific instrumentation, sources, and climate-relevant properties below. For further details on many of the instrumental methods discussed below, readers are directed to excellent reviews on analysis of atmospheric aerosol (Laskin et al., 2016; Prather et al., 2008), mass spectrometry of aerosols (Laskin et al., 2018, 2013; Pratt & Prather, 2012a, 2012b), and spectroscopy and microscopy of aerosols (Ault & Axson, 2017; Power & Reid, 2014). Additionally, specific aspects of aerosol composition and processes have been discussed in a number of reviews, including brown carbon (Laskin et al., 2015; Yan et al., 2018), light absorbing carbon (e.g., BC; Bond et al., 2006; Lack et al., 2014), organic aerosol (Glasius & Goldstein, 2016; Hallquist et al., 2009; Shrivastava et al., 2017), biomass burning aerosol (Chen et al., 2017b), metal-containing aerosol (Popoola et al., 2018), bioaerosols (Fröhlich-Nowoisky et al., 2016), sea spray aerosol (Brooks & Thornton, 2018; Quinn et al., 2015), mineral dust (Cwiertny et al., 2008; Usher et al., 2003), acidic aerosol (Craig & Ault, 2018), ultrafine and newly formed particles (Bzdek et al., 2012), phase separations (Freedman, 2017), and particle viscosity (Power & Reid, 2014; Reid et al., 2018).

Aerosol physicochemical properties and their evolution are a complex and expanding area of research. In this paper, we focus our discussion of physicochemical properties and mixing state on particle shape and structure, which represent a distribution of morphologies. Implications for climate of the atmospheric aerosol and its constituent particles have been discussed in a number of reviews (McNeill, 2017), including CCN (Farmer et al., 2015; McFiggans et al., 2006), INPs (DeMott et al., 2016; Knopf et al., 2018), and aerosol optical properties (Bond et al., 2006; Moise et al., 2015). While substantial advances have been made in the area of low-cost sensors, this technology has not yet advanced to the point of providing useful information regarding mixing state. We therefore will not discuss these techniques further in this review, although advances in this area would greatly benefit the field of aerosol science. Lastly, aerosols have significant impacts on human health globally as one of the largest environmental risk factors (Pope & Dockery, 2006). However, given the complicated nature of connecting aerosol composition to both climate and health, this review will solely focus on connecting aerosol composition and mixing state to climate, with readers directed to detailed reviews relating aerosol composition, air quality, and health (Brook et al., 2010; Pope & Dockery, 2006; Von Schneidemesser et al., 2015).

In this review we start in section 2 with an overview of mixing state terminology, followed in section 3 by a review of experimental tools that are used to measure mixing state. Section 4 summarizes mixing state representations in aerosol models. Section 5 presents our current understanding of mixing state metrics, and then section 6 summarizes the state of knowledge about the role of mixing state in aerosol climate impacts. Section 7 summarizes our main points and outlines future research needs with respect to aerosol mixing state. A list of abbreviations used in the paper is given in the Abbreviations section.

## 2. Mixing State Terminology

To begin the discussion on aerosol mixing state, we will define our terminology in sections 2.1 and 2.2, contrasting the terminology used to describe single particles and particle populations.

### 2.1. Terminology: Single Particles

The extant literature on mixing state uses a variety of sometimes-incompatible terminologies to describe an aerosol, particles within an aerosol, and particle populations, so in this review we start by establishing precise definitions for the terminology used with respect to particles, aerosols, and mixing state. Our approach is based on the notion that it is useful to distinguish between per-particle properties (described in this section) and population-level properties (see section 2.2).

We begin with describing a particle chemically. The *chemical composition* (or *composition*) of a particle is the mass of each chemical species in the particle. A chemical species is commonly defined as an ensemble

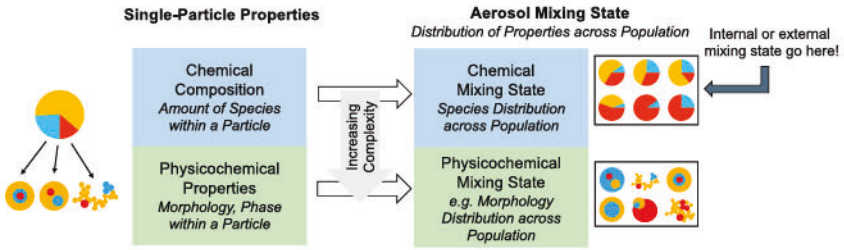


**Figure 3.** Illustration of our terminology. We separate the properties that describe single particles (section 2.1) from the distribution of these properties across the population (section 2.2). It is further useful to separate the aspects that pertain to chemical composition and its distribution across the population from the aspects that include not only chemical composition but also morphology and phase, which together constitute the physicochemical properties for individual particles and the physicochemical mixing state of the population.

of identical molecules. As it is not feasible to measure or model each of the thousands of chemical species present in many atmospheric particles, species is often generalized to refer to a group of similar molecules. This is often determined by the measurement technique (see section 3 for more details) or by the level of detail available in the aerosol model representation. Common examples of how the term species tends to be used in aerosol studies include ammonium sulfate, ions such as nitrate (often referred to irrespective of its counterion, such as sodium), or more complex mixtures treated as surrogate species, such as secondary organics to refer to the hundreds or more distinct organic species present in many individual particles. Ambient particles differ dramatically in the number of chemical species they contain. That is, they have different compositional *diversities*. For example, a freshly emitted combustion particle could be described as containing just two species, BC (i.e., graphitic carbon) and primary organic carbon, so it would have low diversity. Again, we are using primary organic carbon as a generalized surrogate species for the many of the organic species in the condensed phase at the time of emission. After some time in the atmosphere this combustion particle might acquire additional aerosol species as material condenses on it, such as secondary inorganic or organic species, thereby increasing its compositional diversity. The definition of diversity will be made more precise in section 5.1 by introducing the concept of the number of effective species in a particle.

The way these chemical species are arranged spatially within an individual particle brings us to the definition of particle morphology. The *morphology* of a particle is the gross structure and shape of the particle, including the relationship of its components and variation of properties inside the particle. A *component* of an aerosol particle is a subset of the particle with distinct properties. These might include chemical composition, phase, or even a unique shape and will be application dependent. Figure 3 illustrates the fact that a particle of a given composition can assume many different morphologies. For example, the particle with the same mass of three different components could have the components arranged as a spherical core-shell morphology, as a number of inclusions embedded in a spherical host particle, or as a nonspherical, fractal aggregate particle. We summarize common metrics for morphology, or morphometrics, for aerosol particles in section 5.4.

While composition and morphology describe many aspects of a particle, we frequently need more physical or chemical properties to completely quantify the particle state. The *physicochemical properties* of a particle include its composition, morphology, and any additional features needed to fully characterize the particle. Examples of additional features include phase and charge and will be application dependent. Additional properties such as refractive index or hygroscopicity are best regarded as functions of the particle's composition and morphology, but in certain situations may be treated as independent physicochemical properties.

A fundamentally important, but complex, feature of an atmospheric particle is its *size*, usually reported as diameter. The diameter of a particle within an aerosol has traditionally been defined by its behavior while suspended and interacting with the gas it is suspended in (aerodynamic diameter) or while being acted on by an external force (electrical mobility diameter). To connect to composition and species, size can be defined by the diameter of a particle whose volume is determined by summing the masses of the species present and using the species material densities. However, semivolatile species, particularly water, are often difficult to account for in measurements and models and vary with environmental conditions. Another factor that can impact the diameter reported for a particle is its morphology, requiring the use of shape factors and fractal dimensions (DeCarlo et al., 2004). While in fields such as biology it is common to regard size as an

aspect of morphology (Encyclopædia Britannica, 2018), in atmospheric science and the aerosol community morphology typically only refers to additional shape descriptions beyond size. In line with the typical usage of morphology for aerosols, we primarily focus on composition and other physical properties and readers are directed to a number of other comprehensive overviews of the definitions and implications of aerosol size (DeCarlo et al., 2004; Friedlander, 1977; Fuchs, 1964; Hinds, 1999).

### 2.2. Terminology: Defining an Aerosol, Particle Populations, and Mixing State

Having defined our terminology for single particles in section 2.1, we now consider an aerosol, which is a population of particles suspended in a gas. Thus, it is common to discuss the atmospheric aerosol for a specific location as referring to all of the particles suspended at that location.

The *mixing state* of an aerosol is the distribution of properties across the particles in the population. Analogous to the single-particle properties in section 2.1, we distinguish between two different levels that differ in their complexity. We start with the simpler chemical mixing state and then move to the more detailed physicochemical mixing state, as shown in Figure 3.

The *chemical mixing state* of an aerosol is the distribution of chemical species across the particles in the population (Winkler, 1973). When describing the chemical mixing state of a population, it is often helpful to think of it as being more or less internally or externally mixed.

An aerosol is a *fully internal mixture* if all particles in the population contain the same species in the same mass fractions. In other words, the per-particle mass fractions are all equal to the mass fractions of the bulk aerosol. This means that if the population is fully internally mixed and we know the bulk composition, we also know what each particle is made of. Correspondingly, an aerosol contains an *external mixture* if every particle contains just one species (or surrogate species, such as primary organic carbon). Of course, a real-world chemical mixing state will be in between those two extremes, with both internal and external mixing characteristics. We will more precisely define the extent to which a population is internally mixed in section 5.1.

The terms external and internal mixture can also be applied to particle types within the particle population of an aerosol. By *aerosol particle type*, we mean subpopulations of particles within an aerosol, such as particles in the same size range, particles from the same source, particles with similar composition, or particles with other similar properties. A common method of determining particle types is through a mass spectrometry cluster analysis, discussed in section 3.4.2. As an example of describing the mixing state of particle types, an external mixture of combustion particles and sea spray particles means that particles from the two sources exist as separate particles. The particles of each type can consist of different chemical species, each having their own diversity. For example, there can be differing amounts of organic material in sea spray particles, even if that population is distinct from combustion particles. In contrast, an internal mixture from combustion and sea spray sources means that the species from combustion and sea spray are combined within individual particles, such as through coagulation, and present in the same amount in each particle.

Chemical mixing state is agnostic to particle morphology, which we indicate in Figure 3 by using generic pie charts for each particle. To fully characterize an aerosol, we need to generalize the chemical mixing state to the physicochemical mixing state. The *physicochemical mixing state* of an aerosol is the distribution of physicochemical properties across the particles in the population (Ault & Axson, 2017). This includes the chemical mixing state, as well as the distribution of morphology, phase, and any other particle characteristics of interest. Two populations can have the same chemical mixing state (e.g., fully internally mixed) but may differ in their physicochemical mixing state due to their distribution of morphologies (e.g., core shell versus homogeneous on a molecular level).

From knowing the full physicochemical mixing state, we can derive the number and mass size distributions of the particle population. This means that aerosol mixing state and the size distribution are not independent from each other, even though in practice we sometimes treat them as such, a point also made by Farmer et al. (2015). Knowing the full physicochemical mixing state also allows us, at least in principle, to calculate other per-particle properties, such as the particles' critical supersaturation or the absorption and scattering cross sections. From these, population-level quantities can be derived, for example, CCN concentrations or absorption and scattering coefficients. Conversely, it is possible to deduce aspects of mixing state by measuring population-level quantities in combination with a diagnostic model of the target quantities, which will be the subject of section 6.1.

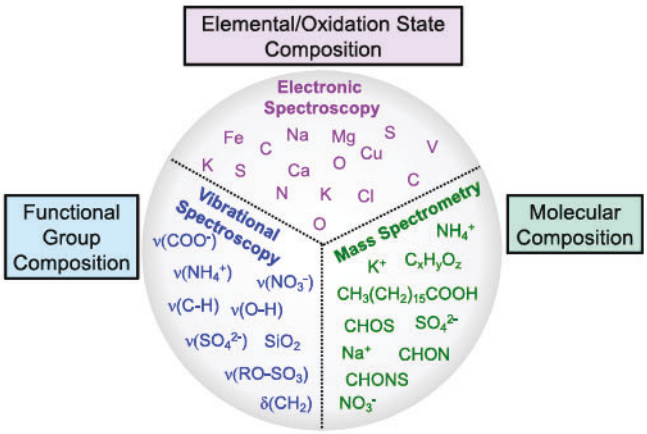


**Figure 4.** Generalized categories of chemical measurements used for mixing state and the type of information provided.

After laying out the concept of individual particle properties on the one hand, and population-level properties of an aerosol on the other hand, it is evident that the term "internal mixture" should not be applied to individual particles, but only to populations. For example, a particle that contains both BC and sulfate is simply a "mixed particle." Assembled in a population, these particles then form an internal mixture of BC and sulfate. Given the complexity of aerosols, particle populations, and mixing state, it is not uncommon to see the occasional, incorrect usage of the term "internally mixed" to refer to individual particles with multiple species. We wish to emphasize that using the terminology of mixing state and aerosol for populations, as done here and in the prior aerosol literature, will help alleviate a potential source of confusion.

## 3. Measurement Techniques for Aerosol Mixing State

To measure aerosol mixing state experimentally, ambient measurements of individual particles are typically combined to define the properties of the overall population. Thus, it is important to understand the available instrumental methods and how they can contribute population-level information on aerosol properties to determine the overall mixing state of an aerosol. Measurements of particle properties that can be related to an aerosol's mixing state predate the term mixing state, such as morphology (e.g., asbestos fibers), optical properties (e.g., different colors of smoke or smog), and water uptake (e.g., haze). The type of information obtained from single-particle measurements (Figure 4) can be roughly grouped into three categories: elemental or oxidation state, functional groups, and molecular composition. Instruments that generally provide this information are electron/X-ray microscopy (elemental or oxidation state), vibrational spectroscopy (functional groups), and mass spectrometry (molecular composition).

Further detail is provided in Tables 1–3, which list specific instrument types (see the Abbreviations section for a list of abbreviations). These tables list important instrument characteristics, including the type of information measured, whether the analysis is conducted at ambient pressure or under vacuum, the coverage of atmospheric species, the level of chemical detail, the level of quantification, whether spatial distributions of species within a particle are mapped, and the number of particles typically analyzed in a day, to give a rough sense of particle statistics. The atmospheric size range measured by each instrument is also listed. These ranges do not necessarily indicate the absolute lower limit of the instrument, but rather the range commonly used in aerosol studies. For some instruments, for example, the online field-based instruments, the upper limit is often dictated by the sampling of aerosol to the instrument or the inlet when an aerodynamic lens is used, with coarse particles being more difficult to sample. An upper limit of 2.0 $\mu$m is listed for instruments using an aerodynamic lens, though each lens will have a different upper limit. For off-line analyses, even though coarse particles are sampled, they can present other challenges related to charging and spreading. Finally, Tables 1–3 also list the potential of each instrument to calculate the mixing state index $\chi$ (sections 5.1 and 5.2), which requires per-particle species masses to be measured.

To compare the methods in the context of species covered and chemical detail, as shown in Figure 5, the methods in Tables 1–3 are grouped on the basis of whether they provide per-particle information about an aerosol or ensemble average (i.e., bulk) information. To provide a historical perspective on mixing state measurement techniques, notable advances in aerosol particle characterization related to mixing state are highlighted in Figure 6. A category of instrumentation discussed later (sections 6.2 and 6.3) are measurements that relate to mixing state indirectly, such as CCN counters, but which are included in the figures to relate to the chemical measurements.

### 3.1. Electron Microscopy and X-ray Spectroscopy

Electron microscopy has been used for over 50 years to study individual atmospheric particles (Heard & Wiffen, 1969; Larner, 1964), and its application to aerosols has increased in recent years (Ault & Axson, 2017). See Table 1 for an overview of microscopy instruments. For both scanning electron microscopy (SEM) and transmission electron microscopy (TEM) an electron beam is directed at a sample, typically a substrate where particles have been collected by inertial impaction, and the interaction of the electrons with particles

Reviews of Geophysics

10.1029/2018RG000615

**Table 1**
*Electron Microscopy/X-ray Spectroscopy*

| Technique | Measures | Analysis conditions | Species coverage | Chemical detail | Identification/ quantification | Mapping (spatial distribution) | Particle statistics (per day)[a] | Size range Atm. studies ($\mu$m) | $\chi$ usage/ potential |
|---|---|---|---|---|---|---|---|---|---|
| *Single particle* | | | | | | | | | |
| SEM-EDX | Elemental | Vacuum | Most | Low | Semiquantitative | Yes | $10^2$–$10^4$ | >0.08 | Already used |
| TEM-EDX | Elemental | Vacuum | Most | Low | Semiquantitative | Yes | $10^2$ | >0.01 | High potential |
| TEM-EELS/EF-TEM | Elemental and oxidation state | Vacuum | Some | Low | Identification | Yes | $10^1$ | >0.01 | Low potential |
| STXM-NEXAFS | Oxidation state (electronic transitions) | Ambient | Some | Medium | Semiquantitative | Yes | $10^2$–$10^3$ | >0.2 | Already used |
| *Ensemble average* | | | | | | | | | |
| XPS | Oxidation state (electronic transitions) | Ambient | Some | Medium | Identification | Surface specific | N/A | 0.1–2.0 | N/A |

*Note.* N/A = not applicable. SEM/EDX = scanning electron microscopy/energy dispersive X-ray spectroscopy; TEM/EDX = transmission electron microscopy/energy dispersive X-ray spectroscopy; TEM-EELS/EF-TEM = transmission electron microscopy-electron energy loss spectroscopy/energy filtered-transmission electron microscopy; STXM-NEXAFS = scanning transmission X-ray microscopy-near edge X-ray absorption fine structure spectroscopy; XPS = X-ray photoelectron spectroscopy.
[a]Order-of-magnitude approximation of the number of particles that are typically analyzed from a sample or in a 1-day sampling period.

Reviews of Geophysics

10.1029/2018RG000615

**Table 2**
*Vibrational Spectroscopy/Optical Methods*

| Technique | Measures | Analysis conditions | Species coverage | Chemical detail | Identification/ quantification | Mapping (spatial distribution) | Particle statistics (per day)[a] | Size range Atm. studies ($\mu$m) | $\chi$ usage/ potential |
|---|---|---|---|---|---|---|---|---|---|
| *Single particle* | | | | | | | | | |
| Micro-FTIR | Functional groups | Ambient | Some | High | Semiquantitative | Yes | $10^2$–$10^3$ | >5.0 | Medium potential |
| EPMA/ATR-FTIR | Functional groups | Ambient | Some | High | Semiquantitative | Yes | $10^2$ | >1.0 | Medium potential |
| Raman Microspectroscopy | Functional groups | Ambient/ controlled | Some | High | Semiquantitative | Yes | $10^2$–$10^3$ | >0.8 | Medium potential |
| SERS/TERS | Functional groups | Ambient | Some | High | Semiquantitative | Yes | $10^1$–$10^2$ | >0.01 | Low potential |
| AFM-IR | Functional groups | Ambient | Some | High | Semiquantitative | Yes | $10^1$ | 0.09–10 | High potential |
| SP2 | Incandescence (optical) | Ambient | Few (soot) | Medium | Semiquantitative | N/A | N/A | 0.07–0.5 | Low potential |
| Fluorescence Microscopy/WIBS | Fluorescence (optical) | Ambient | Few (biological) | Medium | Identification | N/A | N/A | 0.5–50 | Low potential |
| *Ensemble average* | | | | | | | | | |
| FTIR | Functional groups | Ambient | Some | High | Semiquantitative | N/A | N/A | N/A | N/A |
| SFG/SHG | Functional groups/chirality | Ambient | Some | Medium | Identification | N/A (surface only) | N/A | N/A | N/A |

*Note.* N/A = not applicable. Micro-FTIR = Fourier transform infrared spectroscopy coupled to optical; EPMA/ATR-FTIR = energy probe X-ray microanalysis/attenuated total reflectance-Fourier transform infrared; SERS/TERS = surface-enhanced Raman spectroscopy/tip-enhanced Raman spectroscopy; AFM/IR = atomic force microscope/infrared; WIBS = wide issue bioaerosol spectrometer; SFG/SHG = sum frequency generation/sum harmonic generation.
[a]Order-of-magnitude approximation of the number of particles that are typically analyzed from a sample or in a 1-day sampling period.

Reviews of Geophysics

10.1029/2018RG000615

**Table 3**
*Mass Spectrometry*

| Technique | Measures | Analysis conditions | Species coverage | Chemical detail | Identification/ quantification | Mapping (spatial distribution) | Particle statistics (per day)[a] | Size range Atm. studies ($\mu$m) | $\chi$ usage/ potential |
|---|---|---|---|---|---|---|---|---|---|
| *Single particle* | | | | | | | | | |
| Single-particle mass spectrometers (PALMS, ATOFMS, RSMS, SPLAT, ALABAMA, LAMPAS, etc.) | Molecules and fragments[b] | Vacuum[c] | Most | Medium | Semiquantitative | No[d] | $10^4$–$10^6$ | 0.07–5.0 | Already used |
| NAMS | Molecules and fragments[b] | Vacuum | Most | Low | Semiquantitative | No | $10^3$–$10^4$ | 0.007–0.030 | Medium potential |
| Laser microprobe MS (LMMS, LAMMS, and LAMMA) | Molecules and fragments[b] | Vacuum | Most | Low | Semiquantitative | No | $10^2$–$10^3$ | >1.0 | Medium potential |
| SIMS | Molecules and fragments[b] | Vacuum | Most | Medium | Semiquantitative | Yes | $10^2$–$10^4$ | > 1.0 | Medium potential |
| NanoSIMS | Molecules and fragments[b] | Vacuum | Most | Low | Semiquantitative | Yes | $10^2$–$10^4$ | >0.1 | Low potential |
| *Ensemble average* | | | | | | | | | |
| SP-AMS | Molecules and fragments | Vacuum | Few (soot) | Medium | Semiquantitative | No | N/A | 0.07–1.0 | N/A |

*Note.* PALMS = particle analysis by laser mass spectrometry; ATOFMS = aerosol time-of-flight mass spectrometry; RSMS = rapid single-particle mass spectrometry; SPLAT = single-particle laser ablation time-of-flight mass spectrometer; ALABAMA = Aircraft-based Laser Ablation Mass Spectrometer; LAMPAS = laser mass analysis of particles in the airborne state; NAMS = nanoaearosol mass spectrometer; MS = mass spectrometer; LMMS = laser microprobe mass spectrometry; SIMS = secondary ion mass spectrometry; NanoSIMS = nano secondary ion mass spectrometry; SP-AMS = soot particle-aerosol mass spectrometer; N/A = not applicable.

[a]Order-of-magnitude approximation of the number of particles that are typically analyzed from a sample or in a 1-day sampling period. [b]Although the chemical analysis is conducted under vacuum, the duration in vacuum is typically very brief (see section 3.3 for details). [c]Some single-particle mass spectrometers obtain partial spatial information by varying the laser power (e.g., Ault et al., 2013a). [d]The degree of fragmentation varies widely depending on the method of ionization and amount of energy input into the molecule (see section 3.3 for details).

produces an image. The electron beam sensitivity of many submicron aerosol components has traditionally led to SEM being applied to particles greater than 0.1 $\mu$m, while higher-resolution TEM has often been used to probe particles down to ~20 nm (Ault et al., 2013b; Prather et al., 2013; Utsunomiya et al., 2004). Certain detectors used in electron microscopy provide contrast as a function of atomic number ($Z$) or $Z^2$, such that heavier elements appear brighter. These include backscattered electron detectors or high-angle annular dark-field (HAADF) detectors used during scanning transmission electron microscopy (STEM). These can give an indication of compositional variability but do not provide quantifiable data for mixing state analysis. Electron microscopy has also been used for morphological analysis of aerosol particles (e.g., soot) and particles taken up into precipitation (rain water or snow; Adachi et al., 2007; Axson et al., 2014; Creamean et al., 2016; Katrinak et al., 1993; Pósfai et al., 2003). A traditional limitation of SEM and TEM has been the high vacuum in which samples are analyzed, leading to losses of semivolatile materials. However, recent work has moved toward analyzing even delicate aerosol particles, such as liquid-liquid phase separations and intact cells, closer to their native condition via environmental SEM (ESEM), environmental TEM (E-TEM), and cryo-TEM (Laskin et al., 2005; Patterson et al., 2016; Semeniuk et al., 2007; Veghte et al., 2013, 2014; Wise et al., 2007).

Decomposition due to the electron beam and X-ray diffraction were some of the first approaches used to infer composition (Heard & Wiffen, 1969; Larner, 1964). Subsequent work gave some of the first examples of particle-to-particle variability and direct evidence that ambient aerosols are not a pure internal mixture. For example, the thin film vapor method, which exposed samples to vapors such as copper, barium (II) chloride, benzidine, or silver nitrate prior to analysis, enabled detection of a range of compounds at the individual particle level, such as sulfuric acid, sulfates, nitrates, persulfates, and halides, as reported by Bigg et al. (1974) for ambient particles and by Mamane and De Pena (1978) for laboratory-generated standard particles. Early applications of coupling electron microscopy with X-ray spectroscopy for elemental analysis included fly ash particles from coal-fired power plant plumes and particles collected in Antarctica (Parungo et al., 1979; 1978). The analysis of X-rays emitted from samples during electron microscopy is referred to by many different names, including energy dispersive X-ray spectroscopy (EDX), energy dispersive spectroscopy (EDS), X-ray energy dispersive spectroscopy (XEDS), and energy dispersive X-ray microanalysis (EDXMA), but will be referred to EDX throughout this paper for consistency. It is the most common chemical analysis associated with electron microscopy, as EDX can analyze all elements heavier than beryllium ($Z = 4$) and is well suited to higher-$Z$ elements, such as heavy metals. EDX provides atomic percentages for specific elements and can be used for whole-particle characterization or to map elements spatially within an individual particle. To obtain sufficient statistics, computer-controlled (CC) automation of SEM (CCSEM) was developed and has been applied with EDX analysis for source apportionment modeling of specific aerosol particle types (Allen et al., 2015; Ault et al., 2012; Bondy et al., 2018; Casuccio et al., 1983, 2004).

Electron energy loss spectroscopy (EELS) is often coupled with TEM analysis (though not with SEM). EELS detects inelastically scattered electrons, rather than X-rays and, compared to EDX, provides better measurements of certain low-$Z$ elements, as well as chemical bonding information (Ault & Axson, 2017; Conny et al., 2014; Fletcher et al., 2011; Laskin et al., 2016). A limitation of EELS is that it can only be applied to elements that have an electronic transition in the appropriate energy window, such as the carbon 1s (also known as K-edge) transition, as opposed to EDX, which is more universal. When a specific energy window with an EELS spectrum is mapped, this is referred to as energy filtered TEM (EF-TEM), which has been applied to map the chemical composition of marine, organic, dust, and metal-containing particles (Ault et al., 2013b; Deboudt et al., 2010, 2012). Since both EDX and EF-TEM can be used to determine the distribution of chemical elements within particles through mapping, they have the potential to be used to help determine physicochemical mixing state.

A method that provides more detailed electronic structure and bonding information than EELS is scanning transmission X-ray microscopy with near edge X-ray absorption fine structure spectroscopy (STXM-NEXAFS). A highly energy-resolved X-ray beam, typically at a light source such as the advanced light source at Lawrence Berkeley National Laboratory, is focused into a beam and used to analyze samples on a TEM grid (Moffet et al., 2010). STXM-NEXAFS is based on absorption using a Beer's law relationship, which can be used to analyze many electronic states, such as the carbon 1s (K-edge), nitrogen 1s (K-edge), or sulfur 2p (L-edge). STXM-NEXAFS was first applied to aerosol particle analysis in the early 2000s (Maria et al., 2003; Russell et al., 2002) and has been automated to generate the data needed for mixing state analysis (Moffet et al., 2010). While only elements whose energies fall within the available window of the light sources

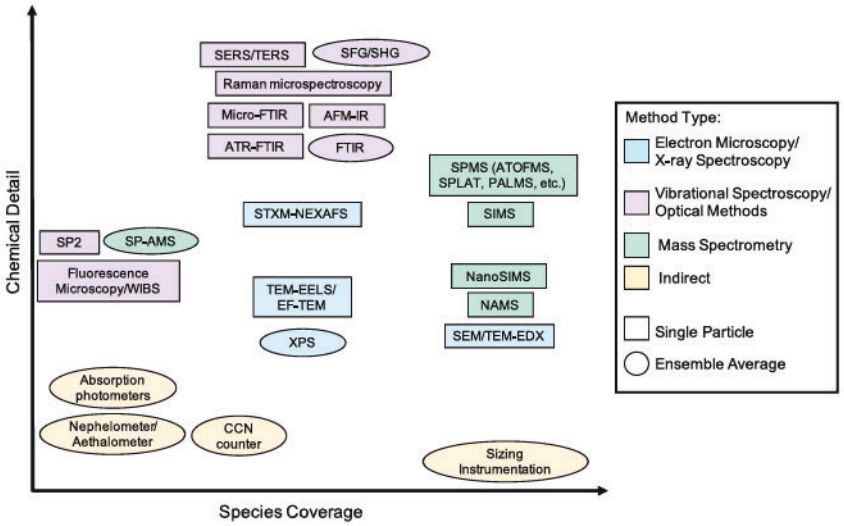


**Figure 5.** Summary of measurement techniques in terms of species coverage and chemical detail. Oval symbols refer to techniques that measure ensemble averages for the entire aerosol. Rectangular symbols refer to techniques that probe properties on the single-particle level. Indirect methods will be discussed in sections 6.2 and 6.3.1.
SERS = surface-enhanced Raman spectroscopy; TERS = tip-enhanced Raman spectroscopy; SFG = sum frequency generation; SHG = sum harmonic generation; Micro-FTIR = Fourier transform infrared spectroscopy coupled to optical; ATR/FTIR = attenuated total reflectance-Fourier transform infrared; AFM/IR = atomic force microscope-infrared; FTIR = Fourier transform infrared; SPMS = single-particle mass spectrometer; ATOFMS = aerosol time-of-flight mass spectrometry; SPLAT = single-particle laser ablation time-of-flight mass spectrometer; PALMS = particle analysis by laser mass spectrometry; STXM = scanning transmission X-ray microscopy; NEXAFS = near edge X-ray absorption fine structure spectroscopy; SIMS = secondary ion mass spectrometry; SP/AMS = soot particle aerosol mass spectrometer; WIBS = wide issue bioaerosol spectrometer; TEM/EELS = transmission electron microscopy/electron energy loss spectroscopy; EF/TEM = energy filtered/transmission electron microscopy; XPS = X-ray photoelectron spectroscopy; NAMS = nanoaearosol mass spectrometer; SEM = scanning electron microscopy; EDX = energy dispersive X-ray spectroscopy; CCN = cloud condensation nuclei.

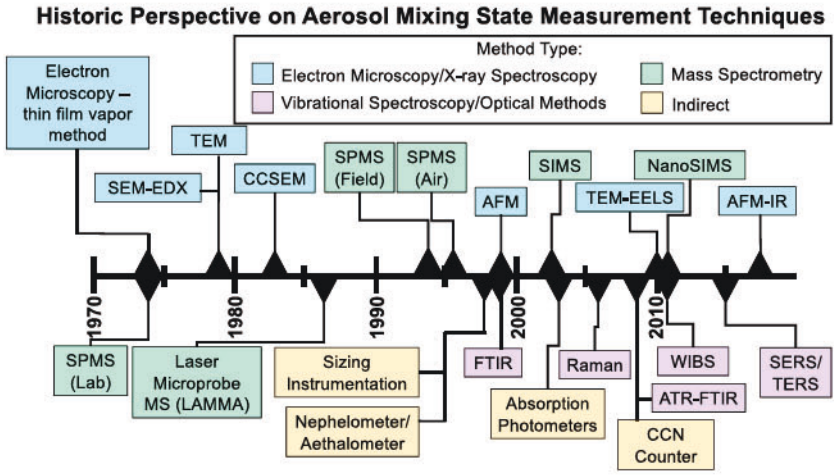


**Figure 6.** Time line of the use of various measurement techniques to study aerosol mixing state. It should be noted that this time line aims to highlight when these techniques were applied for the study of aerosol mixing state. The time frame does not necessarily correlate with the development or first application of the various methods.
SEM/EDX = scanning electron microscopy/energy dispersive X-ray spectroscopy; TEM = transmission electron microscopy; CCSEM = computer-controlled scanning electron microscopy; SPMS = single-particle mass spectrometer; AFM = atomic force microscope; SIMS = secondary ion mass spectrometry; TEM/EELS = transmission electron microscopy/electron energy loss spectroscopy; NaniSIMS = nano secondary ion mass spectrometry; AFM/IR = atomic force microscope/infrared; FTIR = Fourier transform infrared; WIBS = wide issue bioaerosol spectrometer; ATR/FTIR = attenuated total reflectance/Fourier transform infrared; CCN = cloud condensation nuclei; SERS/TERS = surface-enhanced Raman spectroscopy/tip-enhanced Raman spectroscopy.

can be probed, STXM-NEXAFS has been used to analyze a range of sources, including sea spray aerosol (Ault et al., 2013b; Kirpes et al., 2018), biomass burning (Fraund et al., 2017) SOA (Takahama et al., 2007), and soot (Moffet et al., 2013). For higher-$Z$ elements (e.g., metals) X-ray absorption near edge spectroscopy (XANES) is also available at some synchrotrons (De Santiago et al., 2014; Oakes et al., 2012). Single-particle imaging using diffraction from a synchrotron X-ray beam has also been coupled with single-particle mass spectrometry (Bogan et al., 2010; Loh et al., 2012).

When considering methods that have the potential to inform future physicochemical mixing state metrics, surface-specific measurements may be useful. X-ray photoelectron spectroscopy (XPS) is a surface-specific technique, using a monochromatic X-ray beam to measure the energy of ejected electrons from the surface (due to the short mean free path of electrons versus photons). XPS probes electronic transitions, providing oxidation state and bonding information similar to EELS (less resolution than STXM-NEXAFS) but typically only provides ensemble information for bulk samples (Baltrusaitis et al., 2009; Song & Peng, 2009). XPS has been applied to provide carbonaceous aerosol signatures for the identification of soot sources (Vander Wal et al., 2011). XPS has also been used to monitor heterogeneous reactions of sea spray aerosol with nitric acid (Ault et al., 2014). Through XPS analysis, distinct elemental and oxidation states at particle surfaces have been observed to vary as a function of particle size (Guascito et al., 2015; Xu et al., 2016).

Hundreds of studies using electron microscopy and X-ray spectroscopy methods to investigate aerosol particles have been published over the years, ranging from studies characterizing the constituents of specific types of aerosol, such as marine, mineral, dust, and biomass (Buseck & Pósfai, 1999; Li et al., 2003; Pósfai et al., 1994, 2003) to those focused specifically on characterizing per-particle composition and morphology (Deboudt et al., 2010; Pósfai et al., 1999), phase transitions (Wise et al., 2005), hygroscopic behavior (Okada, 1985; Semeniuk et al., 2007), phase separation (Ault et al., 2013a; Freedman, 2017; Losey et al., 2016; O'Brien et al., 2015; You et al., 2012), and other important aerosol physicochemical properties that impact mixing state. However, only in the past few years have these methods begun to be used to quantify aerosol mixing state, the examples of which are discussed later in section 5.2.

### 3.2. Vibrational Spectroscopy and Optical Methods

Vibrational spectroscopy techniques use light to excite and detect vibrational modes, allowing for analysis of specific covalently bonded molecules (e.g., sulfate, nitrate, and ammonium), as well as characterization of functional groups within complex organic material (Ault & Axson, 2017; Lee & Allen, 2012; Murphy et al., 2014). This is useful when attempting to measure an aerosol's mixing state as many species of interest cannot be differentiated solely based on elemental information, such as for nitrogen where ammonium nitrate, and N-containing organic molecules (e.g., amines) all occur in aerosols. See Table 2 for an overview of instruments based on these analysis techniques. Infrared (IR) spectroscopy, specifically Fourier transform IR (FTIR), has been used to obtain ensemble average data from bulk samples or large particles since the early 2000s, when Maria et al. (2002) characterized mixing of African mineral dust and organic compounds in aerosol samples collected in the Caribbean. However, the lack of individual particle data limited its application to mixing state. Micro-FTIR, where an IR spectrometer is coupled to an optical microscope, has been used mostly to study >5-$\mu$m particles. For example, micro-FTIR has been used to study keto-enol tautomerism and hygroscopic properties of mixed salt and organic particles (Ghorai et al., 2011, 2014; Liu et al., 2008). A key limitation for FTIR and mixing state is that the spatial resolution is low due to the long wavelengths of IR radiation and the diffraction limit at those wavelengths. Additionally, the spatial resolution changes with wavelength, causing different resolutions across a spectrum (unlike Raman, discussed below). Thus, FTIR has traditionally been limited in its ability to study aerosol mixing state through measurements of individual particles at atmospherically relevant sizes. One approach to gain more detailed information from IR spectroscopy has been to couple energy probe X-ray microanalysis (EPMA) with attenuated total reflectance FTIR (ATR-FTIR). EPMA is similar to EDX but has improved capabilities for lower atomic number elements. Multiple studies have shown that IR spectra for particles down to ~1 $\mu$m can be obtained using these techniques (Jung et al., 2014; Ryu & Ro, 2009; Song et al., 2010).

Another vibrational spectroscopy technique, Raman microspectroscopy, has been used with increasing frequency since the early 2000s for single aerosol particle analysis. In contrast to IR, Raman spectroscopy uses a single wavelength, often in the visible range, resulting in higher spatial resolution and a lower particle size limit of ~0.8 $\mu$m (Ault & Axson, 2017). Single-particle data from Raman spectroscopy have been used to characterize mixing of species within individual sea spray aerosol (Ault et al., 2013c; Deng et al., 2014;

Ebben et al., 2013; Laskina et al., 2015), mineral dust (Laskina et al., 2013; Sobanska et al., 2012), organic particles (Gaffney et al., 2015), along with ambient samples (Baustian et al., 2012; Craig et al., 2017a). Unlike electron microscopy, Raman analysis is conducted at atmospheric temperature and pressure and, as such, has been used to probe challenging properties impacted by semivolatile (e.g., water) loss under vacuum, such as aerosol acidity (Bondy et al., 2017a; Craig et al., 2017b; Rindelaub et al., 2016). Similar to CCSEM, a few automated methods for Raman analysis have been developed and used to characterize chemical composition of both laboratory-generated and ambient aerosol particles, including computer-controlled Raman (CC-Raman; Craig et al., 2017a) and the automated aerosol Raman spectrometer (Doughty & Hill, 2017).

To probe smaller particles and improve the potential for Raman spectroscopic analysis of interparticle and intraparticle variation, applications of surface-enhanced Raman spectroscopy (SERS) and tip-enhanced Raman spectroscopy (TERS) to the study of aerosols have recently been developed. A SERS method using particles deposited on nanoparticle-coated substrates to enhance the Raman signal was introduced by Craig et al. (2015), followed by several variations, such as electrospray SERS (ES-SERS) and surface-enhanced resonance Raman spectroscopy (SERRS; Craig et al., 2015; Gen & Chan, 2017; Sivaprakasam et al., 2017). TERS uses an atomic force microscope (AFM) tip with a noble metal (e.g., silver) nanoparticle tip to generate enhanced Raman spectra. TERS was first used for aerosol particle analysis by Ofner et al. (2016) to study the chemical composition of SOA particles during formation and photochemical aging.

AFM, mentioned above, can provide information regarding particle size, phase, and height with nanoscale spatial resolution for aerosol particles larger than ~10 nm by the use of an oscillating cantilever whose tip interacts with the surface of a material (i.e., a particle). Early applications of AFM were to study water loss (Pósfai et al., 1998) and classify aerosol particles as organic, graphitic, or inorganic, as well as obtain size distributions (Lehmpuhl et al., 1999). Since then, AFM has been used, most often in tandem with other analysis techniques, to characterize aerosol mixing state in urban and marine-influenced urban environments (Sobanska et al., 2014; Vester et al., 2007), as well as during Chinese wintertime haze events (Chen et al., 2017a). More recently, AFM studies have incorporated more detailed analysis of specific properties, such as surface tension (Lee et al., 2017a, 2017b) and hygroscopicity (Ghorai et al., 2014; Morris et al., 2016). An exciting advancement for AFM has been coupling with a scanning IR laser to conduct photothermal IR spectroscopy (Bondy et al., 2017b; Kwon et al., 2018; Or et al., 2018). The operating principle of AFM-IR is that when the tunable IR laser interacts with the sample at a frequency where it absorbs, the sample expands slightly causing the oscillation of the cantilever to change, and that signal can be converted back to an IR spectrum. This has been used for particles down to 90 nm (Bondy et al., 2017b; Or et al., 2018), which were previously inaccessible to IR spectroscopic analysis. The incorporation of IR spectra with AFM have increased the potential for more detailed direct characterization of mixing state via AFM analysis.

As with the XPS above, surface-selective spectroscopies have also been applied to aerosol particles, typically for ensemble averages. Sum frequency generation (SFG) uses two lasers to probe noncentrosymmetric vibrations, which occur at interfaces. As with other vibrational spectroscopies (and unlike XPS), SFG is conducted at atmospheric pressure and temperature. SFG has been used to probe both laboratory standards and model systems (Jubb et al., 2012; Tang et al., 2010; Xu et al., 2009), as well as field samples (Ault et al., 2013c; Ebben et al., 2013, 2011, 2012, 2014), providing information on properties such as chirality (Martinez et al., 2011). A recent advance has been the application of sum harmonic generation (SHG) to suspended aerosols, where a surface-selective dye was probed (Wu et al., 2016). When considering the importance of surface properties, further advancement of methods that are truly surface selective has the potential to assist with physicochemical mixing state determination.

It should be noted that optical trapping and tweezing coupled with vibrational spectroscopy techniques have also been used for more detailed characterization of the chemical and physical properties of single aerosol droplets during dynamic multiphase processes (Bzdek et al., 2016; David et al., 2015, 2016; Davies & Wilson, 2016; Sullivan et al., 2018), such as coagulation and uptake of water or organics (Hopkins et al., 2004; Mitchem et al., 2006). With our focus on building a population-level understanding of atmospheric particles, these methods are beyond the scope of this review, though they are providing valuable information toward understanding physicochemical properties of individual particles.

Methods focusing on specific subpopulations, such as soot and bioaerosols, have seen expanded usage in recent years. The single-particle soot photometer (SP2) is used to study individual soot particles (Gao et al., 2007) but has been expanded to other absorbing aerosol (Adachi et al., 2016). Briefly, it measures

incandescence after particle absorption in two wavelength ranges (350–800 and 630–800 nm). The SP2 has been used to study coatings on soot particles (Sedlacek et al., 2012; Taylor et al., 2015), impacts on morphology (Sedlacek et al., 2015), and water uptake (Hersey et al., 2013). Following a similar principle, an additional approach to soot particles has been the soot particle aerosol mass spectrometer (SP-AMS; Onasch et al., 2012). Fluorescence spectroscopy is increasingly being used for bioaerosol detection, an early version of which was the ultraviolet aerodynamic particle sizer (UV-APS; Kanaani et al., 2007). Newer methods, including the wide issue bioaerosol spectrometer (WIBS) and a cellular phone attachment, have been used to measure ultraviolet light induced fluorescence for the detection of biological aerosols (Gabey et al., 2010; Huffman et al., 2016). Though chemical speciation is limited in comparison to other spectroscopy methods, studies have shown regional, seasonal, and diurnal variation in primary biological aerosol particles (PBAPs) and thus also variation in aerosol mixing state (Gabey et al., 2010; Perring et al., 2015; Toprak & Schnaiter, 2013). Fluorescence microscopy has also been used to detect aerosols emitted from harmful algal blooms (HABs; May et al., 2018a).

The use of spectroscopic methods to probe individual aerosols, ensemble averages, surface properties, and other properties important for mixing state has expanded considerably in the past decade. Their continued development will provide meaningful information, often at room temperature and ambient pressure for use in aerosol mixing state calculations and modeling of aerosol behavior sensitive to pressure and temperature, such as liquid-liquid phase separations (Pye et al., 2017).

### 3.3. Mass Spectrometry Methods

The use of mass spectrometry to probe aerosols has revolutionized the understanding of aerosol chemical composition through a wide array of instruments coupling a range of ionization sources and mass analyzers, which, as mentioned above, have been the subject of numerous insightful reviews (Laskin et al., 2018, 2013; Noble & Prather, 2000; Pratt & Prather, 2012a, 2012b; Suess & Prather, 1999; Sullivan & Prather, 2005). For this review, we focus on single-particle mass spectrometers (SPMSs), which provide individual particle size and chemical composition in real time. With respect to composition, SPMSs measure most species, though due to how ions are generated species can be fragmented or not ionized well, leading to medium chemical detail. SPMS data have significant potential for mixing state calculations, as SPMSs can analyze a large number of particles, providing higher temporal resolution than microscopy (section 3.1). See Table 3 for an overview of mass spectrometry instruments.

The first real-time SPMSs were developed in the 1970s when particles were introduced into vacuum and collected on a filament, after which the particle was vaporized and either a magnetic sector or a quadrupole mass analyzer was used (Davis, 1973; Myers & Fite, 1975). These methods relied initially on the intensity of the ion signal for sizing and were stationary, thus suitable only for laboratory studies. In the 1980s two key steps forward were the introduction of aerodynamic sizing and laser desorption ionization (LDI) to a scanning mobility particle sizer (SMPS; Sinha et al., 1982). The 1990s saw a rapid expansion in the development and use of real-time SPMS, with the development of rapid single-particle mass spectrometry (RSMS; Carson et al., 1995), particle analysis by laser mass spectrometry (PALMS; McKeown et al., 1991), aerosol time-of-flight mass spectrometry (ATOFMS; Nordmeyer & Prather, 1994; Prather et al., 1994), and laser mass analysis of particles in the airborne state (LAMPAS; Hinz et al., 1994). Key advancements included the use time-of-flight mass analyzers (McKeown et al., 1991), coupling time-of-flight sizing with time-of-flight mass spectrometry (Prather et al., 1994), and dual polarity mass spectra for individual particles (Gard et al., 1997; Hinz et al., 1996). During the 1990s SPMS left the laboratory for ambient sampling with field-deployable instruments (Gard et al., 1997) and a flight capable instrument being developed (Murphy et al., 1998b). These field-deployable instruments have provided single-particle size and chemical composition for a wide range of locations globally (Dall'Osto et al., 2010; Fitzgerald et al., 2015; Guazzotti et al., 2001a; Murphy et al., 1998c). Additional developments with relevance to mixing state have included coupling to optical properties (Moffet & Prather, 2009, 2005) and two-step laser desorption followed by ionization to increase reproducibility of mass spectra (Morrical et al., 1998; Zelenyuk et al., 2009).

More recently developed SPMSs include the single-particle laser ablation time-of-flight mass spectrometer (SPLAT; Zelenyuk & Imre, 2005; Zelenyuk et al., 2008a), Aircraft-based Laser Ablation Mass Spectrometer (ALABAMA; Brands et al., 2011), nanoaearosol mass spectrometer (NAMS; Wang et al., 2006), and light

scattering soot particle AMS (LS-SP-AMS). Given that there are so many different SPMSs, it is not feasible to discuss the details of each instrument, but Murphy (2007) provides a useful discussion of the instrumental design choices for SPMSs and Pratt and Prather (2012a) provide a useful review of instruments and capabilities. In Table 3, these methods are listed together, but each has its own unique capabilities.

In addition, off-line analysis of single particles has been conducted with laser microprobe mass spectrometry (LMMS, LAMMS, or LAMMA) and secondary ion mass spectrometry (SIMS; Kaufmann, 1986; Klaus, 1986; Verbueken et al., 1985; Wieser & Wurster, 1986), though this has decreased in recent years. More recently, time-of-flight (TOF) SIMS has been coupled used for individual particle analysis (Boman et al., 2004; Tervahattu et al., 2002) and coupled with many of the electron microscopy and spectroscopy methods listed above (Hopkins et al., 2008). The more recently developed NanoSIMS has also been applied to atmospheric particles (Pöhlker et al., 2012, 2010).

As listed in Table 3, mass spectrometry provides information on the molecular species and fragments present, but the degree of fragmentation varies widely depending on the method of ionization and amount of energy input into the molecule. Some rely on the fragmentation patterns for quantification (e.g., SP-AMS and PALMS), while others try and minimize fragmentation to observe higher mass-to-charge peaks that provide more information on the molecules present. Even for two methods using the same ionization approach, such as LDI, PALMS uses a 193-nm laser that has more energy per photon and leads to greater fragmentation than the 266-nm laser used by the ATOFMS. In addition, some instruments can use two-step desorption ionization, which is considerably softer than a single higher energy laser pulse for LDI. Thus, although Table 3 lists the "measures" column as "molecules and fragments," there is great heterogeneity in terms of what each instrument provides.

It is also important to note that, while mass spectrometers conduct the chemical analysis under vacuum ($10^{-6}$ to $10^{-8}$ torr), the analysis is typically very rapid (<1 ms) and occurs before particles equilibrate to the vacuum conditions. In addition, sizing is typically being conducted at higher pressures, so the particles do not experience high vacuum for very long.

For mixing state the central appeal of mass spectrometers analyzing single particles is that they measure the size of and chemical species in individual particles. In addition, they typically have much higher throughput than the electron/X-ray and vibrational methods above (sections 3.1 and 3.2), thus generating greater particle statistics and facilitating a more detailed understanding of the overall particle population in the atmospheric aerosol. The challenge with SPMSs is that most rely on LDI, which makes determining exact mass fractions at the single-particle level challenging due to shot-to-shot variability. However, no other approach can provide as much single-particle data over a comparable time period, making efforts to overcome the complexity of the data worth pursuing.

### 3.4. Defining Particle Types for Chemical and Physicochemical Mixing State

#### 3.4.1. Identifying Particle Types

Using aerosol particle types as a mechanism for thinking about certain subpopulations is useful as it provides a simplification that can make classifying aerosols from different sources or that have undergone similar atmospheric aging more manageable. As an example, in Figure 2 over the urban area the sources of particles, such as mineral dust, soot/elemental carbon, primary organic carbon, secondary organic carbon, and metals-rich particles from industry, are often referred to as particle types. This manner of thinking about aerosol particles is useful for trying to determine the sources of particles that lead to overall particulate matter (PM) concentrations (e.g., source apportionment) or the number concentrations of cloud-activating particles (e.g., CCN or INP).

However, there is not a standard definition of particle types. The challenge of defining the properties of a particle type results from the fact that it is not as simple as knowing the source of a particle, since secondary aerosol can form and secondary species can mix at the individual particle level with particles from different sources. In source apportionment this is often treated by including a SOA class in addition to all of the primary sources. However, this does not account for the fact that particles from the same source often have a range of compositions and have undergone varying degrees of atmospheric aging, making aging not uniform across all particles in a population. To build on the Figure 2 example above, consider a soot particle emitted from a diesel vehicle's tailpipe. Initially, the "fresh soot" particle may be a fractal aggregate with a low mass fraction of secondary species (e.g., sulfate) and hydrophobic (i.e., a poor CCN). However, over the course of

its atmospheric lifetime that particle may take up secondary species, collapse into a nearly spherical core, and have a coating of soluble, hygroscopic species form on it (e.g., ammonium sulfate). The question becomes, is the now "aged soot" particle part of the same particle type as the fresh soot? Both are from the same source, but in terms of their optical (fractal versus core shell) and cloud nucleating (hydrophobic versus hygroscopic) properties they are different.

One approach to handling subpopulation variability is to have distinct subpopulations (e.g., fresh soot and aged soot). However, then a cutoff in time, mass fraction, or morphology must be established to determine when a fresh particle transitions to an aged particle (Riemer et al., 2010). This is somewhat arbitrary as the reality is more likely a continuum between fresh and aged. Finding a balance between having a manageable number of particle types, while representing the range of composition and climate-relevant properties, requires making these types of decisions. This example illustrates that even within a single subpopulation or particle type connecting back to the climate (or health) relevant properties of a subpopulation can necessitate characterizing the mixing state within a subpopulation.

Having established that there are multiple particle types and that there is variability within these types, it is important to understand how measurements and models handle these subpopulations, specifically through particle types. For measurements, single-particle data are often sorted, typically using clustering algorithms, into different particle types based on mathematical comparisons of the individual particle composition (or other properties). The types produced from this can be broken down at differing levels of chemical detail from a broad level (soot, organic carbon, biomass burning, dust, sea salt, and industrial) to a more detailed level (cars versus trucks, metal-containing particles from different industrial sources, biomass burning enriched in sulfate versus nitrate, and bloom versus nonbloom sea spray aerosol) depending on the scientific questions being addressed. Section 3.4.2 will discuss some of the methods, including clustering, used to classify individual particle properties into particle types. Section 4.3.3 will discuss how modal models define and handle particles types. As with snowflakes, each particle is unique and the number of subpopulations, how they are distinguished, and the degree to which heterogeneity is accounted for is important when evaluating the impacts of aerosol mixing state.

#### 3.4.2. Clustering and Classification Approaches for Single-Particle Spectra

For ambient measurements of single particles, early classification approaches were developed for CC scanning electron microscopy coupled with EDX (CCSEM) and typically relied upon user-defined rules that determined which category a particle was assigned to (Casuccio et al., 1983; Kim et al., 1987). These data sets often had data for hundreds to thousands of particles for ~15–30 elements, data volumes that could still be spot-checked manually. The development of field-deployable real-time single-particle mass spectrometry (Hinz et al., 1994; McKeown et al., 1991; Prather et al., 1994) resulted in more complicated spectra (hundreds of mass-to-charge, $m/z$, values per spectrum). These mass spectrometers also led to increases in data volumes with data sets initially on the order of tens of thousands of particles, which now are often on the order of millions to tens of millions of particles. These advancements meant that rules-based classification was no longer practical for characterizing the volume and breadth of data being generated. Early on, traditional analytical classification was used, such as principal component analysis (Hinz et al., 1996), but the unique nature of single-particle data led to the development of more specialized approaches.

Song et al. (1999a) first applied a neural network approach to classifying single-particle spectra using adaptive resonance theory 2a (ART-2a). The following is a brief description of the application of ART2a to single-particle data from an ATOFMS to illustrate how clustering is utilized, but each mass spectrometer described above has its own slightly different approach to cluster analysis. Each mass spectrum from an ATOFMS is discretized, providing a vector, typically of 350 values for a mass range of 1–350 $m/z$ or 700 values for dual polarity spectra (both positive and negative ions) at unit mass resolution (one $m/z$), though higher $m/z$ can be used (Pratt et al., 2009a). An initial set of cluster centroids are chosen randomly from single particles within the data set and the remaining single-particle mass spectra are compared to the cluster centers to determine if there were similar enough to be included in that cluster, mathematically known as the vigilance factor (Anderson et al., 2005; Rebotier & Prather, 2007; Song et al., 1999b). If a particle did not fit into any cluster, it is placed in its own cluster. After all particles are either placed in a cluster or a new cluster is defined, new cluster centroids are determined based on the average spectra within a cluster. The amount the cluster centroid could move after an iteration through the assignment process is the learning rate. After generating new cluster centroids, the assignment process repeats and all particles are assigned to

the new centroids. Clusters can merge or split during this process. The analysis typically involves 20 iterations to reach stable cluster assignments, though could be varied depending on data set properties. The final product is typically a large number of clusters, with most particles (80–90%) in the most populated clusters (typically <50) and a large number of small clusters with few particles. Data are typically presented for the most abundant clusters using a threshold, such as 90%, based on the diversity of mass spectra in a data set.

Building on this clustering approach, Bhave et al. (2001) used ART-2a cluster analysis results for source apportionment. Additionally, an approach using spectra from specific sources as "seeds" and then matching the ambient spectra to those seeds has been used for ambient source apportionment (Toner et al., 2008), distinguishing cars from trucks (i.e., light duty vehicles from heavy duty diesel vehicles; Shields et al., 2007; Song et al., 2001) and other source-specific applications (Ault et al., 2009; Fitzgerald et al., 2015; Pratt et al., 2009b; Qin & Prather, 2006). Seed matching has also been implemented for on-the-fly source apportionment (Pratt et al., 2009a).

Additional clustering algorithms have been tested for single-particle mass spectral classification, including k-means and k-medians (Anderson et al., 2005; Rebotier & Prather, 2007), as well as hierarchical approaches (Rebotier & Prather, 2007). The key difference for the k-means and k-medians algorithms is that instead of two user-defined variables (vigilance factor and learning rate), the number of clusters is the sole variable defined at the beginning of the clustering process. The typical manner for checking the efficacy of a specific number of clusters is to use different numbers of clusters and compare the difference between all particles and their cluster centroid with the distance between all particles and the population (overall) cluster centroid (effectively the centroid if there is only one cluster). This value decreases with more clusters approaching an asymptote, and the optimal number of clusters can be determined based on how many it takes to approach that asymptote (Gross et al., 2010). Either ART2a or k-means/k-medians can be effective if applied correctly, though each has their strengths and weaknesses. Multiple studies have expanded upon or further tested clustering of single-particle mass spectrometry data, such as ClusterSculptor by Zelenyuk et al. (2008b).

In addition to single-particle mass spectra, other single-particle analysis methods such as CCSEM-EDX have used the single-particle clustering algorithms described above, particularly k-means. Ault et al. (2012) took the single-particle mass spectrometry clustering approach and applied it to atomic percentages from EDX and used it to cluster CCSEM-EDX data sets (Ault et al., 2012; Shen et al., 2016). There have been an increasing number of ambient studies with CCSEM-EDX spectra (Ault et al., 2013b; Axson et al., 2016a, 2016b; Bondy et al., 2018, 2017c; Coz et al., 2010, 2009; Creamean et al., 2016; Kirpes et al., 2018; May et al., 2018b; Shen et al., 2016), which has also led to source EDX spectra from a range of studies that could be used as seeds for matching in the future, analogously to the ATOFMS matching above.

The increased use of Raman microspectroscopy spectra has also led to spectral classification approaches. Craig et al. (2017a) used (CC-Raman) microspectroscopy to increase throughput and collect hundreds to thousands of spectra, after which hierarchical clustering algorithms were applied to group spectra by aerosol particle type. Cochran et al. (2017) recently developed a library of Raman spectra and an approach to look at linear combinations using chi-square analysis. This has recently been applied in the Arctic to look at chemical mixing state with respect to the distribution of sulfate across an particle population, where Kirpes et al. (2018) found that sulfate is mixed with other species (i.e., sources) across the population and not present as externally population sulfate particles within the aerosol. Other methods for classifying single-particle spectra from different instrumentation have also been developed (Doughty & Hill, 2017).

#### 3.4.3. Field Observations of Particle Types

Having defined the measurement techniques used to study mixing state, it is useful to briefly discuss what is known about aerosol mixing state in different environments and locations. With over 2,000 publications on aerosol mixing state it is not practical to cover all of the literature on the topics, but examples are provided, as are useful reviews. Going back to the concept of particle types defined in section 3.4.1, mixing state is often discussed in terms of the major sources of aerosols within a population. Common particle types are mostly primary (soot, organic carbon, biomass burning, mineral dust, sea salt, and industrial; Andreae & Rosenfeld, 2008; Prather et al., 2008). An exception is SOA, which is secondary, but often listed as its own source. Typically, accumulation mode particles (80–1,000 nm) are a mix of combustion particles and secondary particles with a mixture of SOA and secondary inorganic species (sulfate, nitrate, and ammonium; Qin et al., 2012). Particles larger than 1,000 nm are typically dominated by mechanically generated particle types, such as mineral dust and sea salt.

Studies characterizing specific sources have long been carried out to understand particle type properties at the point of emission, including light duty vehicles (e.g., cars; Sodeman et al., 2005; Toner et al., 2008), heavy duty diesel vehicles (e.g., trucks; Gross et al., 2000; Shields et al., 2007; Toner et al., 2008), ship emissions (Ault et al., 2010, 2009), biomass burning (Pratt & Prather, 2010; Silva et al., 1999), industrial processes (Dall'Osto et al., 2012), sea spray aerosol (Ault et al., 2013b; Frossard et al., 2014; Hawkins & Russell, 2010; Prather et al., 2013), lake spray aerosol (Axson et al., 2016a; May et al., 2016, 2018b, 2018a), mineral dust (Guazzotti et al., 2001a; Murphy & Thomson, 1997; Silva et al., 2000), fireworks (Liu et al., 1997), grass mowing (Drewnick et al., 2008), and many more. Single-particle source characterization approaches are not limited to primary sources either and have been used to probe SOA (Middlebrook et al., 2003), amines (Pratt et al., 2009b), oxalic acid (Sullivan & Prather, 2007), oligomers (Denkenberger et al., 2007), organosulfates (Hatch et al., 2011a, 2011b), methanesulfonate (Gaston et al., 2010), hydroxymethanesulfonate (Whiteaker & Prather, 2003), sulfate (Kirpes et al., 2018; Lake et al., 2004), and secondary chloride (Sullivan et al., 2007b) as a few examples. A challenge when defining primary sources and mixing state is that in heavily aged areas a particle may have a 100-nm core from a primary sources (e.g., soot) with 500-nm coating of sulfate and SOA. It is challenging to define whether this is a primary or secondary particle. Pratt and Prather (2009) studied this through the use of a thermal denuder, which revealed primary cores at the center of many particles heavily coated with secondary material.

Beyond analyzing the single-particle properties associated with specific sources, it is valuable to understand how atmospheric aging changes the mixing state of specific subpopulations. Mixing state studies focused on specific particle types have included soot (Adachi et al., 2010; Jacobson, 2001; Moffet & Prather, 2009; Pósfai et al., 2003; Riemer et al., 2009; Schwarz et al., 2008; Zhang et al., 2008), biomass burning (Bi et al., 2011; Healy et al., 2013; Moffet et al., 2008; Pósfai et al., 2003; Spencer et al., 2008), sea spray aerosol (Ault et al., 2009; Gard et al., 1998; Guazzotti et al., 2001a, 2001b), and mineral dust (Deboudt et al., 2010; Fitzgerald et al., 2015; Geng et al., 2014; Li et al., 2016; Sobanska et al., 2012; Sullivan et al., 2007a) to name a few.

It is important to characterize the mixing state of particle populations at specific locations or in different environments. Example studies have probed mixing state in urban (Qin et al., 2012; Reinard et al., 2007; Toner et al., 2008), marine (Ault et al., 2009; Decesari et al., 2011; Furutani et al., 2008; Guazzotti et al., 2001b; Murphy et al., 1998a; Spencer et al., 2008), forested (Creamean et al., 2011; Gunsch et al., 2018), rural (Bondy et al., 2018; Whiteaker et al., 2002), and Arctic locations (Gunsch et al., 2017). Specific studies focused on the mixing state during unique events, such as during strong biomass burning influence (Pratt & Prather, 2010; Qin & Prather, 2006) or dust transport (Bauer et al., 2013; Creamean et al., 2015; Fitzgerald et al., 2015). Beyond the mixing state at different locations, vertical variation in mixing state is both important and understudied (Creamean et al., 2013; Hudson et al., 2004; Murphy et al., 2006; Pratt & Prather, 2010).

To summarize, single-particle studies focused on mixing state have probed sources, the distribution secondary species, a range of types of environments, vertical distributions, and unique conditions (e.g., fires and dust transport). However, despite all of this information about single-particle composition globally, relatively few studies have connected this single-particle composition data to quantifiable mixing state metrics, as will be discussed in section 5.2.

## 4. Representation of Mixing State in Aerosol Models

Concurrent with advances in experimental methods, our modeling tools have been advanced over the last two decades to better capture the aerosol microphysics processes, including the evolution of the chemical mixing state of aerosols. In this section we will first cover the mathematical framework of aerosol composition space (section 4.1) and the governing equation (section 4.2) and then describe existing modeling approaches (section 4.3).

### 4.1. Aerosol Composition Space

It is common to visualize and analyze aerosols in terms of number distributions or mass distributions as a function of particle size (Seinfeld & Pandis, 2016, Chapter 8)—after all, particle size is of first-order importance for aerosol impacts on health and climate. However, for characterizing aerosol mixing state, size distributions are limiting, since the same size distribution can represent many different mixing states.

An aerosol particle in an population contains mass $\mu_a \geq 0$ of species $a$, for $a = 1, \ldots, A$, so that the particle composition is described by the $A$-dimensional composition vector $\vec{\mu} \in \mathbb{R}^A$. Each aerosol particle

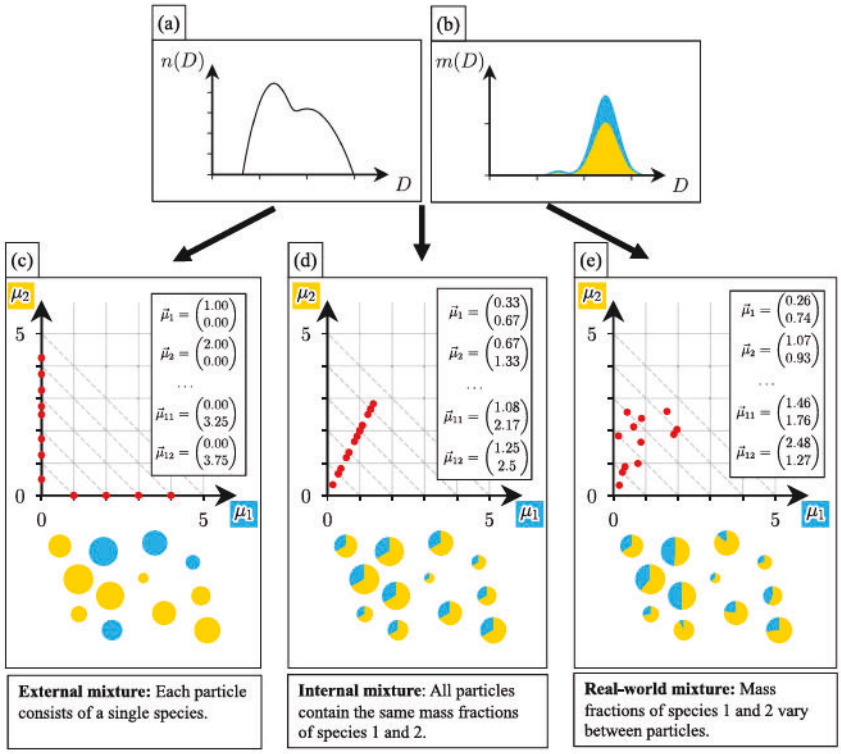


**Figure 7.** The concept of aerosol composition space for a population consisting of two chemical species. (a) Example of a number size distribution, (b) corresponding mass size distribution, (c–e) composition space depictions of example particles from populations that are consistent with the distributions shown in (a) and (b).

represents therefore a point in the $A$-dimensional *composition space*. Figure 7 illustrates this concept for a particle population that has a number distribution as shown in Figure 7a and consists of two species ($A = 2$) with mass distribution as shown in Figure 7b. Figures 7c–7e show how particle samples from three possible populations populate the composition space. The composition space is in this case two dimensional, so each particle is represented by a vector $\vec{\mu} = (\mu_1, \mu_2)$. The broken gray lines are lines of constant diameter (assuming spherical particles). These populations are all consistent with the number and mass distribution above, but they differ in their mixing state. Figures 7c–7e also show corresponding pictorial representations of each population. At this point we are only concerned with the chemical composition, so the fact that the particles can have different shapes and structures is not represented, and the particles are shown as generic pie charts with the size and colors representing particle size and composition, respectively.

Figure 7c depicts the classic "external mixture," where each particle only contains one of the two species. In the composition space graph, the particles are arranged along the two axes, and one of the two components of their composition vector is zero. In contrast, Figure 7d shows the classic "fully internal mixture," where each particle contains the same mixture of species 1 and 2. These particles are therefore arranged along a line through the origin in the composition space graph, with slope of 3/2, since the mass ratio of the two species is 3:2 in each particle. Figure 7e shows a state in between, neither fully internally nor externally mixed. Such a population is more akin ambient aerosols than the extreme cases mentioned above, and mixing state metrics as presented in section 5 below will help quantifying this more precisely. In reality the composition space of an aerosol is high dimensional, including tens or even hundreds of different dimensions (one for each chemical species). We will see in section 4.3 that common aerosol modeling approaches work with low-dimensional projections of this high-dimensional space.

Aerosol particles experience continuous transformations during their lifetime in the atmosphere as a result of coagulation events, the condensation of secondary aerosol material, and multiphase processes—processes that are often summarized with the term "aerosol aging" (Rudich et al., 2007). In other words, particles move in composition space due to aerosol processes acting on them. For example, if species 2 in Figure 7 was semivolatile, we would observe the particles moving parallel to the $\mu_2$ axis as species 2 condenses on the

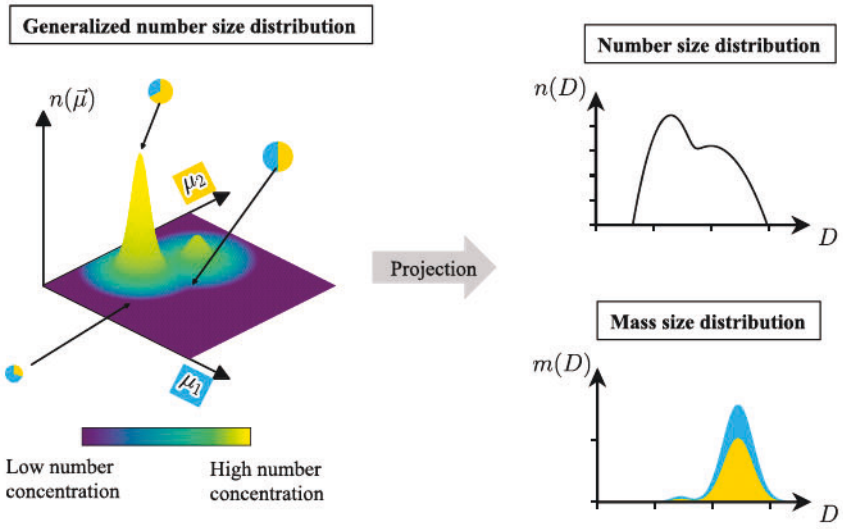


**Figure 8.** Two-dimensional number distribution ($A = 2$) in equation (1), corresponding to the "real-world" mixture in Figure 7. The arrow indicates that the one-dimensional size distributions for number and mass can be obtained by projecting the two-dimensional distribution. The details of how the particles are placed in composition space are lost by this procedure.

particles or evaporates from the particles. Hence, condensation and evaporation can be seen as an advection process in composition space. In contrast, coagulation is a stochastic, discontinuous jump process that produces a particle that will be placed according to the sum of the vector components of its parent particles. In summary, aerosol mixing state is a dynamic quantity that changes continuously as the particles' compositions change and also as particles are added to the population by new particle formation, emissions, or transport or removed from the population by dry or wet deposition. The impact of these changes on mixing state can be quantified more precisely by the use of mixing state metrics as explained in section 5.

So far we have discussed composition space in the context of chemical composition—each entry in a particle's composition vector is the amount of a chemical species. We can extend this concept by adding more components to the composition vector to characterize shape and structure. Candidate quantities are the particle's fractal dimension, the particle viscosity, surface tension, or information about the quantity and location of inclusions within the particle. Note that in industrial applications of aerosol modeling this is also called the state space (Sander et al., 2009).

### 4.2. Continuous Number Distribution and Governing Equation

It is common to use a continuous number distribution function to represent the aerosol state and then use this function to formulate the governing equation that predicts its evolution. In aerosol science, we are used to formulating this number distribution as a function of particle size. However, it is important to realize that in doing so, we project the high-dimensional composition space introduced in section 4.1 onto one dimension (size), thereby losing critical information, such as about mixing state.

We therefore introduce here a generalized number distribution as follows. The cumulative aerosol number distribution at constituent masses $\vec{\mu} \in \mathbb{R}^A$ is $N(\vec{\mu})$ ($\mathrm{m}^{-3}$), which is defined to be the number concentration of aerosol particles that contain less than $\mu_a$ mass of species $a$, for all $a = 1, \ldots, A$. Considering that the number distribution also depends on three dimensions of space and one dimension of time, the full aerosol state is $(4 + A)$ dimensional. The aerosol number distribution at time $t$, location $\vec{x}$, and constituent masses $\vec{\mu} \in \mathbb{R}^A$ is $n(\vec{\mu}, t, \vec{x})$ ($\mathrm{m}^{-3}\, kg^{-A}$), which is defined by

$$n(\vec{\mu}, t, \vec{x}) = \frac{\partial^A N(\vec{\mu}, t, \vec{x})}{\partial \mu_1 \partial \mu_2 \ldots \partial \mu_A}. \quad (1)$$

Figure 8 shows the distribution that corresponds to the "real-world mixture" in Figure 7. The particles in this distribution contain two species ($A = 2$). The one-dimensional number and mass distributions shown in the right column of Figure 8 are projections of this two-dimensional distribution, by relating the diameter $D$

to the constituent masses $\mu_1$ and $\mu_2$ and the corresponding densities $\rho_1$ and $\rho_2$, assuming spherical particles, by $(\pi/6)D^3 = \mu_1/\rho_1 + \mu_2/\rho_2$.

The mean evolution of the stochastic particle coagulation process in the limit of a large number of particles, neglecting fluctuations and correlations between the number of particles of different sizes (Gillespie, 1972), is the classical Smoluchowski coagulation equation (von Smoluchowski, 1916a, 1916b), which for a multidimensional aerosol distribution with gas coupling is

$$\begin{aligned}\frac{\partial n(\vec{\mu},t,\vec{x})}{\partial t} &- \underbrace{\nabla\cdot\left(K_h(t,\vec{x})\nabla n(\vec{\mu},t,\vec{x})\right)}_{\text{turbulent transport}} + \underbrace{\nabla\cdot\left(\vec{v}(\vec{\mu},t,\vec{x})n(\vec{\mu},t,\vec{x})\right)}_{\text{advection transport}} \\ &= \underbrace{\frac{1}{2}\int_0^{\mu_1}\int_0^{\mu_2}\cdots\int_0^{\mu_d} K(\vec{\mu}',\vec{\mu}-\vec{\mu}')n(\vec{\mu}',t,\vec{x})n(\vec{\mu}-\vec{\mu}',t,\vec{x})\mathrm{d}\mu_1'\mathrm{d}\mu_2'\ldots\mathrm{d}\mu_d'}_{\text{coagulation gain}} \\ &- \underbrace{\int_0^{\infty}\int_0^{\infty}\cdots\int_0^{\infty} K(\vec{\mu},\vec{\mu}')n(\vec{\mu},t,\vec{x})n(\vec{\mu}',t,\vec{x})\mathrm{d}\mu_1'\mathrm{d}\mu_2'\ldots\mathrm{d}\mu_d'}_{\text{coagulation loss}} \\ &+ \underbrace{\dot{n}_{\text{emit}}(\vec{\mu},t,\vec{x})}_{\text{emission}} - \underbrace{\sum_{a=1}^{A}\frac{\partial}{\partial\mu_i}(I_a(\vec{\mu},\vec{g},t)n(\vec{\mu},t,\vec{x}))}_{\text{gas-particle transfer}} \\ &+ \underbrace{J_{\text{nuc}}(\vec{g})\delta(\vec{\mu}-\vec{\mu}_{\text{nuc}})}_{\text{nucleation}} + \underbrace{\frac{1}{\rho_{\text{dry}}(t,\vec{x})}\frac{\mathrm{d}\rho_{\text{dry}}(t,\vec{x})}{\mathrm{d}t}n(\vec{\mu},t,\vec{x})}_{\text{air density change}}.\end{aligned} \tag{2}$$

In equation (2), $K_h(t,\vec{x})$ (m$^2$/s) is the diffusion coefficient of heat, $\vec{v}(\vec{\mu},t,\vec{x})$ (m/s) is the advection velocity including size-dependent settling, $K(\vec{\mu}_1,\vec{\mu}_2)$ (m$^3$/s) is the coagulation rate between particles with constituent masses $\vec{\mu}_1$ and $\vec{\mu}_2$, $\dot{n}_{\text{emit}}(\vec{\mu},t,\vec{x})$ (m$^{-3}\cdot$kg$^{-A}\cdot$s$^{-1}$) is the number distribution rate of aerosol emissions, $I_a(\vec{\mu},\vec{g},t)$ (mol/s) is the condensation or evaporation flux of aerosol species $a$, $J_{\text{nuc}}(\vec{g})$ (m$^{-3}\cdot$s$^{-1}$) is the formation rate of particles by nucleation, $\delta$ is the Kronecker delta function, $\vec{\mu}_{\text{nuc}}$ is the particle composition vector of each nucleated particle, and $\rho_{\text{dry}}(t,\vec{x})$ (kg/m$^3$) is the density of dry air. Many of the rates, coefficients, and functions also depend on the environmental conditions, but we have not written this dependence explicitly.

Equation (2) must be augmented with appropriate boundary conditions in both physical and composition space, which are chosen on physical grounds to ensure that the constituent masses of particles cannot become negative and mass is conserved. As such, dry deposition is incorporated as a boundary condition.

Water is treated just like any other chemical species in equation (2). That is, it is present both in the gas phase and in the condensed (liquid) phase on aerosol particles, and it transfers between these phases due to condensation and evaporation. In this setting, cloud and rain droplets are not a distinct type of particle but are simply large particles whose composition vectors $\vec{\mu}$ are almost entirely water. Wet deposition, in which aerosol particles are scavenged by cloud or rain drops, is thus modeled by the coagulation terms between particles.

Having cast the problem in equation (2), the question arises how to discretize this equation for the numerical solution. Common methods for population balance equations are using modal approaches (assuming several overlapping log-normal functions), method-of-moment approaches, or finite volume ("sectional") methods. Since these methods scale exponentially with the number of dimensions in composition space, they become infeasible as the number of species $A$ exceeds 3 or 4. Therefore, when using modes or sections, this equation is usually projected down to a low-dimensional version, which we will formulate in section 4.3. For reasonably large values of $A$, a stochastic particle-resolved approach is suitable; see also section 4.3.

### 4.3. Model Approaches

Aerosol models can be categorized by the way they discretize the aerosol number distribution function, $n(\vec{\mu},t,\vec{x})$. We distinguish bulk models, modal models, moment models, sectional models, and particle-resolved models, as shown in Table 4 and Figure 9. In this section we present how these main categories of modeling approaches handle the representation of aerosol mixing state. For distribution-based

**Table 4**
*Overview of Model Representations*

| Representation | Number of variables | Quality of size resolution | Quality of mixing state resolution |
|---|---|---|---|
| Bulk 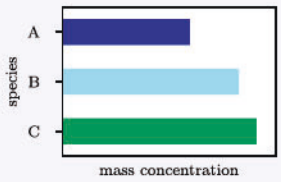  | 1 per species | None | None |
| Modal (3 modes) 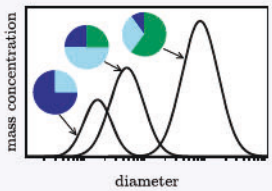  | 3 × (# of species + 1) | Medium | Poor |
| 1-D sectional 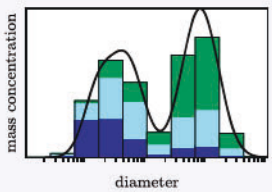  | # of sections × # of species | Good | Poor |
| Modal (> 3 modes) 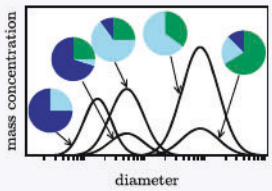  | # of modes × (# of species + 1) | Good | Medium |
| Multi-distribution sectional 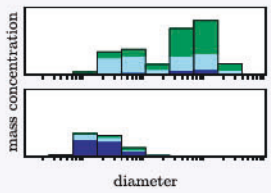  | # of distributions × # of sections × # of species | Good | Medium |
| Higher dimensional sectional 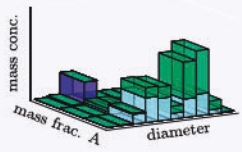  | # of sections × # of species | Good | Good |
| Particle-resolved 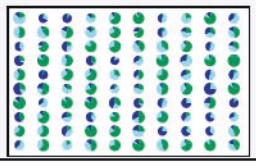 | # of particles × # of species | Excellent | Excellent |

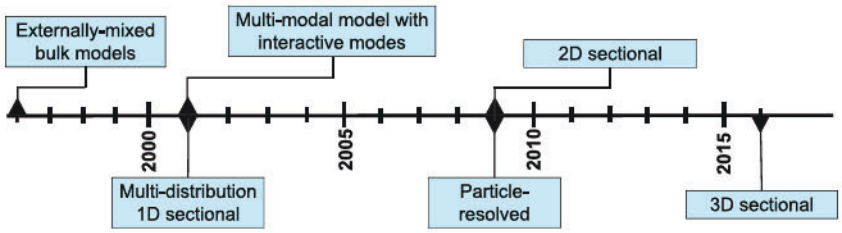


**Figure 9.** Time line of the use of different modeling techniques to represent mixing state.

models, such as modal and sectional models, rules need to be defined to handle the interactions of the various subpopulations, which can introduce difficult-to-quantify uncertainties. Univariate sectional approaches can be expanded to approaches with multivariate bin structures using two or three dimensions; however, these approaches become quickly computationally infeasible as their cost scales exponentially with the number of dimensions.

Particle-resolved models are suitable for explicitly resolving high-dimensional composition spaces that are common for atmospheric aerosols, as introduced in section 4.1. They are computationally expensive, but not infeasible, and provide a tool for benchmarking more simplified, but computationally more efficient, aerosol models with respect to chemical mixing state. Note that at this point, even particle-resolved models need to make assumptions regarding the particle morphology, as the information about shape, fractal dimension, and the internal structure of the particles is not tracked. Modeling capabilities exist that explicitly treat mass transport and chemical reactions *within* particles, thereby resolving concentration gradients in the particle bulk (Couvidat & Sartelet, 2015; Shiraiwa et al., 2010a, 2012), but they have not yet been coupled with a particle-resolved modeling framework that at the same time would enable the detailed representation of mixing state.

#### 4.3.1. Bulk Models

Bulk models can be considered as the "first generation" of aerosol models used in global climate models (Adams & Seinfeld, 2002) or for applications on regional scales where computational resources are limited (e.g., the CAMx "coarse-fine" representation, which assumes a single diameter for the coarse and fine mode, respectively, Morris et al., 2005). These models predict the life cycle of individual aerosol chemical species by tracking the species mass concentrations, inherently treating the aerosol as external mixtures of sulfate, BC, organic carbon, sea salt, and dust (Koch, 2001; Schult et al., 1997; Solmon et al., 2006; Tegen & Miller, 1998). The aerosol size distributions are prescribed based on climatological data, rather than dynamically predicted based on microphysical processes. This modeling approach has shaped how the scientific community has been describing aerosol climate impacts for a long time, namely, as if the chemical species exist as external mixtures, independently of each other (Bauer et al., 2013).

Given this simple representation of the atmospheric aerosol, aspects of mixing state have been taken into account in the context of carbonaceous aerosol. To better simulate the lifetime of carbonaceous aerosol, the conversion of fresh (hydrophobic) to aged (hydrophilic) carbonaceous aerosol is often treated as an exponential decay process, with a constant half-life (Cooke & Wilson, 1996) ranging from 24 hr (Lauer et al., 2005) to approximately 40 hr (Lohmann et al., 1999; Koch, 2001).

While this approach is computationally most efficient, the constant aging half-life for BC introduces significant uncertainties. Koch et al. (2009) performed sensitivity studies that yielded BC lifetimes ranging from 7.6 to 13 days, depending on the choice of the aging time scale. On the other hand, we do know, both from field observations and from detailed modeling studies, that the aging time scale depends on the environmental conditions. It can be on the order of only a few hours in polluted regions where low vapor pressure material is abundant to condense on aerosols, or it can be several days in remote region (Fierce et al., 2015, 2017; Riemer et al., 2004; Wang et al., 2010).

#### 4.3.2. Distribution-Based Models

Univariate distribution-based aerosol models take a mechanistic approach to predicting the aerosol size distribution. They solve a one-dimensional version of equation (2); that is, instead of using $n(\vec{\mu}, t, \vec{x})$, the

governing equation is formulated for $n(v, t, \vec{x})$, where the independent variable $v$ is the particle volume. The two variables $n(\vec{\mu})$ and $n(v)$ are related as follows:

$$n(v) = \frac{\partial}{\partial v} \int \cdots \int_{\{\vec{\mu} \mid V(\vec{\mu}) \le v\}} n(\vec{\mu}) \mathrm{d}\vec{\mu}, \tag{3}$$

where $V(\vec{\mu}) = \sum_i \mu_i / \rho_i$ and $\rho_i$ are the aerosol material densities corresponding to $\mu_i$. The multidimensional evolution equation (2) then reduces to a one-dimensional evolution equation:

$$\begin{aligned} \frac{\partial n(v,t,\vec{x})}{\partial t} &- \underbrace{\nabla \cdot \left(K_h(t,\vec{x}) \nabla n(v,t,\vec{x})\right)}_{\text{turbulent transport}} + \underbrace{\nabla \cdot \left(\vec{v}(v,t,\vec{x}) n(v,t,\vec{x})\right)}_{\text{advection transport}} \\ &= \underbrace{\frac{1}{2} \int_0^v K(v', v-v') n(v',t,\vec{x}) n(v-v',t,\vec{x}) \mathrm{d}v'}_{\text{coagulation gain}} \\ &- \underbrace{\int_0^\infty K(v,v') n(v,t,\vec{x}) n(v',t,\vec{x}) \mathrm{d}v'}_{\text{coagulation loss}} \\ &+ \underbrace{\dot{n}_{\text{emit}}(v,t,\vec{x})}_{\text{emission}} - \underbrace{\frac{\partial}{\partial v}\left(I(v,\vec{g},t) n(v,t,\vec{x})\right)}_{\text{gas-particle transfer}} \\ &+ \underbrace{J_{\text{nuc}}(\vec{g}) \delta(v - v_{\text{nuc}})}_{\text{nucleation}} + \underbrace{\frac{1}{\rho_{\text{dry}}(t,\vec{x})} \frac{\mathrm{d}\rho_{\text{dry}}(t,\vec{x})}{\mathrm{d}t} n(v,t,\vec{x})}_{\text{air density change}}. \end{aligned} \tag{4}$$

Equation (4) can be discretized in different ways, which is the basis for modal, sectional, and moment-based models, discussed next.

#### 4.3.3. Modal Models

The underlying assumption of modal models is that the aerosol can be represented by several overlapping subpopulations (modes), and each subpopulation can be described by a log-normal function of the diameter $D_p$ (Whitby & McMurry, 1997). The overall number density distribution is then

$$n(\log D_p) = \sum_{l=1}^{N_{\text{mode}}} \frac{N_{t,l}}{\sqrt{2\pi} \log \sigma_{g,l}} \exp\left(-\frac{(\log D_p - \log D_{pg,l}^2}{2 \log^2 \sigma_{g,l}}\right), \tag{5}$$

where $N_{\text{mode}}$ is the number of modes, $N_{t,l}$ is the total number concentration of mode $l$, $\sigma_{g,l}$ is the geometric standard deviation of mode $l$, and $D_{pg,l}$ is the geometric mean diameter (equal to the median diameter). The distribution function $n(\log D_p)$ is related to $n(v)$ in equation (4) by $n(\log D_p) = (\pi/2)(\ln 10) D_p^3 n(v)$.

Aerosol mixing state can be captured by different overlapping modes having different average compositions. However, composition diversity of the particles within a mode is not tracked. This means that the true population is projected as shown in Figure 10b. Many global and regional models have adopted this modeling framework (Bauer et al., 2008; Binkowski & Roselle, 2003; Grell et al., 2005; Liu et al., 2012; Stier et al., 2005; Vogel et al., 2009).

The choice of number of modes is guided by the different aerosol sources and properties to be considered, with four to seven modes being a common choice. Choices also have to be made regarding which chemical species are present in the various modes, and different models differ in their assumptions. For example, one guiding principle has been to keep freshly emitted carbonaceous aerosol separately from carbonaceous aerosol mixed with secondary species. However, the details vary between different models. For example, in MAM4, BC is emitted with primary organic aerosol (POA) into an accumulation mode, while in MADE3, BC is emitted into Aitken and Accumulation mode, together with dust. A brief overview of the mode configuration of a selection of current modal aerosol models is given in Table 5.

The log-normal distribution is determined by the three parameters, $N_{t,l}$, $\sigma_{g,l}$, and $D_{pg,l}$, hence predicting the distribution evolution requires calculating the change of three size distribution parameters per mode with

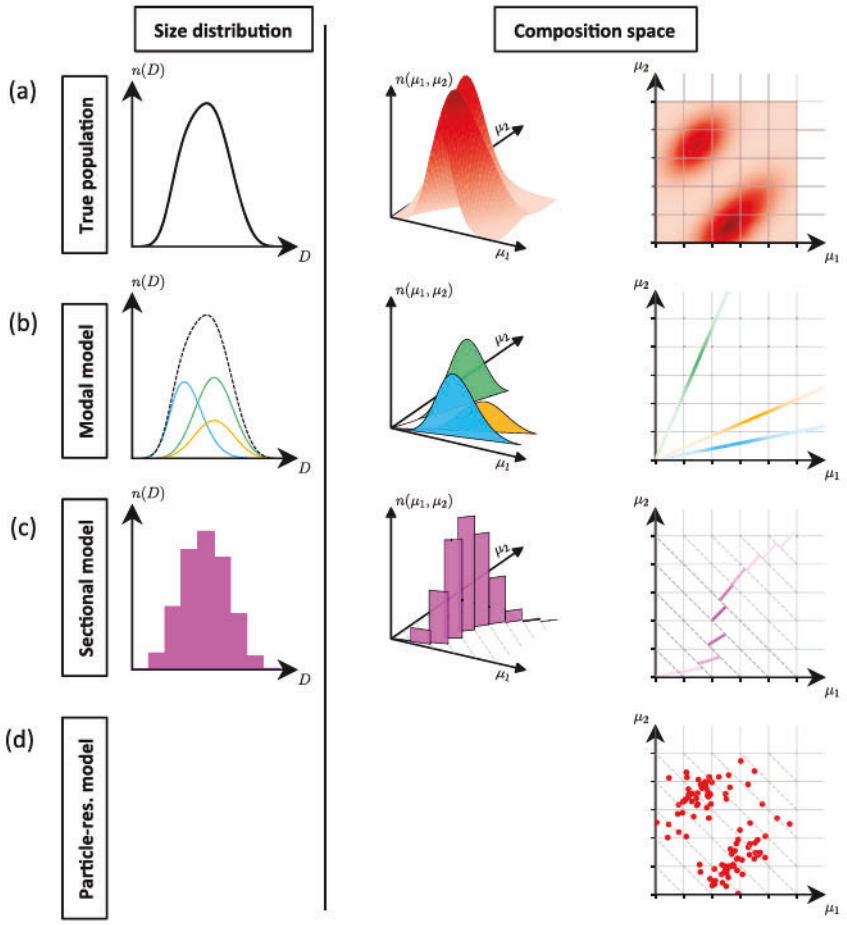


**Figure 10.** Representation of a particle population consisting of two species by different modeling approaches: (a) true population, (b) modal model, (c) sectional model, and (d) particle-resolved model. Left column: number size distribution; middle and right column: representation in composition space.

time. In practice, the geometric standard deviation of each mode is assumed to be constant, and $N_{t,l}$ and $\sigma_{g,l}$ are calculated by formulating prognostic equations for two moments of the distribution, typically the zeroth moment (equal to $N_{t,l}$), and the third moment of the constituent species in each mode (proportional to the mass concentration). From these, the geometric mean diameter can be calculated. Prognostic equations for the $k$th moment are obtained by multiplying equation (4) with $D^k$ and then integrating over $D$.

The aerosol processes of gas/aerosol partitioning and coagulation make it necessary to define rules how the modes interact (Wilson et al., 2001). For example, MAM4 reserves one of its four modes for "fresh" carbonaceous aerosol; that is, carbonaceous aerosol in this mode is not subject to wet deposition (Liu et al., 2012). Condensation of sulfate and SOA on that mode requires moving mass over to the mixed mode accumulation mode when a critical mass fraction of secondary aerosol is exceeded. This is often framed as a criterion based on the equivalent number of "monolayers" (Liu et al., 2012; Vignati et al., 2004), although it comes down to a mass fraction (Riemer et al., 2003). Transfer terms due to coagulation of particles in different modes can be calculated analytically based on Binkowski and Shankar (1995), and rules need to be defined regarding the destination mode after coagulation.

In summary, modal models represent many important aspects of aerosol microphysics with the size distributions and mode compositions changing dynamically over the course of a simulation. The model framework allows for a simplified representation of mixing state, where the high-dimensional composition space is projected down onto a sum of one-dimensional modes. Rules need to be defined for the transfer between modes, and for the set up of destination modes to represent coagulation between modes, which introduce uncertainty.

**Table 5**
*Modal Model Configurations for MAM3 and MAM7 (Liu et al., 2012), MAM4 (Liu et al., 2016), COSMO-Art (Vogel et al., 2009), MADE3 (Kaiser et al., 2014), ECHAM-HAM (Stier et al., 2005), and MATRIX (Bauer et al., 2008)*

| Name | Mode types | Mode composition |
|---|---|---|
| MAM3 | 1 Aitken,<br>1 accumulation,<br>1 coarse | Aitken: Su, SOA, SS;<br>Accumulation: Su, SOA, POA, BC, Du, SS;<br>Coarse: Su, Du, SS. |
| CMAQv5.2 | 1 Aitken,<br>1 accumulation,<br>1 coarse | Aitken: Su, Amm, Nit, POA, BC<br>Accumulation: Su, Amm, Nit, SOA, POA, BC, Du;<br>Coarse: Du, SS, Su, Amm, Nit. |
| MAM4 | 1 Aitken,<br>2 accumulation,<br>1 coarse | As in MAM3, but the second accumulation mode is for freshly emitted BC and POA. |
| MAM7 | 1 Aitken,<br>4 accumulation,<br>2 coarse | As in MAM4, but more detail on dust and sea salt. Additional accumulation modes for "fine dust" {Du, Su, Amm}, "fine sea salt" {SS, Su, Amm}. Coarse modes represent "coarse dust" {Du, Su, Amm}, and "coarse sea salt" {SS, Su, Amm}. |
| ECHAM-HAM | 1 nucleation<br>2 Aitken,<br>2 accumulation,<br>2 coarse | Nucleation: Su;<br>The two Aitken modes separate out freshly emitted BC and POA from {BC, POA, Su};<br>The two accumulation modes separate out Du from {Su, BC, POA, SS, Du};<br>The two coarse modes separate out Du from {Su, BC, POA, SS, Du}. |
| MADE3 | 3 Aitken,<br>3 accumulation,<br>3 coarse | In each size range one mode of fully soluble particles {Su, Amm, Nit, SS, POA}, one mode of insoluble particles {BC, Du}, and one mixed mode (soluble and insoluble components). |
| COSMO-Art | 5 submicron,<br>1 coarse<br>3 dust modes<br>3 sea salt modes | The submicron modes separate out 2 BC-free, 2 BC containing and 1 pure BC mode. The coarse mode contains PM10 emissions. There are also three modes for SS and three modes for Du. |
| MATRIX | 16 modes | The modes separate out dust containing, SS containing, and BC containing populations in the size ranges of Aitken, accumulation, and coarse modes. |

*Note.* The abbreviations of species names are as follows: Amm = ammonium; BC = black carbon; Du = dust; Nit = nitrate; POA = primary organic aerosol; SOA = secondary organic aerosol; SS = sea salt; Su = sulfate.

#### 4.3.4. Moment Models

The method-of-moments approach is closely related to modal models in that it tracks the time evolution of the lower-order moments of the particle size distribution. In contrast to modal models, however, the method of moments does not require the knowledge of the distribution function (Hulburt & Katz, 1964). McGraw (1997) developed the quadrature method of moment (QMOM) to solve the closure problem, which otherwise arises in the traditional formulation of the method-of-moment approach when particle condensational growth is represented.

The original formulation of QMOM was cast for a univariate aerosol distribution and has been applied in that way to multicomponent, internally mixed populations (McGraw & Wright, 2003). The method has been generalized to bivariate populations undergoing coagulation (Wright et al., 2001) and benchmarked with particle-resolved model results (see section 4.3.6; McGraw et al., 2008). Fierce et al. (2017) used the QMOM framework to construct an efficient representation ("sparse particle") of a complex particle population with respect to CCN properties, using moments that are bivariate with respect to dry diameter and hygroscopicity parameter. Benchmark simulations using particle-resolved simulations show that in order to capture CCN properties of a particle-resolved data set with 10,000 computational particles of complex mixing state, a sparse set of just eight weighted particles is needed.

#### 4.3.5. Sectional Models

While modal models use several overlapping log-normal function within a size range, sectional models discretize the aerosol size range into a number of sections and store the total number concentration $N_\ell$ for each section $\ell$, given by

$$N_\ell = \int_{v_{\ell-1}}^{v_\ell} n(v)\,\mathrm{d}v, \qquad \ell = 1 \ldots L, \tag{6}$$

where $L$ is the total number of size sections and $v_{\ell-1}$ and $v_\ell$ are the lower and upper edges of the size section.

Equation (4) can be solved using this discretization; however, it is more common to solve the corresponding equation for the volume or mass size distribution:

$$Q_\ell = \int_{v_{\ell-1}}^{v_\ell} v n(v)\,\mathrm{d}v, \qquad \ell = 1 \ldots L. \tag{7}$$

Another variant of this is to track two moments per size section, as done in Adams and Seinfeld (2002). Working with one univariate distribution allows tracking of size-resolved composition (Spracklen et al., 2005). Figure 10c illustrates the projection of the true composition space that a 1-D sectional model imposes. While size-resolved composition information is provided by this modeling approach, each size bin represents the average in terms of composition. Due to this averaging, it can be the case that size bins are positioned in composition space where only few particles reside for the true population.

Resolving mixing state (i.e., composition differences within a certain size range) can be accomplished by introducing several, potentially interacting univariate distributions (Jacobson, 2002; Kleeman & Cass, 2001). Jacobson (2002) uses 18 different distributions that differ in the chemical species combination (e.g., three BC-containing distributions with different amounts of non-BC components). Eleven of the 18 distributions arise because of coagulation interactions. This approach is computationally more expensive than the modal modeling approach, because more variables are tracked for each distribution. The gain is that, within one distribution, composition can vary with size. A similar approach is chosen by Kleeman and Cass (2001); however, the emphasis here is on tracking the emission sources of the particle distributions.

Another possibility is to use a multivariate bin structure (Lu & Bowman, 2010; Matsui et al., 2013, 2014; Oshima et al., 2009; Zhu et al., 2015). Common feature among several of these models is that they use a two-dimensional sectional framework to represent BC-containing particles, with one dimension being dry diameter and the other dimension being BC mass fraction. The conceptual difference between multivariate models and the univariate/multidistribution models is shown in Figure 11. Building on previous two-dimensional sectional frameworks, the MOSAIC-MIX model (Ching et al., 2016) adds an additional dimension to represent hygroscopicity and shows that this optimizes the calculations of CCN concentrations and aerosol optical properties. The Size-Composition Resolved Aerosol Model (SCRAM; Zhu et al., 2015; 2016a), also a two-dimensional sectional model, uses an alternative discretization based on both size and composition where composition is tracked by mass fractions of different chemical groups such as inorganic hydrophilic, organic hydrophilic, organic hydrophobic, BC, and dust.

#### 4.3.6. Particle-Resolved Models

In contrast to modal and sectional models, particle-resolved models are not distribution based. Instead, the particle population is discretized by a sample of individual computational particles. With this method of discretization, it is possible to solve equation (2) directly.

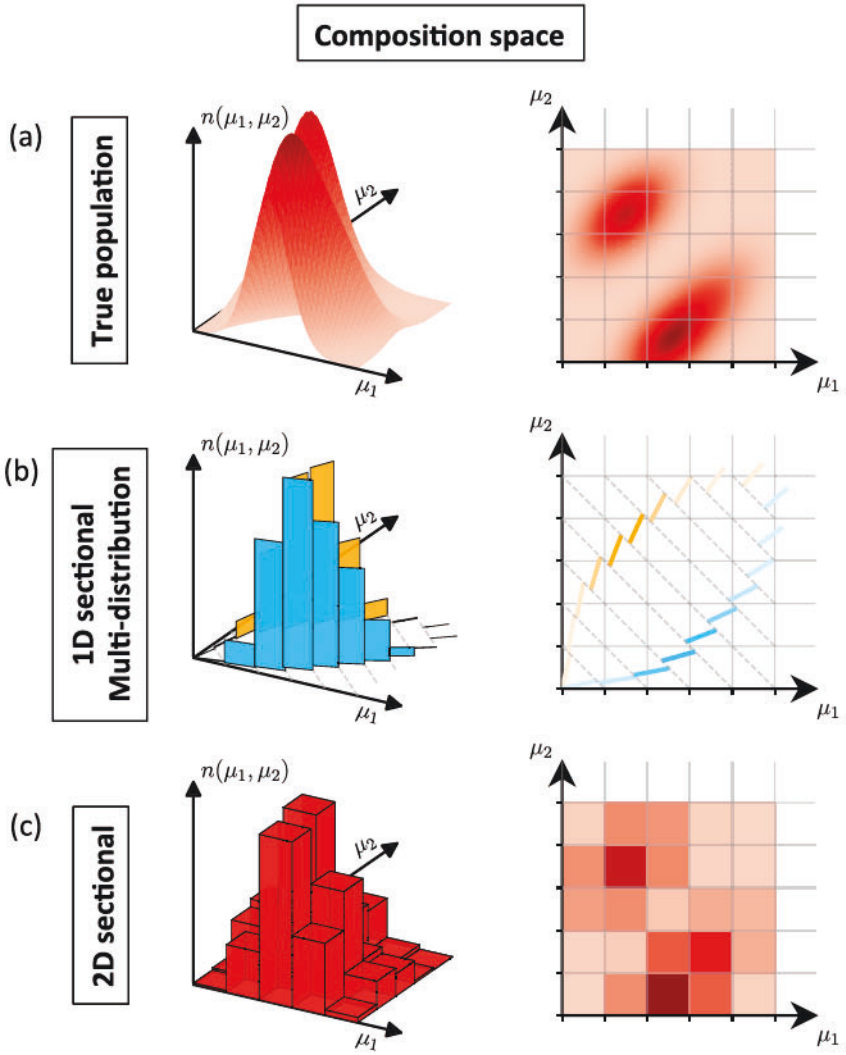


**Figure 11.** Representation of the particle population shown in Figure 10 by two different variants of the sectional modeling approach: (a) true population, (b) 1-D sectional, multidistribution, and (c) 2-D sectional.

One can think of each particle as an $A$-dimensional vector $\vec{\mu}^i \in \mathbb{R}^A$ with components $(\mu_1^i, \mu_2^i, \ldots, \mu_A^i)$, with $\mu_a^i$ being the mass of species $a$ in particle $i$, for $a = 1, \ldots, A$ and $i = 1, \ldots, N_p$. The simulation of the aerosol state proceeds by two mechanisms. First, the composition of each particle can change, changing the components of the vector $\vec{\mu}^i$ for particle $i$ as species condense from the gas phase and evaporate to it, for example. Second, the population $\Pi$ can have particles added and removed, by emissions, dilution, or coagulation events between particles. Emission, dilution, nucleation, and Brownian coagulation are simulated with a stochastic Monte Carlo approach. The relative positions of particles within the computational volume are not tracked.

Applying such a Monte Carlo approach for simulating the evolution of particle distributions dates back to Gillespie (1975), who developed the exact stochastic simulation algorithm (SSA; see also Gillespie, 1976, 1977, 1992) to treat the stochastic collision-coalescence process in clouds. Variants of Gillespie's algorithm are widely used in different fields, including simulations of gene regulatory networks (Samad et al., 2005), chemical kinetics (Gillespie, 2007), and sintering in flames (Wells et al., 2006). For atmospheric aerosol, the approach was first developed and applied with the PartMC-MOSAIC model (Riemer et al., 2009; Zaveri et al., 2008). It is computationally more expensive than modal or sectional approaches; however, the particle-resolved approach directly resolves the composition space, and hence the chemical mixing state, without any approximating assumptions. With the integration of PartMC-MOSAIC into the

**Table 6**
*Aerosol Mass and Mass Fraction Definitions and Notation*

| Quantity | Meaning |
|---|---|
| $\mu_i^a$ | mass of species $a$ in particle $i$ |
| $\mu_i = \sum_{a=1}^{A} \mu_i^a$ | total mass of particle $i$ |
| $\mu^a = \sum_{i=1}^{N} \mu_i^a$ | total mass of species $a$ in population |
| $\mu = \sum_{i=1}^{N} \mu_i$ | total mass of population |
| $p_i^a = \frac{\mu_i^a}{\mu_i}$ | mass fraction of species $a$ in particle $i$ |
| $p_i = \frac{\mu_i}{\mu}$ | mass fraction of particle $i$ in population |
| $p^a = \frac{\mu^a}{\mu}$ | mass fraction of species $a$ in population |

*Note.* The number of particles in the population is $N$, and the number of species is $A$. This table is taken from Riemer and West (2013).

spatially resolved Weather and Research Forecasting (WRF) model (Curtis et al., 2017), it is now possible to conduct particle-resolved simulations for three-dimensional domains.

To evaluate the ability of other model types, such as modal or section, to represent mixing state, Zaveri et al. (2010) developed the framework of *composition-averaging* for particle-resolved models. This entails calculating a quantity of interest (e.g., CCN concentrations) using the full output of the particle-resolved simulation. This result is then compared to a calculation where all particles are assigned the same composition (equal to the average), while keeping the particle sizes unchanged, mimicking the assumption of a fully internal mixture. This average can also be done per size bin to obtain a size-dependent composition assumption. Since this is a postprocessing step, this procedure isolates the error introduced by the model representation of aerosol mixing state.

## 5. Metrics for Mixing State in Measurements and Models

The discussion of mixing state and its impacts is greatly facilitated by appropriate metrics that enable us to quantify the degree of internal/external mixing for any given aerosol. Several approaches exist in the literature, starting with Winkler (1973) who introduced as a metric the standard deviation of the per-particle composition from the bulk composition, $\sigma$. A value of $\sigma = 0$ indicates a perfect internal mixture, since the per-particle composition is the same as the bulk. While Winkler (1973) proposed this as a scalar quantity, the generalization for many aerosol species would be to use the covariance matrix, with an overall mixing state described with a summary statistic such as the trace of the covariance. While simple to define and giving an intuitive value of 0 for an internal mixture, it is less clear how to understand values for fully external mixtures.

In section 5.1 we will focus on the metric by Riemer and West (2013) who proposed a framework for chemical mixing state based on "particle diversity" to calculate an index $\chi$ that ranges from 0% (fully internal mixture)

**Table 7**
*Definitions of Aerosol Mixing Entropies, Particle Diversities, and Mixing State Index*

| Quantity | Name | Units | Range | Meaning |
|---|---|---|---|---|
| $H_i = \sum_{a=1}^{A} -p_i^a \ln p_i^a$ | mixing entropy of particle $i$ | — | 0 to $\ln A$ | Shannon entropy of species distribution within particle $i$ |
| $H_\alpha = \sum_{i=1}^{N} p_i H_i$ | average particle mixing entropy | — | 0 to $\ln A$ | average Shannon entropy per particle |
| $H_\gamma = \sum_{a=1}^{A} -p^a \ln p^a$ | population bulk mixing entropy | — | 0 to $\ln A$ | Shannon entropy of species distribution within population |
| $D_i = e^{H_i} = \prod_{a=1}^{A} (p_i^a)^{-p_i^a}$ | particle diversity of particle $i$ | effective species | 1 to $A$ | effective number of species in particle $i$ |
| $D_\alpha = e^{H_\alpha} = \prod_{i=1}^{N} (D_i)^{p_i}$ | average particle (alpha) species diversity | effective species | 1 to $A$ | average effective number of species in each particle |
| $D_\gamma = e^{H_\gamma} = \prod_{a=1}^{A} (p^a)^{-p^a}$ | bulk population (gamma) species diversity | effective species | 1 to $A$ | effective number of species in the bulk |
| $\chi = \frac{D_\alpha - 1}{D_\gamma - 1}$ | mixing state index | — | 0% to 100% | degree to which population is externally mixed ($\chi = 0\%$) versus internally mixed ($\chi = 100\%$) |

*Note.* In these definitions we take $0 \ln 0 = 0$ and $0^0 = 1$. This table is taken from Riemer and West (2013).

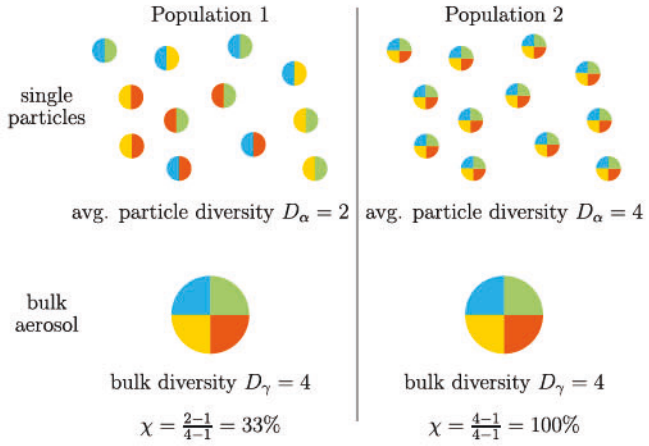


**Figure 12.** The concept of particle diversities $D_\alpha$ and $D_\gamma$ for two different example populations. Both populations have the same bulk composition, with four species present in equal amounts; however, the mixing state is distinctly different. The particles in Population 1 have a lower average diversity than the particles in Population 2. This results in a lower mixing state index $\chi$ for Population 1 compared to Population 2.

to 100% (fully external mixture). We will discuss what is known about the $\chi$ values of real atmospheric aerosols in section 5.2. In section 5.3 we discuss other mixing state metrics, and we will finish this section with a discussion of metrics for the morphological mixing state in section 5.4.

### 5.1. The Entropy-Based Diversity Metric $\chi$ for Chemical Mixing State

Riemer and West (2013) put forward a framework to quantify aerosol chemical mixing state, which was inspired by diversity metrics used in other disciplines such as ecology (Whittaker, 1972), economics (Drucker, 2013), neuroscience (Strong et al., 1998), and genetics (Falush et al., 2007). The fundamental quantity that is used to calculate mixing state metrics are the species mass fractions in each particle, as shown in Table 6. Defining mixing state metrics then includes two distinct aspects: How complex individual particles are (in terms of being composed of different species) and how similar different particles are within a population. Both aspects are quantified by the diversity metrics defined below.

Given a population of $N$ aerosol particles, each consisting of some amounts of $A$ distinct aerosol species, this concept is based on the knowledge of mass of species $a$ in particle $i$, denoted $\mu_i^a$, for $i = 1, \ldots, N$, and $a = 1, \ldots, A$. From this quantity, all other mass-related quantities can be defined, as detailed in Riemer and West (2013) and here listed in Table 6, and the diversity metrics can be constructed as shown in Table 7.

The particle diversity $D_i$ represents the number of "effective species" in particle $i$. For a particle $i$ that consists of $A$ species, the highest possible value for $D_i$ is $A$, and this occurs when all $A$ species are present in equal mass fractions. Knowing the $D_i$ values for all particles, the population-level quantities $D_\alpha$ and $D_\gamma$ can be calculated, with $D_\alpha$ being the average effective number of species in each particle and $D_\gamma$ being the effective number of species in the bulk. Figure 12 illustrates the meaning of $D_\alpha$ and $D_\gamma$. The populations 1 and 2 have the same bulk composition, with four species present in equal amounts; hence $D_\gamma = 4$. However, populations 1 and 2 are different in that Population 1 consists of particles with two species in equal amounts ($D_\alpha = 2$), but several different particle types exist with different species combinations. In contrast, Population 2 contains only one type of particles, which has the same composition as the bulk ($D_\alpha = 4$).

Finally, the mixing state index $\chi$ is defined as

$$\chi = \frac{D_\alpha - 1}{D_\gamma - 1}. \tag{8}$$

The mixing state index $\chi$ varies from 0% (a fully externally mixed population) to 100% (a fully internally mixed population. To quantify mixing state, two of the three metrics ($D_\alpha, D_\gamma, \chi$) are needed, and the third can be derived. For the two examples in Figure 12, $\chi = 33\%$ for Population 1, and $\chi = 100\%$ for Population 2.

It is instructive to map the mixing state metrics of aerosol populations into a mixing state diagram ($D_\alpha, D_\gamma$), as shown in Figure 13 (Healy et al., 2014; Riemer & West, 2013). Particle populations with single-species particles, that is, "externally mixed" populations, have $D_\alpha = 1$ and $D_\gamma$ between 1 and $A$. They are therefore mapped onto the vertical axis ($\chi = 0\%$). This applies to populations $\Pi_2$ and $\Pi_3$ shown in this example. Populations consisting of particles with identical mass fractions map onto the diagonal $\chi = 100\%$, which applies here to populations $\Pi_5$ and $\Pi_7$. Populations $\Pi_3$, $\Pi_4$, and $\Pi_5$ have the same bulk composition and are therefore arranged along the line of constant $D_\gamma$. However, their mixing states vary from

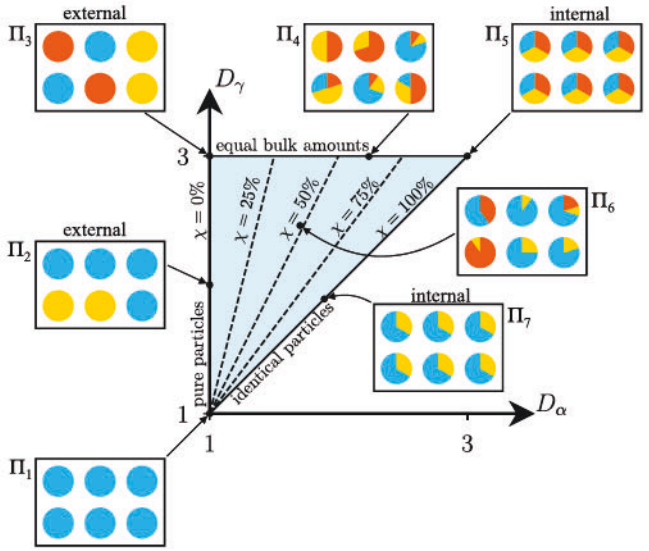


**Figure 13.** Mixing state diagram to illustrate the relationship between average particle diversity $D_\alpha$, bulk population diversity $D_\gamma$, and mixing state index $\chi$ for seven example populations ($\Pi_1$ to $\Pi_7$). Each population consists of six particles, and the colors represent different chemical species ($A = 3$). This figure is adapted from Riemer and West (2013).

10.1029/2018RG000615

**Table 8**
*Field Studies That Used Single-Particle Data to Determine the Aerosol Mixing State Parameter $\chi$*

| Author | Location | Time | Instruments | Species | Size range | Range of $\chi$ |
|---|---|---|---|---|---|---|
| Healy et al. (2014) | Paris, France | 26 January 2010 11 February 2010 | ATOFMS | SO4, NO3, NH4, OA, and BC | 150–900 nm | 37–72% |
| O'Brien et al. (2015) | Sacramento, CA (CARES T0, T1) | 27–28 June 2010 | STXM/NEXAFS | Organic, inorganic, and BC | 0.36–2.5 $\mu$m | 62–93% |
| O'Brien et al. (2015) | Sacramento, CA (CARES T0, T1) | 27–28 June 2010 | CCSEM/EDX | Na, Mg, Al, Si, P, S, Cl, and K, Ca, Mn, Fe, and Zn | 0.1–2.5 $\mu$m | 40–91% |
| Fraund et al. (2017) | Amazon, Brazil (GoAmazon2014/2015 ATTO, ZF2, T3) | Selected days/times during September 2014 and October 2014 | STXM/NEXAFS SEM/EDX | C, N, O, Na, Mg, P, S, and Cl, K, Ca, Mn, Fe, Ni, and Zn | 180–320 nm | >80% |
| Bondy et al. (2018) | Centreville, AL (SOAS) | 5 June - 11 July 2013 STXM/NEXAFS | CCSEM/EDX S, Cl, K, Ca, Ti, and Fe | C, N, O, Na, Mg, Al, Si, and P, | 56 nm to 1.8 $\mu$m | 5%–25 |
| Ye et al. (2018) | Pittsburgh, PA | Aug/Sep 2012, Dec/Jan/Feb 2011/2012 | SP-AMS | SO4, NO3, NH4, OA, and BC | 50 nm to 1 $\mu$m | 36–70% |

*Note.* CARES = Carbonaceous Aerosol and Radiative Effects Study; SOAS = Southern Oxidant and Aerosol Study; ATOFMS = aerosol time-of-flight mass spectrometry; STXM/NEXAFS = scanning transmission X-ray microscopy/near edge X-ray absorption fine structure spectroscopy; CCSEM/EDX = computer-controlled scanning electron microscopy/energy dispersive X-ray spectroscopy; SEM/EDX = scanning electron microscopy/energy dispersive X-ray spectroscopy; SP-AMS = soot particle-aerosol mass spectrometer; OA = organic aerosol; BC = black carbon.

externally mixed $\Pi_3$ to fully internally mixed $\Pi_5$. Population $\Pi_1$, consisting of a single species, is a special case in this framework. Its mixing state index (0/0) is undefined, as it could equally well be said to be perfectly internally or externally mixed.

The mixing state metric $\chi$ has found applications in both modeling and experimental work. Measuring it experimentally requires determining per-particle species masses, as described in section 3.3, while modeling it requires one of the mixing-state-resolving modeling methods, such as particle-resolved models (section 4.3.6).

### 5.2. Measurements and Models of the Diversity Metric $\chi$

To determine the diversity metric $\chi$ from measurements, per-particle mass fractions need to be obtained (section 5.1). A variety of experimental techniques have been used to estimate per-particle mass fractions for this purpose. They range from mass spectrometry with an aerosol time-of-flight mass spectrometer (ATOFMS; Healy et al., 2014) or a soot particle aerosol mass spectrometer (SP-AMS; Ye et al., 2018) to STXM/near edge X-ray absorption fine structure (NEXAFS) and SEM/EDX (Fraund et al., 2017; O'Brien et al., 2015).

All currently available field measurements of $\chi$ are summarized in Table 8. From these studies we learn how chemical mixing state depends on air mass and the time of the day, or how it varies spatially. Common to all studies is that the extreme values of 0% or 100% are never reached. For the MEGAPOLI winter campaign in Paris, France, 2010, Healy et al. (2014) found $\chi$ depending on the air mass that was transported to the measurement site. Values of $\chi$ reached up to 72% during periods when continental pollution was prevalent, while the lowest values of about 37% were reached when the air mass was coming from the ocean, and local pollution mixed with relatively clean air. They also documented a distinct diurnal cycle of $\chi$, with higher values during the night, when ammonium nitrate formation caused the aerosol to become more internally mixed. Ye et al. (2018) quantified aerosol mixing state in different neighborhoods of Pittsburgh, PA, with a mobile measurement platform. The mixing state metric varied between 36% and 70%, with the lowest values close to an interstate highway, and the highest value in rural or suburban regions. This study showed for the first time how mixing state varies on a spatial scale of a city.

Particle diversities and mixing state can be quantified for a subpopulation, as has been done for the subpopulation of BC-containing particles in O'Brien et al. (2015) or within specified size ranges (Healy et al., 2014; O'Brien et al., 2015). For the MILAGRO campaign in Paris, France, Healy et al. (2014) observed an increase of particle diversity with size, as primary carbonaceous particles were accumulating secondary aerosol species, in particular ammonium nitrate.

The mixing state metric $\chi$ has also been used to compare model results to measurements, as in Zhu et al. (2016a). They used the regional mixing-state-resolving SCRAM for the modeling domain of Paris, France, and compared to MEGAPOLI measurements at an urban ground site in Paris (Healy et al., 2014) for the simulation period of about 1 month in winter 2010. The comparison showed that the range of simulated mixing state indices was very similar between observations (37–72%) and modeling resuls (23–90%). The model also reproduced the observed fact that the average single-particle diversity never exceeded the value of 4 (compared to 3.5 in the observations), even when the bulk population diversity reached close to the maximum value of 5. This indicates that some degree of external mixture was always present.

Note that the definition of "species" for calculating the mass fractions depends on the application. It can refer to operationally defined chemical species (Healy et al., 2014; O'Brien et al., 2015; Riemer & West, 2013; Ye et al., 2018), or it can be based on elemental composition (Fraund et al., 2017; O'Brien et al., 2015). Table 8 lists the species definition used the individual field studies that reported the mixing state parameter. It can further refer to species groups, as in Dickau et al. (2016), who quantified mixing state with respect to volatile and nonvolatile components, or Ching et al. (2017) and Hughes et al. (2018), who quantified mixing state with respect to hygroscopic and nonhygroscopic species. The latter is useful when exploring the impact of mixing state on CCN properties. The values of the diversity parameters and the mixing state indices, and hence the conclusion if a population is internally or externally mixed, will depend on the exact definition of species. For example, a population may have relatively low $\chi$ values (i.e., appears externally mixed) with respect to its individual chemical species, but it can appear more internally mixed with respect to the mixture of hygroscopic and nonhygroscopic species. The relationship between $\chi$ values for the same population determined by different species definitions should be explored in more detail in future work.

### 5.3. Other Mixing State Metrics for Measurements and Models

A detailed comparison of model simulations and measurements with respect to mixing state has proven challenging, as it can be difficult to find a common metric between the model and the measurement technique that could form the basis of a quantitative comparison, beyond the studies using $\chi$ described in section 5.2.

A fairly straightforward match are measurements of BC core sizes and associated amounts of coating with the SP2 instrument and model results obtained with a 2-D sectional modeling approach (section 4.3.5) that resolves the mass fraction of BC core and the mass fraction of non-BC aerosol in each size bin (Matsui et al., 2013; Oshima et al., 2009). Oshima et al. (2009) compared low-dimensional aggregate model results using a Lagrangian parcel model version of the MADRID-BC model to aggregated aircraft data from the PEACE-C campaign sampling the outflow from Japanese anthropogenic sources (Moteki et al., 2007). The metric used for comparison was the mass fraction of thickly coated BC particles, with "thickly coated" defined as the particles with the ratio of total diameter to BC diameter larger than 2. It was shown that the model was able to capture the general trends found in the observations, which showed an increase of the mass fraction of thickly coated BC particles with increasing photochemical age of the air mass.

Matsui et al. (2013) compared model simulations from a 2-D sectional aerosol model embedded in the regional air quality model WRF-Chem for the regional of East Asia with SP2 measurements obtained during the A-FORCE campaign in 2009. They used size-dependent number fractions of BC-containing and BC-free particles and averaged coating thicknesses as metrics for comparison. Their model simulations generally reproduced the observed trends and were able to show with sensitivity simulations that the thinly coated BC particles are produced by condensation processes, while coagulation events are needed to produce thickly coated BC particles. Challenges associated with this comparison include the fact that the SP2 is only sensitive to particles having BC cores with mass-equivalent diameter of 75–850 nm and the fact that the assumed BC refractive index had an appreciable impact on determining the coating thickness (Matsui et al., 2013).

Comparing a modal model with SP2 data comes with additional challenges because of the modal structure (Aquila et al., 2011). The size range of BC cores that is detectable from SP2 data represents only a slice of the modal model's BC-containing accumulation mode. Comparing the mixing state of the entire simulated BC-containing mode would not be correct, because particles with BC cores outside the SP2 detection window are represented by the mode. Keeping these caveats in mind, Aquila et al. (2011) showed a comparison of global model simulation results (EMAC with MADE-in) with SP2 data during the CR-AVE campaign over Costa Rica (Schwarz et al., 2008). The metric of comparison was the vertical profile of number fraction of internally mixed BC particles. The model results showed higher fractions of internally mixed BC than the observations, which might mean that the aging process of BC is too rapid in the model. However, Aquila et al. (2011) pointed out that this conclusion should be interpreted with caution, because of the limited comparability between observations and model results.

Bauer et al. (2013) were the first to compare global model simulation results using the modal aerosol model MATRIX and ATOFMS field campaign data. To make this comparison possible, the 16 MATRIX modes needed to be mapped onto the ATOFMS classes, and then the number fractions in each mode/class were compared. For example, the modes that represent mineral dust in the accumulation mode and the coarse mode with an inorganic mass fraction of less than 5% were both mapped to the ATOFMS class "fresh dust." The two BC-containing modes that contain more than 5% inorganic material were both mapped onto the "aged EC" class. The authors concluded that to make a comparison possible between a large-scale model and detailed particle level measurements, observations should be averaged over a period of 1 month to characterize the aerosol that is representative for a given location. Because of the detection limit of the sizing instrument used for scaling (APS), only number concentrations above 500 nm could be compared, which in general tended to be rather aged by condensation and coagulation processes. It was also not possible to compare mass concentrations, and the authors suggested a multi-instrument analysis to accomplish this.

A different method of characterizing aerosol mixing state is that of Su et al. (2010), who developed a framework based on the distribution of the hygroscopicity parameter $\kappa$ (Petters & Kreidenweis, 2007). They use the geometric standard deviation of the $\kappa$ distribution, $\sigma_\kappa$, as a metric to quantify diversity in terms of hygroscopicity. If two or more subpopulations exist with different hygroscopicites, this indicates that the population is externally mixed with respect to hygroscopicity. This approach was used to evaluate mixing state with respect to hygroscopicity by Holmgren et al. (2014) who sampled aerosols at the high-altitude site Puy de Dôme, France, and found three different hygroscopic modes (less hygroscopic, hygroscopic, and more

hygroscopic). Schill et al. (2015) used the framework to characterize hygroscopic mixing state for sea spray aerosol and show that population-weighted distributions of $\kappa$ parameters can be retrieved from size-resolved CCN measurements.

### 5.4. Morphometrics

To go beyond chemical mixing state metrics to the full physicochemical mixing state, it is necessary to quantify the morphology of individual aerosol particles. It is practical to distinguish between metrics that characterize the overall shape of a particle and, for particles containing more than one component, metrics that characterize the spatial arrangement of particle components within the particle.

Regarding the overall shape of the particle, a fundamental quantity is the dynamic shape factor, which is defined as the ratio of the particle's drag force and the drag force of a sphere that has a diameter equal to the particle's volume equivalent diameter (Seinfeld & Pandis, 2016, Chapter 9.7.1). It is an important quantity for particle sizing (DeCarlo et al., 2004). The dynamic shape factor of irregular particles is usually larger than 1, an exception being certain streamlined shapes (Hinds, 1999). For example, the shape factor of a cube is 1.08, and that of a compact cluster consisting of three spheres is 1.15 (Hinds, 1999, Table 3.2).

Another class of shape descriptors are ratios of two particle size measurements, such as the aspect ratio, the roundness, or the convexity (Hentschel & Page, 2003). The aspect ratio is popular for characterizing dust particles (Kandler & Schütz, 2007; Kandler et al., 2011) and is also common to characterize the habits of ice particles (Um et al., 2015). These metrics are typically derived from projected two-dimensional imaging, even though particle shape is in fact a three-dimensional characteristic. Using a two-dimensional image, gives rise to the possibility of misinterpretations (Powers et al., 2007). Adachi et al. (2007) retrieved the 3-D structure of soot aggregates using electron tomography with a transmission electron microscope and demonstrated that metrics such as the fractal dimension and the projected area differ greatly from the ones determined from a 2-D analysis. Nevertheless, working with 2-D projections is deemed still useful in practice if it can be assumed that the particle orientation is random and that the particles are approximately isotropic (Hentschel & Page, 2003).

A special case of irregular particles is aggregates (DeCarlo et al., 2004), which can be described by a fractal formalism, including the fractal dimension, size of primary particles, radius of gyration, and the structural coefficient (Sorensen, 2011; Naumann, 2003). These metrics have been used to characterize ambient carbonaceous aerosol (China et al., 2013, 2015).

Given that many particles are mixtures, several metrics exist that quantify the interior arrangement of the particles' components. Spherical particles that consist of a host particle with inclusions can generally be described by the number, the size distribution, the position, and the phase of the inclusions. When considering a large collective of particles, the mean number of inclusions per particle can be used (Efendiev & Zachariah, 2002). A special case of this type of morphology is the core-shell morphology, where we track core diameter, position of the core, and coating thickness (Fuller et al., 1999).

A variety of morphologies can be expected in any given environment, so to move toward characterizing the full physicochemical mixing state as defined in section 2.2, a large ensemble of particles needs to be analyzed. Generally, particles contain different components and are not spherical, and the arrangement of the components is anisotropic (Adachi et al., 2010; Scarnato et al., 2013), so the selection of metrics varies between different studies. Kandler et al. (2011) analyzed nearly 50,000 particles in a mineral dust-dominated region in Cape Verde and reported size-resolved distributions of particle aspect ratio, contrasting dry and wet particles. A combination of metrics has been used by Moffet et al. (2016) with scanning transmission X-ray microscopy (STXM) particle data from the Carbonaceous Aerosol and Radiative Effects Study (CARES) campaign in California in 2010. For a collective of about 1,900 particles, they grouped the particle samples according to their size-resolved composition maps that map the BC inclusion, the organic dominant regions, and the inorganic dominant regions within individual particles. They further quantified the size of BC inclusions compared to the overall particle size, the BC inclusion convexity, and the location of BC inclusion within the particle. Based on SEM imaging, China et al. (2013) classified carbonaceous aerosol particles into four different categories based on the shape of the BC component and the non-BC coating.

To summarize, metrics for morphology are not as unified as for the chemical mixing state but rather dependent on the system under consideration. An important issue relates to the use of projected two-dimensional images to determine the various metrics, which necessarily limits the ability to infer the full 3-D

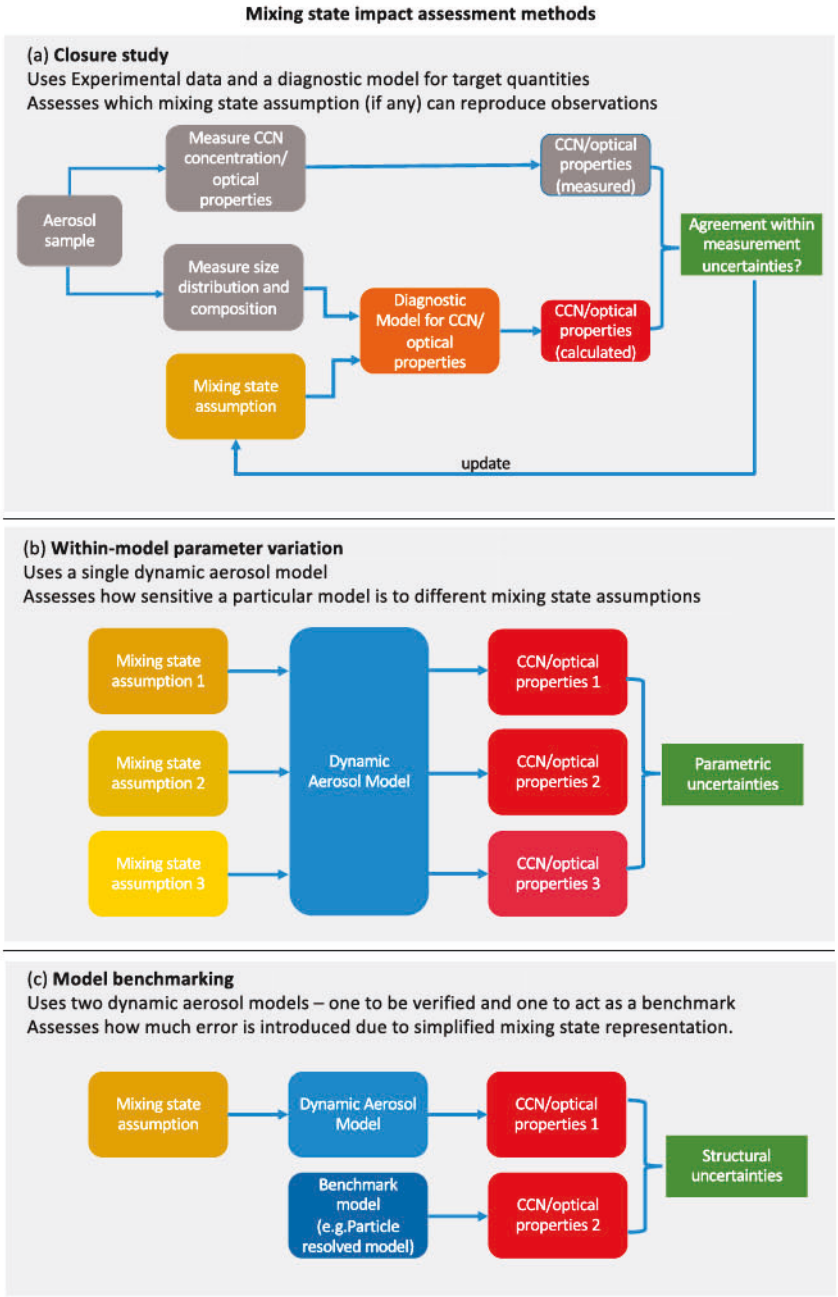


**Figure 14.** Overview of methods used to assess impacts of mixing state. (a) Closure studies, involving the comparison of measurements to calculations with a diagnostic model of target quantities (here cloud condensation nuclei, CCN, concentration and optical properties). (b) Within-model parameter variation, involving the comparison of several dynamic aerosol model runs that differ in parameter choices with respect to their mixing state representation. (c) Model benchmarking, involving comparison of a dynamic aerosol model to a benchmark model that resolves mixing state explicitly.

morphology. At the present time, atmospheric aerosol models generally do not resolve particle morphology with any detail, so the available information we have on environmental physicochemical mixing state is almost entirely from measurements.

## 6. Impacts of Aerosol Mixing State on Climate-Relevant Aerosol Properties

Considering the complexity of aerosol mixing state, the question arises of how important the knowledge of mixing state is when assessing aerosol impacts on climate. This question typically focuses on

climate-relevant aerosol properties that depend on individual particle physicochemical properties, such as optical properties for the direct effect and cloud droplet or ice crystal nucleation for the indirect effect. Do we really need to know the details of aerosol mixing state to quantify aerosol climate impacts, or are simplifying assumptions (e.g., assuming a fully external or a fully internal mixture) good enough? Can we determine how large the errors are associated with such assumptions?

### 6.1. Methods to Assess Mixing State Impacts

There are several ways to assess the impacts of mixing state. Three of the most common ways are schematically illustrated in Figure 14. These are the following: (1) closure studies for CCN concentrations or optical properties, (2) modeling studies to assess the sensitivity to parameters related to aerosol mixing state, and (3) error quantification studies using a benchmark model to quantify the structural uncertainty of mixing state approximations. We now discuss each of these in turn.

A closure study involves measuring a property of the aerosol (e.g., CCN concentrations or one or several of the optical properties in Figure 14a) and then calculating the property from a diagnostic model that is based on other independently measured quantities (Quinn & Coffman, 1998). In many applications, the diagnostic model for CCN is $\kappa$-Köhler theory (section 6.3.1), and for optical properties it is Mie theory (section 6.2).

Closure studies provide an indirect way of determining mixing state, since the calculations of CCN concentration or optical properties are generally sensitive to mixing state assumptions. The mixing state for which the best closure is achieved is then identified as the most likely mixing state for a given scenario, and the quality of closure yields insights into the fidelity of the diagnostic model being used. While closure studies are a useful approach to infer mixing state in a given environment, it is important to remember that even if closure is achieved, it does not mean that we have predictive capabilities for aerosol properties in any given environment. Moreover, since the aerosol composition space is high dimensional (section 4.1), many different mixing states may give reasonable closure for a given set of measurements.

Another way of determining the sensitivity toward mixing state assumptions involves conducting sensitivity studies with a given dynamic aerosol model (Figure 14b). These studies quantify the parametric model uncertainty by varying a mixing-state-related parameter and evaluating the change in an impact measures. For example, to parameterize the aerosol aging process, multimodal models use certain threshold criteria to move aerosol mass between modes (section 4.3.3). Performing sensitivity simulations where the threshold is varied, and comparing the resulting differences in CCN concentration or aerosol optical depth, quantifies the parametric uncertainty with respect to the choice of the threshold parameter (Liu et al., 2012). This method, however, does not assess the sensitivity to the model's structural choices (e.g., for the example of modal models the fact that a small number of modes are used to represent the aerosol).

To determine the sensitivity due to structural choices, a higher-detail model is required that can serve as a benchmark model, as shown in Figure 14c. Particle-resolved methods provide such benchmark capabilities, and comparisons of this kind allow the determination of how much error is introduced by the simplified mixing state representation in the model under study (Fierce et al., 2016).

In the following sections 6.2 and 6.3 we will see how these three techniques have been used in attempts to understand how mixing state impacts the calculation of aerosol optical properties and aerosol-cloud interactions.

### 6.2. Mixing State and Aerosol Optical Properties

Aerosol optical properties are closely tied to mixing state, since the macroscopic absorption and scattering of an aerosol population are determined by the absorption/scattering cross sections of individual particles. In this section we will focus our discussion on particle populations containing BC, although there is substantial evidence that mixing state is relevant for the optical properties of other aerosol types as well, such as mineral dust (Merikallio et al., 2011) or brown carbon (Lack et al., 2012). BC typically only represents a small fraction of the total aerosol mass concentration at a given location but is one of the few aerosol species that absorb light, acting as a short-lived climate forcer (Jacobson, 2001).

The physicochemical mixing state of BC is very complex. BC-containing particles (or "soot") are inherently nonspherical, fractal aggregates, which are found in the atmosphere at various stages of compaction (China et al., 2015; Naumann, 2003; Pósfai et al., 1999) and are partially or completely coated with other inorganic or organic aerosol material (Adachi & Buseck, 2013; China et al., 2013; Moffet et al., 2016). Their composition and morphology depend on the fuel type, the burning conditions and on aging processes (Schwarz et al.,

2008). See the review of Bond et al. (2013) for a comprehensive summary of the current state of knowledge about BC aerosols (and also the reviews of Bond & Bergstrom, 2006 and Andreae & Gelencsér, 2006).

Several approaches exist to calculate aerosol optical properties based on particle-level composition, size, and shape information. By far the most common approach is to assume spherical particles and to apply Mie (1908) theory. This requires as inputs the particle size, the wavelength of the incoming radiation, and the refractive index of the chemical compound that the particle consists of. For a multicomponent aerosol, assumptions need to be made regarding the mixing state and regarding the particles' morphologies, that is, how the chemical species are arranged within one particle (Sloane, 1983). The simplest assumption is that each particle contains only one species, that is, the external mixture assumption; however, we know that this is rarely the case in the real atmosphere. If the population is internally mixed, different "mixing rules" can be applied to compute the refractive index of the mixed particles (Chýlek et al., 2000; Lesins et al., 2002). Common assumptions are that the particles consist of a concentric or eccentric core that is coated (core-shell assumption), that the particles are homogeneously mixed on a molecular level (volume-mixing assumption), or that the mixture on the particle level can be described by embedded inclusions within a host particle (effective medium assumption; Adachi et al., 2010). These different assumptions lead to very different results in the particle's extinction cross section, single-scattering albedo, and phase function (Adachi et al., 2010; Kahnert et al., 2012).

Challenges related to the definition of a chemical species in models add fundamentally to uncertainties in the refractive indices used as inputs to any optical model, particularly in the case of BC and organic carbon. The way the refractive indices of these species are retrieved can lead to large differences in their numerical values (Saleh et al., 2016). Stier et al. (2007) showed that the basic assumption regarding the refractive index of BC plays a key role in the calculation of radiative forcing.

Many studies have explored the parametric uncertainty of different mixing rules on global climate predictions by performing sensitivity studies (Chung & Seinfeld, 2005; Jacobson, 2000, 2001; Lesins et al., 2002; Stier et al., 2007). While the aerosol model representation differs between these studies, they all found that changing the mixing rule produces large changes in BC radiative forcing. For example, Jacobson (2000) found that the core-shell assumption results in a 50% higher BC forcing compared to the externally mixed assumption and in a 40% lower BC forcing compared to the volume-mixing assumption. If feedbacks of radiation on the meteorology are included, changes in precipitation patterns and cloud coverage are also documented (Chung & Seinfeld, 2005).

The optical properties of an aerosol can be determined by measuring their light scattering or absorption. A nephelometer is the most common instrument for measuring aerosol light scattering and has been primarily used for studies of the direct effect of aerosols on climate, specifically radiative forcing (Anderson & Ogren, 1998; Heintzenberg & Charlson, 1996). For measurements of light absorption, a range of absorption photometer instrumentation has been developed, such as an aethalometer (Hansen et al., 1984), photoacoustic spectrometer (PAS; Arnott et al., 1999), particle soot absorption photometer (PSAP; Virkkula et al., 2005), and multiangle absorption photometer (MAAP; Petzold et al., 2005).

There is extensive experimental evidence that the absorption of BC-containing particles can be enhanced by coatings. However, the value of absorption enhancement ranges from 1.05 to 3.5 depending on the experimental conditions, including the amount and nature of the coating material, the exact particle morphology, and the size distribution (Khalizov et al., 2009; Schnaiter et al., 2005; Shiraiwa et al., 2010b). Field observations of absorption enhancement also show a large variability depending on the environmental conditions, ranging from negligible observed enhancement (Cappa et al., 2012) to enhancement factors of 1.67 in Detling, UK (Liu et al., 2015), or up to 2.2 in an urban area of the North China Plain, with a recognizable diurnal pattern that exhibits maximum values in the afternoon and minimum values during the evening (Chen et al., 2017a). See Wu et al. (2018) for a compilation of enhancement values, which vary between 1.06 and 2.25.

Several laboratory studies performed closure studies to test how well Mie theory reproduces the observed optical properties of BC-containing aerosol, including the absorption enhancement. They found that for thickly coated particles the absorption enhancement factors are reproduced well by Mie theory assuming a core-shell morphology (He et al., 2015; Schnaiter et al., 2005; Shiraiwa et al., 2010b). However, Schnaiter et al. (2005) also pointed out that closure for other quantities such as the single-scattering albedo, the Ångström

exponent, and the hemispheric backscattering ratio, was not as successful, especially for thinly coated BC particles.

Field closure studies found that complex partially-internally mixed assumptions give the best closure and that the best fit mixing state varies over the course of the day, with spatial location (Cheng et al., 2006, 2009; Ma et al., 2012), with season (Dey et al., 2008), and with level of pollution (Wehner et al., 2009). The fact that a signification variation in enhancement is observed and found to depend on environmental conditions makes it challenging to develop a predictive capability for aerosol optical properties on regional and global scales.

Major gaps in our ability to reliably perform successful closure calculations still exist, as demonstrated by Cappa et al. (2012). Despite having detailed measurements of BC core distributions and the amounts of coating material, using Mie calculations consistently overpredicted the measured absorption enhancements during the 2010 CARES campaign in Sacramento, CA. Multiple possible explanations exist for this finding. The poor closure could be because in the investigated environment the BC-containing particles did not exhibit "core-shell" morphologies, and therefore, the Mie model was inadequate. While determining morphology from single-particle microscopy is challenging after impaction and drying, measurements from different environments do show that the BC component can be at the edge rather than inside of the host particle (Adachi et al., 2010; China et al., 2015), which would lessen the lensing effect.

Another explanation was put forward by Fierce et al. (2016) who used particle-resolved simulations to isolate the effect of the *distribution* of coatings over a population of BC cores on absorption enhancement. Note that this particular aspect was not measured during the campaign. Assuming that the mass fractions of coatings and cores are constant across all core sizes led to a twofold overestimation of absorption enhancement because too much coating material was associated with larger BC cores. Using the coating distributions from the particle-resolved simulations rectified this issue and gave absorption enhancements in line with the observations. An important finding from Fierce et al. (2016) was also that the water content of the aerosol needed to be included in the estimate of absorption enhancement, something that is difficult to achieve with measurements. A similar conclusion regarding the role of aerosol water uptake was reached by Zhu et al. (2016a). They performed simulations for region of Paris, France, with a sophisticated mixing-state-aware model (SCRAMS). Different treatments of chemical mixing state led to differences in aerosol water uptake, causing differences in aerosol optical depths of up to 70%.

To calculate optical properties of particles with arbitrary shape or anisotropic composition, methods such as T-Matrix (Mishchenko et al., 1996) or the discrete dipole approximation (DDA; Draine & Flatau, 1994; Scarnato et al., 2013) need to be used. These methods are far more computationally expensive than Mie theory calculations and are therefore typically applied to a small number of reference particles, which then can be used to benchmark simpler model particles (Kahnert et al., 2012). Closure studies for those methods do not yet exist.

Andersson and Kahnert (2016) framed the question of whether particle morphology "matters" in terms of a comparison to the impact that aerosol microphysics processes have on optical properties (meant here as the processes that contribute to the evolution of the aerosol size distribution and the chemical aerosol mixing state). They coupled a sophisticated optical model to a mixing state-representing regional chemical transport model. Externally mixed BC was represented as fractal aggregates, and for internally mixed BC they used a novel "core-gray-shell" model, which corrects for the fact that the classical core-shell model underpredicts absorption compared to a coated aggregate (Kahnert et al., 2012). They found that the impacts from including sophisticated optics are on the same order of magnitude as the effects of aerosol microphysics. For example, relative differences in aerosol optical depth between the two optics models varied over the modeling domain (Europe) between −28% and 18%, while the differences caused by the inclusion or omission of the aerosol-microphysical processes ranged from −50% to 37%.

The above discussion has primarily focused on absorption, but it is worth remembering that other optical properties, such as the single-scattering albedo, are also sensitive to the aerosol mixing state (Zaveri et al., 2010). Quantities important for remote sensing such as the backscattering coefficient, Ångström exponent, and polarization require more complex knowledge of morphology (Andersson & Kahnert, 2016). Wang and Martin (2007) systematically investigated the impact of chemical mixing state on the accuracy of satellite retrievals of aerosol optical thickness and aerosol effective radius. For an aerosol consisting of sulfate and

BC, they found that assuming an internal or external mixing of the two components significantly affected the single-scattering albedo and the diagnostic relationship of the Ångström exponent to the aerosol effective radius and caused differences in aerosol optical depth of 60%.

In summary, from many different lines of experimental and modeling evidence, we learn that physicochemical mixing state matters for aerosol optical properties. There are several aspects to consider, namely, the chemical mixing state (i.e., how different materials are distributed over the population), the morphology (i.e., how the different materials are distributed within one particle), and as a consequence of both, the water uptake of the particles. Simplified assumptions of the physicochemical mixing state of the atmospheric aerosol can introduce substantial errors in simulated optical properties and radiative fluxes in chemistry-climate models, which then will propagate into the calculation of direct radiative forcing. A chemical transport model capability that can reliably predict aerosol optical properties based on the evolution of the physicochemical mixing state coupled with a sophisticated optical model does not yet exist.

### 6.3. Mixing State and Clouds

#### 6.3.1. Mixing State Impacts on CCN

The formation of cloud droplets or crystals in supersaturated environments is intrinsically a single-particle process. As discussed in Figure 1, even for a population of particles with the same bulk aerosol properties (e.g., mass, bulk composition, and size distribution), without individual particle information, evaluating the climate impact of an aerosol is challenging. To evaluate the potential impact of aerosol mixing state on the CCN activity for cloud droplet formation or INP activity for ice crystal formation, it is necessary to discuss the typical frameworks for studying CCN and INP activity and how they relates to mixing state.

Since the Earth's atmosphere never reaches supersaturations high enough for water droplets to nucleate without a particle, the properties of particles that can act as CCN is central to determining their climate impacts. The ability of a CCN to activate and form a cloud droplet is related to a particle's size, surface tension, composition, which determines hygroscopicity, and the supersaturation of the environment in which it is suspended. Köhler (1936) theory combines the competing Kelvin effect of increased equilibrium vapor pressure over a curved surface with the decreased vapor pressure of a solution via the Raoult effect. The combination of the Kelvin effect and Raoult's law within Köhler theory allows for the determination of the diameter at which a particle in a given supersaturated environment will undergo spontaneous growth to form a cloud droplet. This critical supersaturation and diameter, which corresponds to the maximum on a typical Köhler curve, are considered central to predicting cloud formation. The CCN activity of aerosol particles depends most strongly on their size but is also significantly affected by their composition and other physical properties. This means that the size distribution of an aerosol strongly affects the CCN spectrum, but detailed composition and mixing state knowledge are also needed.

To simplify the incredibly complex physicochemical properties of particles for modeling CCN activity, Petters and Kreidenweis (2007) introduced the hygroscopicity parameter $\kappa$. For a multicomponent homogeneously mixed particle $\kappa$ is the volume-weighted average of the $\kappa$ values of the constituent species. Neglecting kinetic effects (Nenes et al., 2001), the CCN concentration is then the number concentration of particles for whom the environmental supersaturation is higher than their critical supersaturation. To evaluate the impact of aerosol mixing state on cloud droplet formation, we can use $\kappa$-Köhler theory to consider CCN activity or different mixing states.

Figure 15 illustrates the effect of mixing state on CCN. Using our previous schematic of internal and external mixtures, Figure 15a shows a size distribution assumed to be an internal mixture of ammonium sulfate and a hydrophobic organic. Based on $\kappa$-Köhler theory, it is straightforward to determine the critical diameter at a given supersaturation, above which particles will act as CCN and form droplets. For the external mixture in Figure 15b, each of the two distinct populations has its own hygroscopicity, and therefore, two different critical diameters exist. Thus, the hydrophobic particles shown here in blue will activate only at a larger activation diameter to form CCN, while the hygroscopic ammonium sulfate will activate at a lower size. This illustrates the differences in CCN activation for the extremes of the aerosol mixing state range. Figure 15c is typical of how CCN data are presented, with supersaturation shown as a function of diameter and diagonal lines of constant $\kappa$. The $\kappa$ values of our example are highlighted as stars along a line of constant supersaturation.

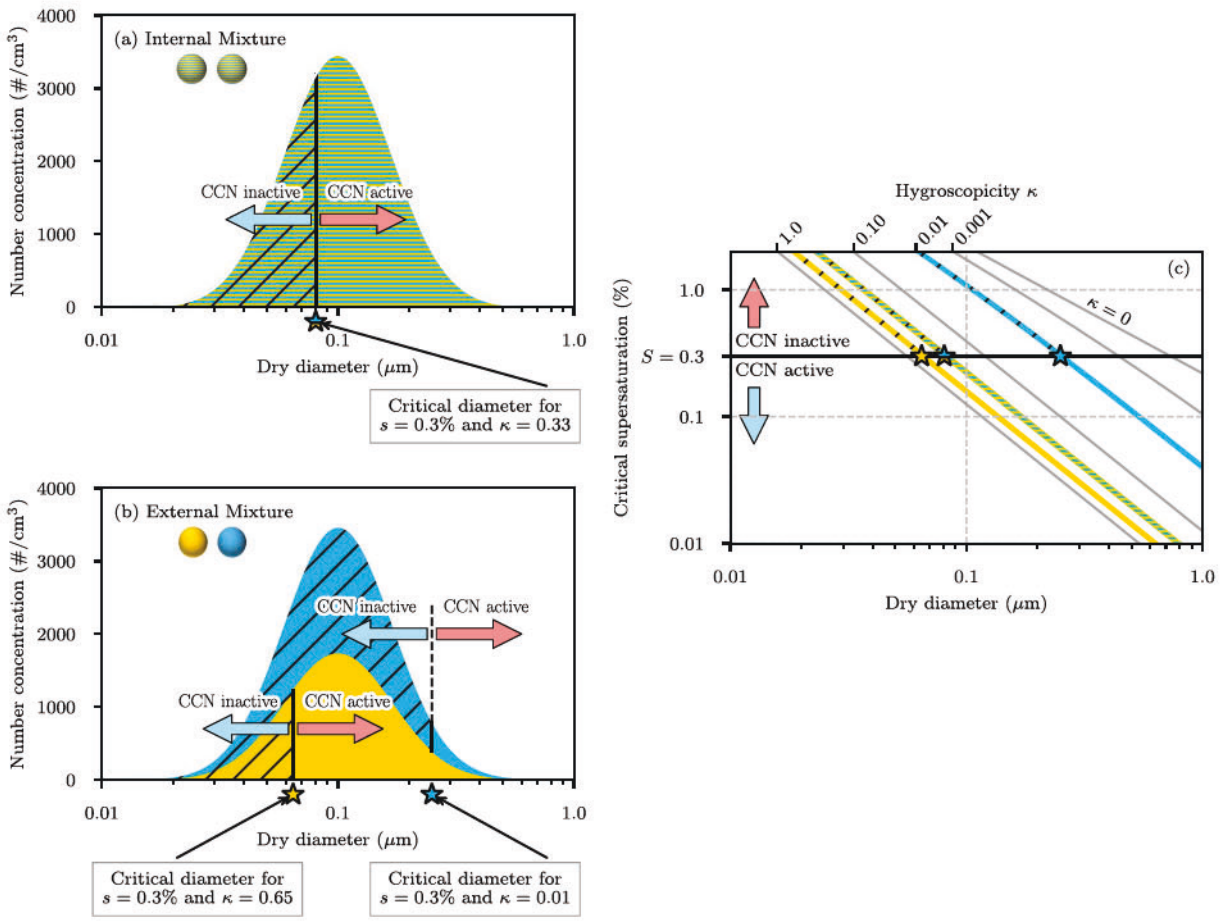


**Figure 15.** Illustration of the effect of mixing state on cloud condensation nuclei (CCN). (a) Size distribution assuming internal mixture. At a given environmental supersaturation (here 0.3% as example), a unique critical diameter exists above which all particles activate, marked with a green star. (b) Size distribution assuming that the population is externally mixed, consisting of two subpopulations with different hygroscopicities. This results in two different critical diameters, marked with a yellow and blue stars, respectively. (c) Mapping of the information in (a) and (b) in supersaturation-diameter space. The yellow, green, and blue stars correspond to the critical diameters in (a) and (b). Particles above the horizontal line for $S = 0.3\%$ are CCN inactive, while particles below the line are CCN active.

To consider a real-world example, Figure 16 shows a number distribution as a function of supersaturation and diameter for a particle population simulated with a particle-resolved model (see section 4.3.6; Ching et al., 2012). The population represents conditions of a polluted urban environment, showing a mixture of fresh and aged emissions from traffic, meat cooking, and background aerosol. The resulting per-particle $\kappa$ values range between close to 0 (for freshly emitted soot particles) and 0.65 (for background particles, consisting of ammonium sulfate). Using 0.3% supersaturation as an example, the overall particle population can be divided into CCN active (all particles below the line) and CCN inactive (all particles above the line). At the given supersaturation, for particles with low $\kappa$ (0.01), the diameter must be smaller than 0.12 $\mu$m for them to be inactive, while for particles with high $\kappa$ (0.65), the diameter must be smaller than 0.06 $\mu$m to remain inactive. If all the data were projected onto the ordinate, we would obtain the number size distribution with a mode of 0.08 $\mu$m for the fresh soot and 0.13 $\mu$m for the aged and background particles. This example illustrates that in the ambient environment different populations with different CCN activities can exist and that mixing state will matter for predicting CCN concentration in such regions.

A critical advance in our ability to understand CCN activity was the development of the CCN counter (Hudson, 1989; Roberts & Nenes, 2005). The basic operation of a CCN counter is that suspended aerosol are exposed to a precisely controlled supersaturation (often 0.2–1.0% supersaturation). The fraction of particles that are activated is then optically detected and compared with the total number of condensation nuclei (CN), which represents all particles. From this the CCN/CN ratio can be obtained at a given supersaturation. Since the CCN counter measures the activation of individual particles, the properties of the aerosol being

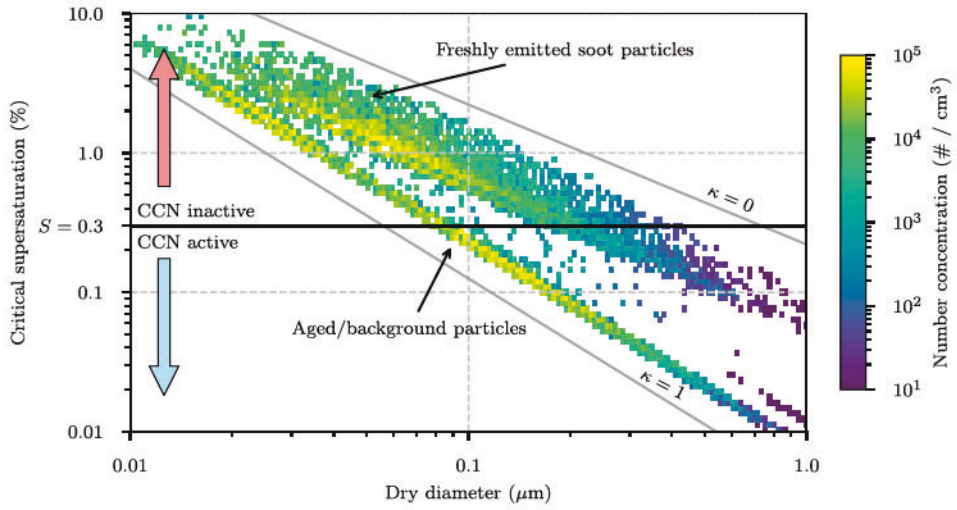


**Figure 16.** Two-dimensional number distribution as a function of particle dry diameter and critical supersaturation. The black horizontal line indicates a given environmental supersaturation threshold (here 0.3% as an example). Based on this the particles can be categorized as cloud condensation nuclei (CCN) inactive and CCN active.

measured can be used for closure studies. To perform an aerosol/CCN closure study, the CCN concentration is measured for an aerosol that is exposed to a particular supersaturation or a set of supersaturations. Independently, the dry particle size distribution and (aspects of) the aerosol composition are also measured.

Mixing state and its relationship to CCN specifically has been explored by a number of laboratory and field studies (Asa-Awuku et al., 2011, 2015; Fofie et al., 2018; Hatch et al., 2008, 2009; Jurányi et al., 2013; Lance et al., 2013; Leck & Svensson, 2015; Maskey et al., 2017; Sullivan et al., 2009; Rose et al., 2011; Vestin et al., 2007; Wang et al., 2010). Laboratory studies for well-characterized internally mixed aerosol with single-component, binary mixtures, or tertiary mixtures agree well with Köhler theory described above (Abbatt et al., 2005; Cruz & Pandis, 1997; Gerber et al., 1977; Katz & Kocmond, 1973). However, as we will discuss below, closure studies using ambient aerosol are not as simple and give mixed results (Broekhuizen et al., 2006), including some cases where closure cannot be obtained with reasonable assumptions. Reasons for this range from incomplete information about composition, hygroscopic properties of organic species, and mixing state to measurement uncertainties in CCN chambers or of particle size distributions.

Intuitively, we expect that assuming internal mixture will result in poor closure when the sampling occurs close to emission sources or at times of high emission rates. This has been confirmed by several closure studies over the years. For example, Wang et al. (2010) and Lance et al. (2013) found a time-of-day dependence for Mexico City during the MILAGRO campaign, with an external mixture assumption needed during the morning rush hour, but not at other times of the day. Similarly, from a synthesis of closure studies at six locations by Ervens et al. (2010), it was found that conditions close to the emission source warranted more complex assumptions about composition, that is, at least information about size-resolved composition or how hygroscopic and nonhygroscopic species are mixed within a size range. Using measurement of the hygroscopic growth of atmospheric aerosols by Kandler and Schütz (2007) and Swietlicki et al. (2008), Wex et al. (2010) used a closure study to argue that an aerosol is often externally mixed with respect to hygroscopicity and that using an average value for $\kappa$ leads to an overestimation of CCN concentration by up to a factor of two. Cubison et al. (2008) found that closure was best achieved for the SOAR-1 field campaign in Riverside when using size-resolved composition, combined with the assumption that elemental carbon and small-mode organics are externally mixed with respect to the background population.

When performing closure studies, different studies have considered different possible mixing state hypotheses. For example, Ervens et al. (2010) explored the impact of four different composition assumptions, carbonaceous and inorganic fractions externally or internally mixed, combined with the assumption of soluble or insoluble organics. In contrast, Cubison et al. (2008) compared five cases, and Bhattu and Tripathi (2015) included eight cases. It is important to point out that the "composition assumptions" that are typically made in closure studies are rather simplistic, and even though closure may be achieved reasonably

well for a certain case, one should not conclude that the true aerosol really looks like as is assumed for that case, as noted by (Ervens et al., 2010). More generally, it is important to separate closure from our ability to predict aerosol properties. From closure studies we learn how much variability is introduced by different assumptions, but due to the intrinsically empirical nature of closure studies, predictive capabilities are not necessarily gained based on the information obtained.

From these studies one might conclude that external mixing states are only encountered in polluted urban environments. However, this can also be the case in remote locations. Collins et al. (2013) showed that sea spray can consist of two externally mixed modes, one consisting of sea salt and organic material and the other consisting of insoluble organic material. In this case, three different subpopulations with different $\kappa$ values were needed to explain the data. Similarly, Moore et al. (2011) and Lathem et al. (2013) found that assuming external mixing provided the best agreement between measured and predicted CCN activity in the Arctic. Meskhidze et al. (2011) showed that model assumptions on mixing state of marine primary organic matter impact CCN concentrations. In particular, they concluded that treating sea spray in global climate models as internal mixture of marine POA and sea salt will lead to an underestimation in CCN concentration, which is not consistent with observations over biologically active ocean areas.

Composition and mixing state matter least when the aerosol is internally mixed with a hygroscopic salt as one of the components, because the hygroscopic salt will dominate the CCN activity of the particle. For example, in Figure 15 particles that are 50% ammonium sulfate ($\kappa = 0.65$) and 50% organic carbon ($\kappa = 0.01$) have critical diameters that are very close to the critical diameter of pure ammonium sulfate and very far from the critical diameter of pure organic carbon. That is, the particle's CCN activity is largely determined by the hygroscopic salt (ammonium sulfate). For highly aged aerosol where the particle population is assumed to be internally mixed, a well-constrained size distribution can thus be sufficient for CCN closure (Broekhuizen et al., 2006; Dusek et al., 2006; Gunthe et al., 2009).

Regional modeling studies using modal and sectional models are useful for directly comparing the impact of assuming internal versus external mixing assumptions. In this context, Lee et al. (2016) used source-oriented WRF/Chem simulations in the Californian Central Valley and found a decrease in CCN/CN from 94% with an internal mixture assumption to 80% with a source-oriented mixture. Zhu et al. (2016b) simulated an episode of several days for the greater Paris Region using the SCRAM and found changes of up to 72% in CCN concentrations evaluated at 0.02% supersaturation in the rural areas surrounding the Paris center.

Zaveri et al. (2010) used a particle-resolved model and a composition-averaging framework (section 4.3.6) and found that ignoring mixing state heterogeneity caused CCN concentrations to be overestimated by up to 40% for conditions that represented a polluted urban plume. Fierce et al. (2017) used particle-resolved modeling to provide estimates for the time that an initially externally mixed aerosol must be aged to become fully internally mixed with respect to CCN activity. This time scale can range from a few hours for polluted environments to several days for environments with low production rates of hygroscopic secondary aerosol (e.g., sulfate) that makes them more CCN active (Ma et al., 2017). This is consistent with the findings by Dusek et al. (2006) and Ervens et al. (2010) in that assuming a fully internal mixture is adequate for simulating CCN concentration of populations away from source regions. However, in regions where fresh emissions mix with aged aerosol, more detailed mixing state representations are required, such as multimodal approaches or multidistribution sectional approaches. Also using particle-resolved modeling, Ching et al. (2017) quantified the error when assuming internal mixture as a function of the mixing state index $\chi$ (see section 5). They found that CCN concentrations were up to 100% overpredicted for low-$\chi$ populations when internal mixing was assumed, but were well predicted for high-$\chi$ populations.

The supersaturation at which the CCN activity is being evaluated can determine whether detailed mixing state information is needed, because different parts of the particle population are more sensitive at different supersaturations, as shown in Figure 15 above. In general, it might be high or low supersaturations that require more mixing state information and the effect of neglecting mixing state can have either sign, depending on the details of the aerosol. For example, Bhattu and Tripathi (2015) showed for measurements in Kanpur, India, that the quality of closure depended on the supersaturation at which the CCN concentration was evaluated. This is consistent with the results by Cubison et al. (2008) and Wex et al. (2010), who found that more detailed mixing state information was needed when the supersaturation was below 0.2%. The modeling study of Zaveri et al. (2010) also found a dependence on the supersaturation cutoff, although there it was the higher supersaturations (around 0.5%) that required more mixing state information. When

modeling the MEGAPOLI campaign, Zhu et al. (2016b) also found supersaturation dependence, with an internal mixing assumption reducing CCN concentration at low supersaturations but increasing it at high supersaturations.

So far we have exclusively discussed the relevance of chemical mixing state for CCN activity. However, for particles that contain organic and inorganic components, particle morphology can become important (Facchini et al., 1999; Shulman et al., 1996; Topping et al., 2007). If liquid-liquid phase separation occurs, a complete or partial coating of a hygroscopic particle core by a hydrophobic organic-rich phase will form (Song et al., 2013), which lowers the surface tension and the critical supersaturation that is required to activate the aerosol (Ruehl et al., 2016; Ovadnevaite et al., 2017). Experimentally determining the surface tension of atmospherically relevant systems is an active topic of research (Boyer & Dutcher, 2017; Petters & Petters, 2016).

To summarize, a full internal mixture across all sizes (submicron and supermicron) is not found in the ambient atmosphere (Bauer et al., 2013). Even for submicron particles, complex mixing states can exist, particularly close to aerosol source regions. Assuming internal mixtures will then incur appreciable errors (on the order of 100%) in predicting CCN concentration. For these environments, assumptions about the degree of internal versus external mixing within a size range need to be made, but it is generally a priori unclear exactly which assumptions to make, as this appears to vary on a case-to-case basis. For these cases, our predictive capability with respect to CCN activity is limited. In contrast, in locations, where the aerosol is aged and fresh emissions are not added to the population, assuming an internal mixture with respect to CCN for submicron sized particles is reasonable for predicting CCN activity. These tend to be remote regions, but even for those, natural fresh emissions, such as sea spray, can add heterogeneity to an aerosol, resulting in a mixing state that is not completely internally mixed. These findings lead to the conclusion that including aerosol mixing state information in chemical transport models is warranted if the prediction of CCN concentrations is desired. At the same time, suitable observations are needed to validate the simulated mixing state.

#### 6.3.2. Mixing State Impacts on Ice Nucleating Particles (INPs)

It has long been known that particles, called ice nucleating particles (INPs), enable the heterogeneous freezing of the droplets at temperatures above those required for homogeneous freezing (Dufour, 1862; DeMott et al., 2011; Schaefer, 1949). This process is critical for cloud formation, evolution, lifetime, and precipitation in mixed phase and ice clouds. However, typically only one in $10^5$ particles is able to act as an INP (DeMott et al., 2010), which is believed to strongly depend on its physicochemical properties, such as whether phase state is solid, viscous, or liquid. Thus, the ability to predict cloud behavior and the impacts on the hydrological cycle as a whole depends on connecting ice crystal formation to individual particle properties.

The propensity to form ice at elevated temperatures relative to homogeneous freezing is usually reported for different particle types and subpopulations of those types (e.g., different types of mineral dust, soot, or biological particles; Kanji et al., 2017). From field studies using single-particle analysis techniques on ice residuals, we also know that ice nuclei are mixtures of species (Schill & Tolbert, 2014; Schaefer, 1949; Wise et al., 2012, 2010), for example, mineral dust and organic material. Specific particle types observed in clouds include dust and biological particles, which are also observed in the resulting precipitation (Creamean et al., 2013, 2014, 2015; Pratt et al., 2009c). Since ice nucleation is a process that depends on the surface properties of the particles, it is inherently tied to aerosol mixing state (Ault et al., 2011; Creamean et al., 2013; Pratt et al., 2009c).

Some laboratory studies have shown that coatings on INPs can reduce or inhibit the ability to nucleate ice in the deposition mode (i.e., ice nucleates from supersaturated vapor with respect to ice directly on an INP; Cziczo et al., 2009; Hoose & Möhler, 2012; Niedermeier et al., 2011; Sullivan et al., 2010), where details, such as the thickness or the completeness of the coating, matter (Cziczo et al., 2009). However, ice can still form via the immersion freezing pathway (i.e., ice nucleation initiated by an INP immersed in an aqueous solution or water droplet via activation of CCN followed by freezing at supercooled temperatures), which then requires that supersaturation with respect to water is reached. This means that aerosol mixing state to some extent governs which freezing pathway is accessed.

Quantifying the ice nucleation rates is expected to depend on the details of the aerosol composition and morphology, in particular, on which species reside at the surface of the aerosol particle and the properties of

that surface (Knopf & Alpert, 2013). However, in contrast to the process of cloud droplet formation, where Köhler theory provides us an accurate model, we do not yet have a first-principles understanding of the process of ice crystal formation, and how it depends on the details of aerosol composition and morphology (Knopf et al., 2018; Murray et al., 2012). Unlike with CCN or optical properties, INP closure studies do not yet exist. While the importance of mixing state for INPs is well recognized within the community, its quantification is hampered by the lack of fundamental process models.

It is currently greatly debated how to best parameterize heterogeneous ice nucleation, even for "simple" (externally mixed) aerosol types (Hoose et al., 2010; Hoose & Möhler, 2012; Phillips et al., 2008). The two fundamentally different approaches are a stochastic description based on classical nucleation theory, which yields a nucleation rate coefficient, and a deterministic (singular) description, which yields the number of ice nucleation active sites. Within each of these frameworks, different parameter choices produce diverging results for cloud properties such as the onset of the Wegener-Bergeron-Findeisen process (Findeisen, 1938; Wegener, 1911), liquid water and ice water content (Ervens & Feingold, 2012; Wright & Petters, 2013). Since INP parameterizations have traditionally been formulated for different particle types, they intrinsically rely on an understanding of the aerosol mixing state. As parameterizations expand to include more types of freezing and multiple particle types (Beydoun et al., 2017), knowledge of the overall aerosol mixing state will be critical for accurate predictions.

The modal representation of aerosol in global and regional models (see section 4.3.3) lends itself to a "type-based approach" of representing ice nucleation, where different ice nucleation propensities are assigned to the various particle types (e.g., dust, biological particles, and soot; Hoose et al., 2010). Within large-scale modeling studies, complexities due to morphology and mixing state have been largely not yet explored, with the exception of INP deactivation by coatings. Overall, while it is known that it is important to connect aerosol mixing state with primary cloud ice crystal formation, the ability of models to incorporate both detailed aerosol mixing state information and INP predictions is currently quite limited.

## 7. Conclusions and Future Needs

This review has covered our current understanding of aerosol mixing state and its impacts. We began in section 2 with definitions of the chemical mixing state, which is the distribution of chemical species across the particles in an aerosol, and the physicochemical mixing state, which also includes the distribution of morphology, phase, and other particle characteristics. We have emphasized the need to distinguish between single-particle properties, such as the number of chemical species or the particle shape, and the mixing state, which captures the *distribution* of these properties across a population.

Over the past few decades considerable progress has been made in measuring the composition and physical properties of individual particles necessary to determine aerosol mixing state and to evaluate its impacts. However, as described in section 3, no single instrument is able to completely capture physicochemical mixing state across all particle sizes. For example, gaps in data can be related to the sizes of particles measured by a certain instrument (e.g., ultrafine particles might not be captured) or stem from challenges measuring specific species (e.g., water or refractory material might not be detected). To characterize aerosol mixing state at a given time or location therefore necessitates the combination of multiple instruments that simultaneously sample the same aerosol. This can be challenging, and often a single measurement is all that is available to determine mixing state from field measurements. Though not the norm, studies taking an integrative approach have provided useful information on mixing state and serve as a guide for future efforts (Bondy et al., 2018; Fraund et al., 2017; Gunsch et al., 2017; Healy et al., 2013; Jung et al., 2014; Li et al., 2016; May et al., 2018b; Moffet et al., 2010; Murphy et al., 2006; O'Brien et al., 2015; Qin et al., 2012; Sobanska et al., 2014). It would be extremely helpful to conduct more observations in which a complete characterization of aerosol samples is achieved, that is, studies that determine chemical, and morphological properties simultaneously.

The development of new measurement techniques and methodologies represents an exciting direction of research for improving our understanding of aerosol mixing state. This includes both sophisticated instrumentation to measure challenging or integrated properties, simpler measurements that can complement existing approaches, field-portable versions of laboratory instrumentation, and new approaches for properties that are currently not measured effectively. As an example of a measurement that would be valuable, direct determination of aerosol liquid water content at the single-particle level would complement exist-

ing measurements of dry components. New instrumentation does not need to provide precise mass of each component at the individual particle level to be valuable and worth pursuing to improve our understanding of mixing state in the ambient atmosphere.

Aerosol models used in regional or global climate-chemistry models increasingly include representations of aerosol mixing state, ranging from comparatively simple multimodal approaches (e.g., MAM4 Liu et al., 2016) to more sophisticated multidimensional sectional approaches (e.g., SCRAM Zhu et al., 2015, ATRAS Matsui et al., 2014) and to very detailed particle-resolved approaches (e.g., WRF-PartMC Curtis et al., 2017). Section 4 laid out how the different modeling approaches represent the aerosol composition space, and what the trade-offs are in terms of detail in representation and computational demands.

A challenge when trying to evaluate the quality of the simulated aerosol mixing state is the scarcity of measurement data (Stier et al., 2007), which is not surprising, given that the data suitable for comparisons are mostly complex, expensive, and labor intensive to obtain. We are not yet at the point where we can routinely characterize the mixing state of aerosols with high detail, over large areas, and with high temporal frequency. Improved measurement capabilities that can provide increased spatial resolution or broader time scales than typical field studies are needed. Challenges also remain around the compatibility of the quantities that models track and the quantities that are experimentally determined. All mixing-state-aware models are aiming at predicting the distribution of masses of different model species across the population. Quantitative information about species masses are challenging to extract from experimental single-particle approaches, and frequently, the species tracked in models do not easily map to the species that are measured.

For any of these modeling approaches, aerosol emission inventories are important input data. For many significant emission sources, the aerosol already has a complex mixing state at the time of emission (e.g., car emissions Willis et al., 2016). Much work will be needed to include this information in emission inventories, so that mixing-state-aware models can make use of it.

To fully allow the representation of not only the chemical mixing state but the physicochemical mixing state in models, predictive models of particle morphology are needed, for example, models that can capture the restructuring of fractal carbonaceous particles as part of the aerosol aging process or models that capture the occurrence of liquid-liquid phase separation. This goes well beyond simply storing morphological information, as it is the evolution of the morphology which must be accurately captured. As well as model development, targeted experimental data sets from the lab and field will be needed to guide the development of truly predictive morphology models.

For studying aerosol mixing state, quantitative metrics of the mixing state are key tools. Such metrics measure the degree to which an aerosol or subpopulation is internally or externally mixed and allow the direct comparison of mixing state from different instruments or models. The most widespread metric of chemical mixing state at present is the mixing state index $\chi$ described in sections 5.1 and 5.2, although other metrics exist that are tailored to specific aerosol features (section 5.3).

Measuring or modeling the value of $\chi$ raises two of our central themes, namely, the need to measure per-particle mass fractions of species and the need to choose what constitutes a species. Progress on these two items has already enabled comparisons between the measured and modeled mixing state in several studies, and we have some preliminary quantitative understanding of how the mixing state index relates to errors in predicted aerosol impacts (section 5.2).

While the mixing state index $\chi$ has provided a framework for quantifying chemical mixing state, we currently lack generally accepted metrics for the full physicochemical mixing state. There are numerous metrics for single-particle morphology (section 5.4), but these still need to be integrated into metrics for the morphological state and variability of an entire particle population. This is important for understanding heterogeneous and multiphase reactions, as well as impacts that are sensitive to particle structure such as optical properties.

Different approaches exist for quantifying the impact of aerosol mixing state on aerosol optical properties, as well as CCN and INP activity (section 6). This includes closure studies, sensitivity studies that determine parametric uncertainty with respect to mixing state assumptions, and comparisons to higher-detail models that determine structural uncertainty of models that use a simplified mixing state representation. From these studies we learn that to predict these target quantities, mixing state matters in many conditions. For example, different mixing state assumptions will introduce errors in CCN concentration predictions by up to

100%, and predictions of absorption enhancement of BC will be overestimated by a factor of 2 if the mixing state is oversimplified.

To accurately predict aerosol impacts, it is generally necessary to both predict the physicochemical mixing state of the aerosol and to understand how the target quantities depend on this mixing state. As discussed above, both measurements and models have made progress in quantifying and predicting mixing state of an aerosol. When it comes to predicting target quantities from a known mixing state, our understanding is generally better for CCN (section 6.3.1) than for optical properties (section 6.2), which in turn is significantly better than for INPs (section 6.3.2). For CCN, $\kappa$-Köhler theory generally gives reasonable results, unless there are surface effects. For optical properties, Mie theory and core-shell models are physically well founded when they apply, but understanding when and how they apply remains an active area of research (section 6.2). For INPs, there does not yet exist a consensus on the appropriate physical models, which results in a current lack of predictive models for INPs in a range of atmospheric conditions.

## Abbreviations

| | |
|---|---|
| AFM | atomic force microscopy |
| AFM-IR | atomic force microscopy with infrared spectroscopy |
| A-FORCE | Aerosol Radiative Forcing in East Asia |
| ALABAMA | aircraft-based laser ablation mass spectrometry |
| AMS | aerosol mass spectrometer |
| ART-2a | adaptive resonance theory 2a |
| ATOFMS | aerosol time-of-flight mass spectrometry |
| ATRAS | Aerosol Two-dimensional bin module for foRmation and Aging Simulation |
| ATR-FTIR | attenuated total reflectance Fourier transform infrared spectroscopy |
| ATTO | Amazonia Tall Tower Observatory |
| BC | black carbon |
| CAMx | Community Atmosphere Model |
| CARES | Carbonaceous Aerosol and Radiative Effects Study |
| CCN | cloud condensation nuclei |
| CC-Raman | computer-controlled Raman microspectroscopy |
| CCSEM | computer-controlled scanning electron microscopy |
| CMAQ | Community Multiscale Air Quality Modeling System |
| COSMO-Art | Consortium for Small-scale Modelling-Aerosol and Reactive Trace gases |
| CPC | condensation particle counter |
| CR-AVE | Costa Rica Aura Validation Experiment |
| Cryo-TEM | transmission electron cryomicroscopy |
| DDA | discrete dipole approximation |
| DMA | differential mobility analyzer |
| ECHAM | comprehensive atmospheric general circulation model developed at the Max Planck Institute for Meteorology |
| ECHAM-HAM | ECHAM model including an aerosol module |
| EDX | energy dispersive X-ray spectroscopy |
| EDXMA | energy dispersive X-ray microanalysis |
| EELS | electron energy loss spectroscopy |
| EMAC | ECHAM/MESSy Atmospheric Chemistry |
| EPMA | energy probe X-ray microanalysis |
| ESEM | environmental scanning electron microscopy |
| E-TEM | environmental transmission electron microscopy |
| EF-TEM | energy filtered transmission electron microscopy |
| ES-SERS | electrospray surface-enhanced Raman spectroscopy |
| FTIR | Fourier transform infrared spectroscopy |
| HAADF | high-angle annular dark-field detector |
| HAB | harmful algal bloom |
| HDMPS | humidifying differential mobility particle sizer |
| HH-TDMA | high humidity hygroscopic tandem differential analyzer |

| | |
|---|---|
| HTDMA | hygroscopic tandem differential analyzer |
| INP | ice nucleating particle |
| IR | infrared |
| LAMPAS | laser mass analysis of particles in the airborne state |
| LDI | laser desorption ionization |
| LMMS | laser microprobe mass spectrometry |
| LS-SP-AMS | light scattering soot particle aerosol mass spectrometer |
| MAAP | multiangle absorption photometer |
| MADE3 | Model Aerosol Dynamics model for Europe |
| MADE-in | modal aerosol dynamics model including insoluble modes |
| MADRID-BC | Model of Aerosol Dynamics, Reaction, Ionization, and Dissolution—Black carbon |
| MAM | Modal Aerosol Model |
| MATRIX | Multiconfiguration Aerosol Tracker of Mixing State |
| MEGAPOLI | Megacities: emissions, urban, regional and global atmospheric pollution and climate effects, and Integrated tools for assessment and mitigation |
| MESSy | Modular Earth Submodel System |
| Micro-FTIR | Fourier transform infrared spectroscopy coupled to optical microscopy |
| MILAGRO | Megacity Initiative: Local and Global Research Observations |
| MOSAIC | Model for Simulating Aerosol Interactions and Chemistry |
| MOSAIC-MIX | mixing-state-resolved sectional aerosol model |
| MS | mass spectrometer |
| NAMS | nanoaerosol mass spectrometry |
| NanoSIMS | nano secondary ion mass spectrometry |
| PALMS | particle analysis by laser mass spectrometry |
| PartMC | particle-resolved Monte Carlo |
| PAS | photoacoustic spectrometer |
| PBAP | primary biological aerosol particle |
| PEACE-C | Pacific Exploration of Asian Continental Emission-C |
| PM | particulate matter |
| POA | primary organic aerosol |
| PSAP | particle soot absorption photometer |
| QMOM | quadrature method of moment |
| RSMS | rapid single-particle mass spectrometry |
| SCRAM | Size-Composition Resolved Aerosol Model |
| SEM | scanning electron microscopy |
| SERS | surface-enhanced Raman spectroscopy |
| SERRS | surface-enhanced resonance Raman spectroscopy |
| SFG | sum frequency generation |
| SHG | sum harmonic generation |
| SIMS | secondary ion mass spectrometry |
| SMPS | scanning mobility particle sizer |
| SOA | secondary organic aerosol |
| SOAR-1 | Study of Organic Aerosol at Riverside |
| SOAS | Southern Oxidant and Aerosol Study |
| SP2 | single-particle soot photometer |
| SP-AMS | soot particle aerosol mass spectrometer |
| SPLAT | single-particle laser ablation time-of-flight mass spectrometry |
| SPMS | single-particle mass spectrometer |
| SSA | stochastic simulation algorithm |
| STEM | scanning transmission electron microscopy |
| STXM | scanning transmission X-ray microscopy |
| STXM-NEXAFS | scanning transmission X-ray microscopy with near edge X-ray absorption fine structure spectroscopy |
| TDMPS | twin differential mobility particle sizer |
| TEM | transmission electron microscopy |

| | |
|---|---|
| TERS | tip-enhanced Raman spectroscopy |
| TOF-SIMS | time-of-flight secondary ion mass spectrometry |
| UV-APS | ultraviolet aerodynamic particle sizer |
| VOC | volatile organic compound |
| VTDMA | volatility tandem differential mobility analyzer |
| WIBS | wide issue bioaerosol spectrometer |
| WRF-Chem | Weather and Research Forecasting model coupled with Chemistry |
| XANES | X-ray absorption near edge spectroscopy |
| XEDS | X-ray energy dispersive spectroscopy |
| XPS | X-ray photoelectron spectroscopy |

**Acknowledgments**
N. Riemer, J. H. Curtis, and M. West were partially supported by DOE grant DE-SC0019192. N. Riemer was partially supported by NSF grant AGS-1254428. J. H. Curtis and M. West were partially supported by NSF grant CMMI-1150490. A. P. Ault was supported by NSF grants CHE-1654149 and AGS-1703019, as well as a Sloan Research Fellowship in Chemistry. R. L. Craig was partially supported by a Susan Lipschutz Fellowship Award from the University of Michigan Rackham Graduate School. Ernie Lewis is thanked for thoughtful comments on the manuscript. Jessie Creamean is thanked for insightful feedback on the INP section.

## References

Abbatt, J., Broekhuizen, K., & Kumar, P. P. (2005). Cloud condensation nucleus activity of internally mixed ammonium sulfate/organic acid aerosol particles. *Atmospheric Environment*, *39*(26), 4767–4778.

Abbatt, J., Lee, A., & Thornton, J. (2012). Quantifying trace gas uptake to tropospheric aerosol: Recent advances and remaining challenges. *Chemical Society Reviews*, *41*(19), 6555–6581.

Adachi, K., & Buseck, P. R. (2013). Changes of ns-soot mixing states and shapes in an urban area during CalNex. *Journal of Geophysical Research: Atmospheres*, *118*, 3723–3730. https://doi.org/10.1002/jgrd.50321

Adachi, K., Chung, S. H., & Buseck, P. R. (2010). Shapes of soot aerosol particles and implications for their effects on climate. *Journal of Geophysical Research*, *115*, D15206. https://doi.org/10.1029/2009JD012868

Adachi, K., Chung, S. H., Friedrich, H., & Buseck, P. R. (2007). Fractal parameters of individual soot particles determined using electron tomography: Implications for optical properties. *Journal of Geophysical Research*, *112*, D14202. https://doi.org/10.1029/2006JD008296

Adachi, K., Moteki, N., Kondo, Y., & Igarashi, Y. (2016). Mixing states of light-absorbing particles measured using a transmission electron microscope and a single-particle soot photometer in Tokyo, Japan. *Journal of Geophysical Research: Atmospheres*, *121*, 9153–9164. https://doi.org/10.1002/2016JD025153

Adams, P. J., & Seinfeld, J. H. (2002). Predicting global aerosol size distributions in general circulation models. *Journal of Geophysical Research*, *107*, 4370. https://doi.org/10.1029/2001JD001010

Allen, H. M., Draper, D. C., Ayres, B. R., Ault, A., Bondy, A., Takahama, S., et al. (2015). Influence of crustal dust and sea spray supermicron particle concentrations and acidity on inorganic $NO_3^-$ aerosol during the 2013 Southern Oxidant and Aerosol Study. *Atmospheric Chemistry and Physics*, *15*(18), 10,669–10,685.

Anderson, B. J., Musicant, D. R., Ritz, A. M., Ault, A., Gross, D., Yuen, M., & Gälli, M. (2005). User-friendly clustering for atmospheric data analysis (MN Technical Report): Carleton College Northfield.

Anderson, T. L., & Ogren, J. A. (1998). Determining aerosol radiative properties using the TSI 3563 integrating nephelometer. *Aerosol Science and Technology*, *29*(1), 57–69.

Andersson, E., & Kahnert, M. (2016). Coupling aerosol optics to the MATCH (v5. 5.0) chemical transport model and the SALSA (v1) aerosol microphysics module. *Geoscientific Model Development*, *9*(5), 1803–1826.

Andreae, M., & Gelencsér, A. (2006). Black carbon or brown carbon? The nature of light-absorbing carbonaceous aerosols. *Atmospheric Chemistry and Physics*, *6*(10), 3131–3148.

Andreae, M., & Rosenfeld, D. (2008). Aerosol–cloud–precipitation interactions. Part 1. The nature and sources of cloud-active aerosols. *Earth-Science Reviews*, *89*(1–2), 13–41.

Aquila, V., Hendricks, J., Lauer, A., Riemer, N., Vogel, H., Baumgardner, D., et al. (2011). MADE-in: A new aerosol microphysics submodel for global simulation of insoluble particles and their mixing state. *Geoscientific Model Development*, *4*(2), 325.

Arnott, W. P., Moosmüller, H., Rogers, C. F., Jin, T., & Bruch, R. (1999). Photoacoustic spectrometer for measuring light absorption by aerosol: Instrument description. *Atmospheric Environment*, *33*(17), 2845–2852.

Asa-Awuku, A., Moore, R. H., Nenes, A., Bahreini, R., Holloway, J. S., Brock, C. A., et al. (2011). Airborne cloud condensation nuclei measurements during the 2006 Texas Air Quality Study. *Journal of Geophysical Research*, *116*, D11201. https://doi.org/10.1029/2010JD014874

Asa-Awuku, A., Sorooshian, A., Flagan, R. C., Seinfeld, J. H., & Nenes, A. (2015). CCN properties of organic aerosol collected below and within marine stratocumulus clouds near Monterey California. *Atmosphere*, *6*(11), 1590–1607. https://doi.org/10.3390/atmos6111590

Ault, A. P., & Axson, J. L. (2017). Atmospheric aerosol chemistry: Spectroscopic and microscopic advances. *Analytical Chemistry*, *89*(1), 430–452.

Ault, A. P., Gaston, C. J., Wang, Y., Dominguez, G., Thiemens, M. H., & Prather, K. A. (2010). Characterization of the single particle mixing state of individual ship plume events measured at the port of Los Angeles. *Environmental Science & Technology*, *44*(6), 1954–1961.

Ault, A. P., Guasco, T. L., Baltrusaitis, J., Ryder, O. S., Trueblood, J. V., Collins, D. B., et al. (2014). Heterogeneous reactivity of nitric acid with nascent sea spray aerosol: Large differences observed between and within individual particles. *The Journal of Physical Chemistry Letters*, *5*(15), 2493–2500.

Ault, A. P., Guasco, T. L., Ryder, O. S., Baltrusaitis, J., Cuadra-Rodriguez, L. A., Collins, D. B., et al. (2013a). Inside versus outside: Ion redistribution in nitric acid reacted sea spray aerosol particles as determined by single particle analysis. *Journal of the American Chemical Society*, *135*(39), 14,528–14,531.

Ault, A. P., Moffet, R. C., Baltrusaitis, J., Collins, D. B., Ruppel, M. J., Cuadra-Rodriguez, L. A., et al. (2013b). Size-dependent changes in sea spray aerosol composition and properties with different seawater conditions. *Environmental Science & Technology*, *47*(11), 5603–5612.

Ault, A. P., Moore, M. J., Furutani, H., & Prather, K. A. (2009). Impact of emissions from the Los Angeles port region on San Diego air quality during regional transport events. *Environmental Science & Technology*, *43*(10), 3500–3506.

Ault, A. P., Peters, T. M., Sawvel, E. J., Casuccio, G. S., Willis, R. D., Norris, G. A., & Grassian, V. H. (2012). Single-particle SEM-EDX analysis of iron-containing coarse particulate matter in an urban environment: Sources and distribution of iron within Cleveland, Ohio. *Environmental Science & Technology*, *46*(8), 4331–4339.

Ault, A. P., Williams, C. R., White, A. B., Neiman, P. J., Creamean, J. M., Gaston, C. J., et al. (2011). Detection of Asian dust in California orographic precipitation. *Journal of Geophysical Research*, *116*, D16205. https://doi.org/10.1029/2010JD015351

Ault, A. P., Zhao, D., Ebben, C. J., Tauber, M. J., Geiger, F. M., Prather, K. A., & Grassian, V. H. (2013c). Raman microspectroscopy and vibrational sum frequency generation spectroscopy as probes of the bulk and surface compositions of size-resolved sea spray aerosol particles. *Physical Chemistry Chemical Physics*, *15*(17), 6206–6214.

Axson, J. L., Creamean, J. M., Bondy, A. L., Capracotta, S. S., Warner, K. Y., & Ault, A. P. (2014). An in situ method for sizing insoluble residues in precipitation and other aqueous samples. *Aerosol Science and Technology*, *49*, 24–34.

Axson, J. L., May, N. W., Colón-Bernal, I. D., Pratt, K. A., & Ault, A. P. (2016a). Lake spray aerosol: A chemical signature from individual ambient particles. *Environmental Science & Technology*, *50*(18), 9835–9845.

Axson, J. L., Shen, H., Bondy, A. L., Landry, C. C., Welz, J., Creamean, J. M., & Ault, A. P. (2016b). Transported mineral dust deposition case study at a hydrologically sensitive mountain site: Size and composition shifts in ambient aerosol and snowpack, Aerosol Air Qual. *Philosophy and Phenomenological Research*, *16*(3), 555–567.

Baltrusaitis, J., Jayaweera, P. M., & Grassian, V. H. (2009). XPS, study of nitrogen dioxide adsorption on metal oxide particle surfaces under different environmental conditions. *Physical Chemistry Chemical Physics*, *11*(37), 8295–8305.

Barger, W., & Garrett, W. (1970). Surface active organic material in the marine atmosphere. *Journal of Geophysical Research*, *75*(24), 4561–4566.

Bauer, S. E., Ault, A., & Prather, K. A. (2013). Evaluation of aerosol mixing state classes in the GISS modelE-MATRIX climate model using single-particle mass spectrometry measurements. *Journal of Geophysical Research: Atmospheres*, *118*, 9834–9844. https://doi.org/10.1002/jgrd.50700

Bauer, S., Wright, D., Koch, D., Lewis, E., McGraw, R., Chang, L.-S., et al. (2008). MATRIX, (Multiconfiguration Aerosol TRacker of mIXing state): An aerosol microphysical module for global atmospheric models. *Atmospheric Chemistry and Physics*, *8*(20), 6003–6035.

Baustian, K. J., Cziczo, D. J., Wise, M. E., Pratt, K. A., Kulkarni, G., Hallar, A., & Tolbert, M. A. (2012). Importance of aerosol composition, mixing state, and morphology for heterogeneous ice nucleation: A combined field and laboratory approach. *Journal of Geophysical Research*, *117*, D06217. https://doi.org/10.1029/2011JD016784

Bellouin, N., Boucher, O., Haywood, J., & Reddy, M. S. (2005). Global estimate of aerosol direct radiative forcing from satellite measurements. *Nature*, *438*(7071), 1138.

Beydoun, H., Polen, M., & Sullivan, R. C. (2017). A new multicomponent heterogeneous ice nucleation model and its application to Snomax bacterial particles and a Snomax–illite mineral particle mixture. *Atmospheric Chemistry and Physics*, *17*, 13,545–13,557.

Bhattu, D., & Tripathi, S. (2015). CCN, closure study: Effects of aerosol chemical composition and mixing state. *Journal of Geophysical Research: Atmospheres*, *120*, 766–783. https://doi.org/10.1002/2014JD021978

Bhave, P. V., Fergenson, D. P., Prather, K. A., & Cass, G. R. (2001). Source apportionment of fine particulate matter by clustering single-particle data: Tests of receptor model accuracy. *Environmental Science & Technology*, *35*(10), 2060–2072.

Bi, X., Zhang, G., Li, L., Wang, X., Li, M., Sheng, G., et al. (2011). Mixing state of biomass burning particles by single particle aerosol mass spectrometer in the urban area of PRD, China. *Atmospheric Environment*, *45*(20), 3447–3453.

Bigg, E., Ono, A., & Williams, J. A. (1974). Chemical tests for individual submicron aerosol particles. *Atmospheric Environment*, *8*(1), 1–13.

Binkowski, F. S., & Roselle, S. J. (2003). Models-3 Community Multiscale Air Quality (CMAQ) model aerosol component 1 Model description. *Journal of Geophysical Research*, *108*(D6), 4183. https://doi.org/10.1029/2001JD001409

Binkowski, F. S., & Shankar, U. (1995). The regional particulate matter model 1. Model description and preliminary results. *Journal of Geophysical Research*, *100*, 26,191–26,209.

Bogan, M. J., Starodub, D., Hampton, C. Y., & Sierra, R. G. (2010). Single-particle coherent diffractive imaging with a soft X-ray free electron laser: Towards soot aerosol morphology. *Journal of Physics B: Atomic Molecular and Optical Physics*, *43*(19), 194013.

Boman, C., Nordin, A., Boström, D., & Öhman, M. (2004). Characterization of inorganic particulate matter from residential combustion of pelletized biomass fuels. *Energy & Fuels*, *18*(2), 338–348.

Bond, T. C., & Bergstrom, R. W. (2006). Light absorption by carbonaceous particles: An investigative review. *Aerosol Science and Technology*, *40*(1), 27–67.

Bond, T. C., Doherty, S. J., Fahey, D. W., Forster, P. M., Berntsen, T., DeAngelo, B. J., et al. (2013). Bounding the role of black carbon in the climate system: A scientific assessment. *Journal of Geophysical Research: Atmospheres*, *118*, 5380–5552. https://doi.org/10.1002/jgrd.50171

Bond, T. C., Habib, G., & Bergstrom, R. W. (2006). Limitations in the enhancement of visible light absorption due to mixing state. *Journal of Geophysical Research*, *111*, D20211. https://doi.org/10.1029/2006JD007315

Bondy, A. L., Bonanno, D., Moffet, R. C., Wang, B., Laskin, A., & Ault, A. P. (2018). The diverse chemical mixing state of aerosol particles in the southeastern United States. *Atmospheric Chemistry and Physics*, *18*, 12,595–12,612. https://doi.org/10.5194/acp-18-12595-2018

Bondy, A. L., Craig, R. L., Zhang, Z., Gold, A., Surratt, J. D., & Ault, A. P. (2017a). Isoprene-derived organosulfates: Vibrational mode analysis by Raman spectroscopy, acidity-dependent spectral modes, and observation in individual atmospheric particles. *The Journal of Physical Chemistry A*, *122*, 303–315.

Bondy, A. L., Kirpes, R. M., Merzel, R. L., Pratt, K. A., Banaszak Holl, M. M., & Ault, A. P. (2017b). Atomic force microscopy-infrared spectroscopy of individual atmospheric aerosol particles: Subdiffraction limit vibrational spectroscopy and morphological analysis. *Analytical Chemistry*, *89*(17), 8594–8598.

Bondy, A. L., Wang, B., Laskin, A., Craig, R. L., Nhliziyo, M. V., Bertman, S. B., et al. (2017c). Inland sea spray aerosol transport and incomplete chloride depletion: Varying degrees of reactive processing observed during SOAS. *Environmental Science & Technology*, *51*(17), 9533–9542.

Boyer, H. C., & Dutcher, C. S. (2017). Atmospheric aqueous aerosol surface tensions: Isotherm-based modeling and biphasic microfluidic measurements. *The Journal of Physical Chemistry A*, *121*(25), 4733–4742.

Brands, M., Kamphus, M., Böttger, T., Schneider, J., Drewnick, F., Roth, A., et al. (2011). Characterization of a newly developed aircraft-based laser ablation aerosol mass spectrometer (ALABAMA) and first field deployment in urban pollution plumes over Paris during MEGAPOLI 2009. *Aerosol Science and Technology*, *45*(1), 46–64.

Broekhuizen, K., Chang, R.-W., Leaitch, W., Li, S.-M., & Abbatt, J. (2006). Closure between measured and modeled cloud condensation nuclei (CCN) using size-resolved aerosol compositions in downtown Toronto. *Atmospheric Chemistry and Physics*, *6*(9), 2513–2524.

Brook, R. D., Rajagopalan, S., Pope, C. A., Brook, J. R., Bhatnagar, A., Diez-Roux, A. V., et al. (2010). Particulate matter air pollution and cardiovascular disease: An update to the scientific statement from the American Heart Association. *Circulation*, *121*(21), 2331–2378.

Brooks, S. D., & Thornton, D. C. O. (2018). Marine aerosols and clouds. *Annual Review of Marine Science*, *10*, 289–313.

Buseck, P. R., & Pósfai, M. (1999). Airborne minerals and related aerosol particles: Effects on climate and the environment. *Proceedings of the National Academy of Sciences*, *96*(7), 3372–3379.

Bzdek, B. R., Pennington, M. R., & Johnston, M. V. (2012). Single particle chemical analysis of ambient ultrafine aerosol: A review. *Journal of Aerosol Science*, *52*, 109–120.

Bzdek, B. R., Power, R. M., Simpson, S. H., Reid, J. P., & Royall, C. P. (2016). Precise, contactless measurements of the surface tension of picolitre aerosol droplets. *Chemical Science*, *7*(1), 274–285.

Cappa, C. D., Onasch, T. B., Massoli, P., Worsnop, D. R., Bates, T. S., Cross, E. S., et al. (2012). Radiative absorption enhancements due to the mixing state of atmospheric black carbon. *Science*, *337*(6098), 1078–1081.

Carson, P. G., Neubauer, K. R., Johnston, M. V., & Wexler, A. S. (1995). On-line chemical analysis of aerosols by rapid single-particle mass spectrometry. *Journal of Aerosol Science*, *26*(4), 535–545.

Casuccio, G. S., Janocko, P. B., Lee, R. J., Kelly, J. F., Dattner, S. L., & Mgebroff, J. S. (1983). The use of computer controlled scanning electron microscopy in environmental studies. *Journal of the Air Pollution Control Association*, *33*(10), 937–943.

Casuccio, G. S., Schlaegle, S. F., Lersch, T. L., Huffman, G. P., Chen, Y., & Shah, N. (2004). Measurement of fine particulate matter using electron microscopy techniques. *Fuel processing technology*, *85*(6-7), 763–779.

Chen, B., Bai, Z., Cui, X., Chen, J., Andersson, A., & Gustafsson, Ö. (2017a). Light absorption enhancement of black carbon from urban haze in Northern China winter. *Environmental Pollution*, *221*, 418–426.

Chen, J., Li, C., Ristovski, Z., Milic, A., Gu, Y., Islam, M. S., et al. (2017b). A review of biomass burning: Emissions and impacts on air quality, health and climate in China. *Science of the Total Environment*, *579*, 1000–1034.

Cheng, Y., Berghof, M., Garland, R., Wiedensohler, A., Wehner, B., Müller, T., et al. (2009). Influence of soot mixing state on aerosol light absorption and single scattering albedo during air mass aging at a polluted regional site in northeastern China. *Journal of Geophysical Research*, *114*, D00G10. https://doi.org/10.1029/2008JD010883

Cheng, Y. F., Eichler, H., Wiedensohler, A., Heintzenberg, J., Zhang, Y. H., Hu, M., et al. (2006). Mixing state of elemental carbon and non-light-absorbing aerosol components derived from in situ particle optical properties at Xinken in Pearl River Delta of China. *Journal of Geophysical Research*, *111*, D20204. https://doi.org/10.1029/2005JD006929

China, S., Mazzoleni, C., Gorkowski, K., Aiken, A. C., & Dubey, M. K. (2013). Morphology and mixing state of individual freshly emitted wildfire carbonaceous particles. *Nature Communications*, *4*, 2122.

China, S., Scarnato, B., Owen, R. C., Zhang, B., Ampadu, M. T., Kumar, S., et al. (2015). Morphology and mixing state of aged soot particles at a remote marine free troposphere site: Implications for optical properties. *Geophysical Research Letters*, *42*, 1243–1250. https://doi.org/10.1002/2014GL062404

Ching, J., Fast, J., West, M., & Riemer, N. (2017). Metrics to quantify the importance of mixing state for CCN activity. *Atmospheric Chemistry and Physics*, *17*(12), 7445.

Ching, J., Riemer, N., & West, M. (2012). Impacts of black carbon mixing state on black carbon nucleation scavenging: Insights from a particle-resolved model. *Journal of Geophysical Research*, *117*, D23209. https://doi.org/10.1029/2012JD018269

Ching, J., Zaveri, R. A., Easter, R. C., Riemer, N., & Fast, J. D. (2016). A three-dimensional sectional representation of aerosol mixing state for simulating optical properties and cloud condensation nuclei. *Journal of Geophysical Research: Atmospheres*, *121*, 5912–5929. https://doi.org/10.1002/2015JD024323

Chung, S. H., & Seinfeld, J. H. (2005). Climate response of direct radiative forcing of anthropogenic black carbon. *Journal of Geophysical Research*, *110*, D11102. https://doi.org/10.1029/2004JD005441

Chýlek, P., Videen, G., Geldart, D. J. W., Dobbie, J. S., & Tso, H. C. W. (2000). Effective medium approximations for heterogeneous particles. In M. I. Mishchenko, & J. W. Hovenier (Eds.), *Light scattering by nonspherical particles: Theory, measurements, and applications*. Travis: Elsevier.

Cochran, R. E., Laskina, O., Trueblood, J. V., Estillore, A. D., Morris, H. S., Jayarathne, T., et al. (2017). Molecular diversity of sea spray aerosol particles: Impact of ocean biology on particle composition and hygroscopicity. *Chem*, *2*(5), 655–667.

Collins, D. B., Ault, A. P., Moffet, R. C., Ruppel, M. J., Cuadra-Rodriguez, L. A., Guasco, T. L., et al. (2013). Impact of marine biogeochemistry on the chemical mixing state and cloud forming ability of nascent sea spray aerosol. *Journal of Geophysical Research: Atmospheres*, *118*, 8553–8565. https://doi.org/10.1002/jgrd.50598

Conny, J. M., Collins, S. M., & Herzing, A. A. (2014). Qualitative multiplatform microanalysis of individual heterogeneous atmospheric particles from high-volume air samples. *Analytical Chemistry*, *86*(19), 9709–9716.

Cooke, W. F., & Wilson, J. N. (1996). A global black carbon aerosol model. *Journal of Geophysical Research*, *101*, 19,395–19,408.

Couvidat, F., & Sartelet, K. (2015). The Secondary Organic Aerosol Processor (SOAP v1. 0,) model: A unified model with different ranges of complexity based on the molecular surrogate approach. *Geoscientific Model Development*, *8*(4), 1111–1138.

Coz, E., Artíñano, B., Clark, L. M., Hernandez, M., Robinson, A. L., Casuccio, G. S., et al. (2010). Characterization of fine primary biogenic organic aerosol in an urban area in the northeastern United States. *Atmospheric Environment*, *44*(32), 3952–3962.

Coz, E., Gómez-Moreno, F. J., Pujadas, M., Casuccio, G. S., Lersch, T. L., & Artíñano, B. (2009). Individual particle characteristics of North African dust under different long-range transport scenarios. *Atmospheric Environment*, *43*(11), 1850–1863.

Craig, R. L., & Ault, A. P. (2018). Aerosol Acidity: Direct Measurement from a Spectroscopic Method. In S. W. Hunt, A. Laskin, & S. A. Nizkorodov (Eds.), *Multiphase Environmental Chemistry in the Atmosphere, ACS Symposium Series, 1299* (pp. 171–191). https://doi.org/10.1021/bk-2018-1299.ch009

Craig, R. L., Bondy, A. L., & Ault, A. P. (2015). Surface enhanced Raman spectroscopy enables observations of previously undetectable secondary organic aerosol components at the individual particle level. *Analytical Chemistry*, *87*(15), 7510–7514.

Craig, R. L., Bondy, A. L., & Ault, A. P. (2017a). Computer-controlled Raman microspectroscopy (CC-Raman): A method for the rapid characterization of individual atmospheric aerosol particles. *Aerosol Science and Technology*, *51*(9), 1099–1112.

Craig, R. L., Nandy, L., Axson, J. L., Dutcher, C. S., & Ault, A. P. (2017b). Spectroscopic determination of aerosol pH from acid–base equilibria in inorganic, organic, and mixed systems. *The Journal of Physical Chemistry A*, *121*(30), 5690–5699.

Creamean, J. M., Ault, A. P., Ten Hoeve, J. E., Jacobson, M. Z., Roberts, G. C., & Prather, K. A. (2011). Measurements of aerosol chemistry during new particle formation events at a remote rural mountain site. *Environmental Science & Technology*, *45*(19), 8208–8216.

Creamean, J. M., Ault, A. P., White, A. B., Neiman, P. J., Ralph, F. M., Minnis, P., & Prather, K. A. (2015). Impact of interannual variations in sources of insoluble aerosol species on orographic precipitation over California's central Sierra Nevada. *Atmospheric Chemistry and Physics*, *15*(11), 6535–6548.

Creamean, J. M., Axson, J. L., Bondy, A. L., Craig, R. L., May, N. W., Shen, H., et al. (2016). Changes in precipitating snow chemistry with location and elevation in the California Sierra Nevada. *Journal of Geophysical Research: Atmospheres*, *121*, 7296–7309. https://doi.org/10.1002/2015JD024700

Creamean, J. M., Lee, C., Hill, T. C., Ault, A. P., DeMott, P. J., White, A. B., et al. (2014). Chemical properties of insoluble precipitation residue particles. *Journal of Aerosol Science*, *76*, 13–27.

Creamean, J. M., Suski, K. J., Rosenfeld, D., Cazorla, A., DeMott, P. J., Sullivan, R. C., et al. (2013). Dust and biological aerosols from the Sahara and Asia influence precipitation in the Western US. *Science*, *339*(6127), 1572–1578.

Cruz, C. N., & Pandis, S. N. (1997). A study of the ability of pure secondary organic aerosol to act as cloud condensation nuclei. *Atmospheric Environment*, *31*(15), 2205–2214.
Cubison, M., Ervens, B., Feingold, G., Docherty, K., Ulbrich, I., Shields, L., et al. (2008). The influence of chemical composition and mixing state of Los Angeles urban aerosol on CCN number and cloud properties. *Atmospheric Chemistry and Physics*, *8*(18), 5649–5667.
Curtis, J. H., Riemer, N., & West, M. (2017). A single-column particle-resolved model for simulating the vertical distribution of aerosol mixing state: WRF-PartMC-MOSAIC-SCM v1.0. *Geoscientific Model Development*, *10*(11), 4057.
Cwiertny, D. M., Young, M. A., & Grassian, V. H. (2008). Chemistry and photochemistry of mineral dust aerosol. *Annual Review of Physical Chemistry*, *59*, 27–51.
Cziczo, D. J., Froyd, K. D., Gallavardin, S. J., Moehler, O., Benz, S., Saathoff, H., & Murphy, D. M. (2009). Deactivation of ice nuclei due to atmospherically relevant surface coatings. *Environmental Research Letters*, *4*(4), 44013.
Dall'Osto, M., Drewnick, F., Fisher, R., & Harrison, R. M. (2012). Real-time measurements of nonmetallic fine particulate matter adjacent to a major integrated steelworks. *Aerosol Science and Technology*, *46*(6), 639–653.
Dall'Osto, M., Harrison, R. M., Highwood, E. J., O'Dowd, C., Ceburnis, D., Querol, X., & Achterberg, E. P. (2010). Variation of the mixing state of Saharan dust particles with atmospheric transport. *Atmospheric Environment*, *44*(26), 3135–3146.
David, G., Esat, K., Hartweg, S., Cremer, J., Chasovskikh, E., & Signorell, R. (2015). Stability of aerosol droplets in bessel beam optical traps under constant and pulsed external forces. *The Journal of Chemical Physics*, *142*(15), 154506.
David, G., Esat, K., Ritsch, I., & Signorell, R. (2016). Ultraviolet broadband light scattering for optically-trapped submicron-sized aerosol particles. *Physical Chemistry Chemical Physics*, *18*(7), 5477–5485.
Davies, J. F., & Wilson, K. R. (2016). Raman spectroscopy of isotopic water diffusion in ultraviscous, glassy, and gel states in aerosol by use of optical tweezers. *Analytical Chemistry*, *88*(4), 2361–2366.
Davis, W. (1973). Surface ionization mass spectroscopy of airborne particulates (Ph.D. thesis), AVS.
De Santiago, A., Longo, A. F., Ingall, E. D., Diaz, J. M., King, L. E., Lai, B., et al. (2014). Characterization of selenium in ambient aerosols and primary emission sources. *Environmental Science & Technology*, *48*(16), 8988–8994.
DeCarlo, P. F., Slowik, J. G., Worsnop, D. R., Davidovits, P., & Jimenez, J. L. (2004). Particle morphology and density characterization by combined mobility and aerodynamic diameter measurements. Part 1: Theory. *Aerosol Science and Technology*, *38*(12), 1185–1205.
DeMott, P. J., Hill, T. C., McCluskey, C. S., Prather, K. A., Collins, D. B., Sullivan, R. C., et al. (2016). Sea spray aerosol as a unique source of ice nucleating particles. *Proceedings of the National Academy of Sciences*, *113*(21), 5797–5803.
DeMott, P. J., Möhler, O., Stetzer, O., Vali, G., Levin, Z., Petters, M. D., et al. (2011). Resurgence in ice nuclei measurement research. *Bulletin of the American Meteorological Society*, *92*, 1623–1635.
DeMott, P. J., Prenni, A. J., Liu, X., Kreidenweis, S. M., Petters, M. D., Twohy, C. H., et al. (2010). Predicting global atmospheric ice nuclei distributions and their impacts on climate. *Proceedings of the National Academy of Sciences*, *107*(25), 11,217–11,222.
Deboudt, K., Flament, P., Choël, M., Gloter, A., Sobanska, S., & Colliex, C. (2010). Mixing state of aerosols and direct observation of carbonaceous and marine coatings on African dust by individual particle analysis. *Journal of Geophysical Research*, *115*, D24207. https://doi.org/10.1029/2010JD013921
Deboudt, K., Gloter, A., Mussi, A., & Flament, P. (2012). Red-ox speciation and mixing state of iron in individual African dust particles. *Journal of Geophysical Research*, *117*, D12307. https://doi.org/10.1029/2011JD017298
Decesari, S., Finessi, E., Rinaldi, M., Paglione, M., Fuzzi, S., Stephanou, E., et al. (2011). Primary and secondary marine organic aerosols over the North Atlantic ocean during the MAP experiment. *Journal of Geophysical Research*, *116*, D22210. https://doi.org/10.1029/2011JD016204
Deng, C., Brooks, S. D., Vidaurre, G., & Thornton, D. C. (2014). Using Raman microspectroscopy to determine chemical composition and mixing state of airborne marine aerosols over the Pacific ocean. *Aerosol Science and Technology*, *48*(2), 193–206.
Denkenberger, K. A., Moffet, R. C., Holecek, J. C., Rebotier, T. P., & Prather, K. A. (2007). Real-time, single-particle measurements of oligomers in aged ambient aerosol particles. *Environmental Science & Technology*, *41*(15), 5439–5446.
Dey, S., Tripathi, S., & Mishra, S. (2008). Probable mixing state of aerosols in the Indo-Gangetic Basin, northern India. *Geophysical Research Letters*, *35*, L03808. https://doi.org/10.1029/2007GL032622
Dickau, M., Olfert, J., Stettler, M. E. J., Boies, A., Momenimovahed, A., Thomson, K., et al. (2016). Methodology for quantifying the volatile mixing state of an aerosol. *Aerosol Science and Technology*, *50*(8), 759–772. https://doi.org/10.1080/02786826.2016.1185509
Doughty, D. C., & Hill, S. C. (2017). Automated aerosol Raman spectrometer for semi-continuous sampling of atmospheric aerosol. *Journal of Quantitative Spectroscopy and Radiative Transfer*, *188*, 103–117.
Draine, B. T., & Flatau, P. J. (1994). Discrete-dipole approximation for scattering calculations. *JOSA A*, *11*(4), 1491–1499.
Drewnick, F., Dall'Osto, M., & Harrison, R. (2008). Characterization of aerosol particles from grass mowing by joint deployment of ToF-AMS and ATOFMS instruments. *Atmospheric Environment*, *42*(13), 3006–3017.
Drucker, J. (2013). Industrial structure and the sources of agglomeration economies: Evidence from manufacturing plant production. *Growth Change*, *44*(1), 54–91. https://doi.org/10.1111/grow.12002
Dufour, L. (1862). Über das Gefrieren des Wassers und über die Bildung des Hagels. *Annalen der Physik*, *190*, 530–554.
Dusek, U., Frank, G., Hildebrandt, L., Curtius, J., Schneider, J., Walter, S., et al. (2006). Size matters more than chemistry for cloud-nucleating ability of aerosol particles. *Science*, *312*(5778), 1375–1378.
Ebben, C. J., Ault, A. P., Ruppel, M. J., Ryder, O. S., Bertram, T. H., Grassian, V. H., et al. (2013). Size-resolved sea spray aerosol particles studied by vibrational sum frequency generation. *The Journal of Physical Chemistry A*, *117*(30), 6589–6601.
Ebben, C., Martinez, I., Shrestha, M., Buchbinder, A., Corrigan, A., Guenther, A., et al. (2011). Contrasting organic aerosol particles from boreal and tropical forests during HUMPPA-COPEC-2010 and AMAZE-08 using coherent vibrational spectroscopy. *Atmospheric Chemistry and Physics*, *11*(20), 10,317–10,329.
Ebben, C. J., Shrestha, M., Martinez, I. S., Corrigan, A. L., Frossard, A. A., Song, W. W., et al. (2012). Organic constituents on the surfaces of aerosol particles from Southern Finland, Amazonia, and California studied by vibrational sum frequency generation. *The Journal of Physical Chemistry A*, *116*(32), 8271–8290.
Ebben, C. J., Strick, B. F., Upshur, M. A., Chase, H. M., Achtyl, J. L., Thomson, R. J., & Geiger, F. M. (2014). Towards the identification of molecular constituents associated with the surfaces of isoprene-derived secondary organic aerosol (SOA) particles. *Atmospheric Chemistry and Physics*, *14*(5), 2303–2314.
Efendiev, Y., & Zachariah, M. (2002). Hybrid Monte Carlo method for simulation of two-component aerosol coagulation and phase segregation. *Journal of Colloid and Interface Science*, *249*(1), 30–43.
Encyclopædia Britannica (2018). Morphology. Britannica Academic, accessed 19th June 2018.

Ervens, B., Cubison, M., Andrews, E., Feingold, G., Ogren, J., Jimenez, J., et al. (2010). CCN, predictions using simplified assumptions of organic aerosol composition and mixing state: A synthesis from six different locations. *Atmospheric Chemistry and Physics*, *10*(10), 4795–4807.

Ervens, B., & Feingold, G. (2012). On the representation of immersion and condensation freezing in cloud models using different nucleation schemes. *Atmospheric Chemistry and Physics*, *12*, 5807–5826.

Facchini, M. C., Mircea, M., Fuzzi, S., & Charlson, R. J. (1999). Cloud albedo enhancement by surface-active organic solutes in growing droplets. *Nature*, *401*(6750), 257.

Falush, D., Stephens, M., & Pritchard, J. K. (2007). Inference of population structure using multilocus genotype data: Dominant markers and null alleles. *Molecular Ecology Notes*, *7*(4), 574–578. https://doi.org/10.1111/j.1471-8286.2007.01758.x

Farmer, D. K., Cappa, C. D., & Kreidenweis, S. M. (2015). Atmospheric processes and their controlling influence on cloud condensation nuclei activity. *Chemical Reviews*, *115*(10), 4199–4217.

Fierce, L., Bond, T. C., Bauer, S. E., Mena, F., & Riemer, N. (2016). Black carbon absorption at the global scale is affected by particle-scale diversity in composition. *Nature Communications*, *7*(12), 361.

Fierce, L., Riemer, N., & Bond, T. C. (2015). Explaining variance in black carbon's aging timescale. *Atmospheric Chemistry and Physics*, *15*(6), 3173–3191.

Fierce, L., Riemer, N., & Bond, T. C. (2017). Toward reduced representation of mixing state for simulating aerosol effects on climate. *Bulletin of the American Meteorological Society*, *98*(5), 971–980.

Findeisen, W. (1938). Kolloid-meteorologische Vorgänge bei Niederschlagsbildung. *Meteorologische Zeitschrift*, *55*, 121–133.

Fitzgerald, E., Ault, A. P., Zauscher, M. D., Mayol-Bracero, O. L., & Prather, K. A. (2015). Comparison of the mixing state of long-range transported Asian and African mineral dust. *Atmospheric Environment*, *115*, 19–25.

Fletcher, R. A., Ritchie, N. W., Anderson, I. M., & Small, J. A. (2011). Microscopy and microanalysis of individual collected particles. In P. Kulkarni, P. A. Baron, & K. Willeke (Eds.), *Aerosol measurement: Principles, Techniques, and Applications*, (pp. 179–232). Hoboken, NJ: Wiley.

Fofie, E., Donahue, N., & Asa-Awuku, A. (2018). Cloud condensation nuclei activity and droplet formation of primary and secondary organic aerosol mixtures. *Aerosol Science and Technology*, *52*(2), 242–251.

Fraund, M., Pham, D. Q., Bonanno, D., Harder, T. H., Wang, B., Brito, J., et al. (2017). Elemental mixing state of aerosol particles collected in Central Amazonia during GoAmazon 2014/15. *Atmosphere*, *8*(9), 173.

Freedman, M. A. (2017). Phase separation in organic aerosol. *Chemical Society Reviews*, *46*(24), 7694–7705.

Friedlander, S. K. (1977). *Smoke, dust and haze: Fundamentals of aerosol behavior*, vol. 1977, pp. 333. New York: Wiley-Interscience.

Fröhlich-Nowoisky, J., Kampf, C. J., Weber, B., Huffman, J. A., Pöhlker, C., Andreae, M. O., et al. (2016). Bioaerosols in the Earth system: Climate, health, and ecosystem interactions. *Atmospheric Research*, *182*, 346–376.

Frossard, A. A., Russell, L. M., Burrows, S. M., Elliott, S. M., Bates, T. S., & Quinn, P. K. (2014). Sources and composition of submicron organic mass in marine aerosol particles. *Journal of Geophysical Research: Atmospheres*, *119*, 12,977–13,003. https://doi.org/10.1002/2014JD021913

Fuchs, N. (1964). *The mechanics of aerosols*. New York: Pagamon.

Fuller, K. A., Malm, W. C., & Kreidenweis, S. M. (1999). Effects of mixing on extinction by carbonaceous particles. *Journal of Geophysical Research*, *104*(D13), 15,941–15,954.

Furutani, H., Dall'osto, M., Roberts, G. C., & Prather, K. A. (2008). Assessment of the relative importance of atmospheric aging on CCN activity derived from field observations. *Atmospheric Environment*, *42*(13), 3130–3142.

Gabey, A., Gallagher, M., Whitehead, J., Dorsey, J., Kaye, P. H., & Stanley, W. (2010). Measurements and comparison of primary biological aerosol above and below a tropical forest canopy using a dual channel fluorescence spectrometer. *Atmospheric Chemistry and Physics*, *10*(10), 4453–4466.

Gaffney, J. S., Marley, N. A., & Smith, K. J. (2015). Characterization of fine mode atmospheric aerosols by Raman microscopy and diffuse reflectance FTIR. *The Journal of Physical Chemistry A*, *119*(19), 4524–4532.

Gao, R., Schwarz, J., Kelly, K., Fahey, D., Watts, L., Thompson, T., et al. (2007). A novel method for estimating light-scattering properties of soot aerosols using a modified single-particle soot photometer. *Aerosol Science and Technology*, *41*(2), 125–135.

Gard, E. E., Kleeman, M. J., Gross, D. S., Hughes, L. S., Allen, J. O., Morrical, B. D., et al. (1998). Direct observation of heterogeneous chemistry in the atmosphere. *Science*, *279*(5354), 1184–1187.

Gard, E., Mayer, J. E., Morrical, B. D., Dienes, T., Fergenson, D. P., & Prather, K. A. (1997). Real-time analysis of individual atmospheric aerosol particles: Design and performance of a portable ATOFMS. *Analytical Chemistry*, *69*(20), 4083–4091.

Gaston, C. J., Pratt, K. A., Qin, X., & Prather, K. A. (2010). Real-time detection and mixing state of methanesulfonate in single particles at an inland urban location during a phytoplankton bloom. *Environmental Science & Technology*, *44*(5), 1566–1572.

Gen, M., & Chan, C. K. (2017). Electrospray surface-enhanced Raman spectroscopy (ES-SERS) for probing surface chemical compositions of atmospherically relevant particles. *Atmospheric Chemistry and Physics*, *17*(22), 14,025–14,037.

Geng, H., Hwang, H., Liu, X., Dong, S., & Ro, C.-U. (2014). Investigation of aged aerosols in size-resolved Asian dust storm particles transported from Beijing, China, to Incheon, Korea, using low-Z particle EPMA. *Atmospheric Chemistry and Physics*, *14*(7), 3307.

George, C., Ammann, M., D'Anna, B., Donaldson, D., & Nizkorodov, S. A. (2015). Heterogeneous photochemistry in the atmosphere. *Chemical Reviews*, *115*(10), 4218–4258.

Gerber, H., Hoppel, W., & Wojciechowski, T. (1977). Experimental verification of the theoretical relationship between size and critical supersaturation of salt nuclei. *Journal of the Atmospheric Sciences*, *34*(11), 1836–1841.

Ghorai, S., Laskin, A., & Tivanski, A. V. (2011). Spectroscopic evidence of keto-enol tautomerism in deliquesced malonic acid particles. *The Journal of Physical Chemistry A*, *115*(17), 4373–4380.

Ghorai, S., Wang, B., Tivanski, A., & Laskin, A. (2014). Hygroscopic properties of internally mixed particles composed of NaCl and water-soluble organic acids. *Environmental Science & Technology*, *48*(4), 2234–2241.

Gillespie, D. T. (1972). The stochastic coalescence model for cloud droplet growth. *Journal of the Atmospheric Sciences*, *29*, 1496–1510.

Gillespie, D. T. (1975). An exact method for numerically simulating the stochastic coalescence process in a cloud. *Journal of the Atmospheric Sciences*, *32*, 1977–1989.

Gillespie, D. T. (1976). A general method for numerically simulating the stochastic time evolution of coupled chemical reactions. *Journal of Computational Physics*, *22*, 403–434.

Gillespie, D. T. (1977). Exact stochastic simulation of coupled chemical reactions. *Journal of Physical Chemistry*, *81*, 2340–2361. https://doi.org/10.1021/j100540a008

Gillespie, D. T (1992). *Markov processes: An introduction for physical scientists*: Academic Press.

Gillespie, D. T. (2007). Stochastic simulation of chemical kinetics. *Annual Review of Physical Chemistry*, *58*, 35–55. https://doi.org/10.1146/annurev.physchem.58.032806.104637

Glasius, M., & Goldstein, A. H. (2016). Recent discoveries and future challenges in atmospheric organic chemistry. *Environmental Science & Technology*, *50*, 2754–2764.

Grell, G. A., Peckham, S. E., Schmitz, R., & McKeen, S. A. (2005). Fully coupled online chemistry within the WRF model. *Atmospheric Environment*, *39*, 6957–6975.

Gross, D. S., Atlas, R., Rzeszotarski, J., Turetsky, E., Christensen, J., Benzaid, S., et al. (2010). Environmental chemistry through intelligent atmospheric data analysis. *Environmental Modelling & Software*, *25*(6), 760–769.

Gross, D. S., Galli, M. E., Silva, P. J., Wood, S. H., Liu, D.-Y., & Prather, K. A. (2000). Single particle characterization of automobile and diesel truck emissions in the Caldecott Tunnel. *Aerosol Science & Technology*, *32*(2), 152–163.

Guascito, M. R., Cesari, D., Chirizzi, D., Genga, A., & Contini, D. (2015). XPS, surface chemical characterization of atmospheric particles of different sizes. *Atmospheric Environment*, *116*, 146–154.

Guazzotti, S. A., Coffee, K. R., & Prather, K. A. (2001a). Continuous measurements of size-resolved particle chemistry during INDOEX-Intensive Field Phase 99. *Journal of Geophysical Research*, *106*(D22), 28,607–28,627.

Guazzotti, S. A., Whiteaker, J. R., Suess, D., Coffee, K. R., & Prather, K. A. (2001b). Real-time measurements of the chemical composition of size-resolved particles during a Santa Ana wind episode, California USA. *Atmospheric Environment*, *35*(19), 3229–3240.

Gunsch, M. J., Kirpes, R. M., Kolesar, K. R., Barrett, T. E., China, S., Sheesley, R. J., et al. (2017). Contributions of transported Prudhoe Bay oil field emissions to the aerosol population in Utqiaġvik, Alaska. *Atmospheric Chemistry and Physics*, *17*(17), 10,879–10,892.

Gunsch, M. J., May, N. W., Wen, M., Bottenus, C. L., Gardner, D. J., VanReken, T. M., et al. (2018). Ubiquitous influence of wildfire emissions and secondary organic aerosol on summertime atmospheric aerosol in the forested Great Lakes region. *Atmospheric Chemistry and Physics*, *18*(5), 3701–3715.

Gunthe, S., King, S., Rose, D., Chen, Q., Roldin, P., Farmer, D., et al. (2009). Cloud condensation nuclei in pristine tropical rainforest air of Amazonia: Size-resolved measurements and modeling of atmospheric aerosol composition and CCN activity. *Atmospheric Chemistry and Physics*, *9*, 7551–7575.

Hallquist, M., Wenger, J., Baltensperger, U., Rudich, Y., Simpson, D., Claeys, M., et al. (2009). The formation, properties and impact of secondary organic aerosol: Current and emerging issues. *Atmospheric chemistry and physics*, *9*(14), 5155–5236.

Hansen, A., Rosen, H., & Novakov, T. (1984). The aethalometer—An instrument for the real-time measurement of optical absorption by aerosol particles. *Science of the Total Environment*, *36*, 191–196.

Hatch, L. E., Creamean, J. M., Ault, A. P., Surratt, J. D., Chan, M. N., Seinfeld, J. H., et al. (2011a). Measurements of isoprene-derived organosulfates in ambient aerosols by aerosol time-of-flight mass spectrometry—Part 1: Single particle atmospheric observations in Atlanta. *Environmental Science & Technology*, *45*(12), 5105–5111.

Hatch, L. E., Creamean, J. M., Ault, A. P., Surratt, J. D., Chan, M. N., Seinfeld, J. H., et al. (2011b). Measurements of isoprene-derived organosulfates in ambient aerosols by aerosol time-of-flight mass spectrometry—Part 2: Temporal variability and formation mechanisms. *Environmental Science & Technology*, *45*(20), 8648–8655.

Hatch, C. D., Gierlus, K. M., Schuttlefield, J. D., & Grassian, V. H. (2008). Water adsorption and cloud condensation nuclei activity of calcite and calcite coated with model humic and fulvic acids. *Atmospheric Environment*, *42*(22), 5672–5684.

Hatch, C. D., Gierlus, K. M., Zahardis, J., Schuttlefield, J., & Grassian, V. H. (2009). Water uptake of humic and fulvic acid: Measurements and modelling using single parameter Köhler theory. *Environmental Chemistry*, *6*(5), 380–388.

Hawkins, L. N., & Russell, L. M. (2010). Polysaccharides, proteins, and phytoplankton fragments: Four chemically distinct types of marine primary organic aerosol classified by single particle spectromicroscopy. *Advances in Meteorology*, *2010*, 612132.

He, C., Liou, K.-N., Takano, Y., Zhang, R., Levy Zamora, M., Yang, P., et al. (2015). Variation of the radiative properties during black carbon aging: Theoretical and experimental intercomparison. *Atmospheric Chemistry and Physics*, *15*(20), 11,967–11,980.

Healy, R., Riemer, N., Wenger, J., Murphy, M., West, M., Poulain, L., et al. (2014). Single particle diversity and mixing state measurements. *Atmospheric Chemistry and Physics*, *14*(12), 6289–6299.

Healy, R. M., Sciare, J., Poulain, L., Crippa, M., Wiedensohler, A., Prévôt, A. S., et al. (2013). Quantitative determination of carbonaceous particle mixing state in Paris using single-particle mass spectrometer and aerosol mass spectrometer measurements. *Atmospheric Chemistry and Physics*, *13*(18), 9479–9496.

Heard, M., & Wiffen, R. (1969). Electron microscopy of natural aerosols and the identification of particulate ammonium sulphate. *Atmospheric Environment*, *3*(3), 337–340.

Heintzenberg, J., & Charlson, R. J. (1996). Design and applications of the integrating nephelometer: A review. *Journal of Atmospheric and Oceanic Technology*, *13*(5), 987–1000.

Hentschel, M. L., & Page, N. W. (2003). Selection of descriptors for particle shape characterization. *Particle & Particle Systems Characterization*, *20*(1), 25–38.

Hersey, S. P., Craven, J. S., Metcalf, A. R., Lin, J., Lathem, T., Suski, K. J., et al. (2013). Composition and hygroscopicity of the Los Angeles aerosol: CalNex. *Journal of Geophysical Research: Atmospheres*, *118*, 3016–3036. https://doi.org/10.1002/jgrd.50307

Hinds, W. C. (1999). *Aerosol technology: Properties, behavior, and measurement of airborne particles*. New York: John Wiley.

Hinz, K.-P., Kaufmann, R., & Spengler, B. (1994). Laser-induced mass analysis of single particles in the airborne state. *Analytical Chemistry*, *66*(13), 2071–2076.

Hinz, K.-P., Kaufmann, R., & Spengler, B. (1996). Simultaneous detection of positive and negative ions from single airborne particles by real-time laser mass spectrometry. *Aerosol Science and Technology*, *24*(4), 233–242.

Holmgren, H., Sellegri, K., Hervo, M., Rose, C., Freney, E., Villani, P., & Laj, P. (2014). Hygroscopic properties and mixing state of aerosol measured at the high-altitude site Puy de Dôme (1465 m asl), france. *Atmospheric Chemistry and Physics*, *14*(18), 9537–9554.

Hoose, C., Kristjánsson, J. E., Chen, J.-P., & Hazra, A. (2010). A classical-theory-based parameterization of heterogeneous ice nucleation by mineral dust, soot, and biological particles in a global climate model. *Journal of the Atmospheric Sciences*, *67*(8), 2483–2503.

Hoose, C., & Möhler, O. (2012). Heterogeneous ice nucleation on atmospheric aerosols: A review of results from laboratory experiments. *Atmospheric Chemistry and Physics*, *12*, 9817–9854.

Hopkins, R. J., Desyaterik, Y., Tivanski, A. V., Zaveri, R. A., Berkowitz, C. M., Tyliszczak, T., et al. (2008). Chemical speciation of sulfur in marine cloud droplets and particles: Analysis of individual particles from the marine boundary layer over the California current. *Journal of Geophysical Research*, *113*, D04209. https://doi.org/10.1029/2007JD008954

Hopkins, R. J., Mitchem, L., Ward, A. D., & Reid, J. P. (2004). Control and characterisation of a single aerosol droplet in a single-beam gradient-force optical trap. *Physical Chemistry Chemical Physics*, *6*(21), 4924–4927.

Hudson, J. G. (1989). An instantaneous CCN spectrometer. *Journal of Atmospheric and Oceanic Technology*, *6*(6), 1055–1065.

Hudson, P. K., Murphy, D. M., Cziczo, D. J., Thomson, D. S., De Gouw, J. A., Warneke, C., et al. (2004). Biomass-burning particle measurements: Characteristic composition and chemical processing. *Journal of Geophysical Research*, *109*, D23S27. https://doi.org/10.1029/2003JD004398

Huffman, D. R., Swanson, B. E., & Huffman, J. A. (2016). A wavelength-dispersive instrument for characterizing fluorescence and scattering spectra of individual aerosol particles on a substrate. *Atmospheric Measurement Techniques*, *9*(8), 3987.

Hughes, M., Kodros, J. K., Pierce, J. R., West, M., & Riemer, N. (2018). Machine learning to predict the global distribution of aerosol mixing state metrics. *Atmosphere*, *9*(1), 15.

Hulburt, H. M., & Katz, S. (1964). Some problems in particle technology: A statistical mechanical formulation. *Chemical Engineering Science*, *19*(8), 555–574.

Jacobson, M. Z. (2000). Physically-based treatment of elemental carbon optics: Implications for global direct forcing of aerosols. *Geophysical Research Letters*, *27*(2), 217–220.

Jacobson, M. Z. (2001). Strong radiative heating due to the mixing state of black carbon in atmospheric aerosols. *Nature*, *409*(6821), 695–697.

Jacobson, M. Z. (2002). Analysis of aerosol interactions with numerical techniques for solving coagulation, nucleation, condensation, dissolution, and reversible chemistry among multiple size distributions. *Journal of Geophysical Research*, *107*, 4366. https://doi.org/10.1029/2001JD002044

Jubb, A. M., Hua, W., & Allen, H. C. (2012). Environmental chemistry at vapor/water interfaces: Insights from vibrational sum frequency generation spectroscopy. *Annual Review of Physical Chemistry*, *63*, 107–130.

Jung, H.-J., Eom, H.-J., Kang, H.-W., Moreau, M., Sobanska, S., & Ro, C.-U. (2014). Combined use of quantitative ED-EPMA, Raman microspectrometry, and ATR-FTIR imaging techniques for the analysis of individual particles. *The Analyst*, *139*(16), 3949–3960.

Junge, C. E. (1952). Die Konstitution des atmosphärischen Aerosols. *Annalen der Meteorologie*, *5*, 1–55.

Jurányi, Z., Tritscher, T., Gysel, M., Laborde, M., Gomes, L., Roberts, G., et al. (2013). Hygroscopic mixing state of urban aerosol derived from size-resolved cloud condensation nuclei measurements during the MEGAPOLI campaign in Paris. *Atmospheric Chemistry and Physics*, *13*(13), 6431–6446.

Kahnert, M., Nousiainen, T., Lindqvist, H., & Ebert, M. (2012). Optical properties of light absorbing carbon aggregates mixed with sulfate: Assessment of different model geometries for climate forcing calculations. *Optics Express*, *20*(9), 10,042–10,058.

Kaiser, J. C., Hendricks, J., Righi, M., RIemer, N., Zaveri, R. A., Metzger, S., & Aquila, V. (2014). The MESSy aerosol submodel MADE3 (v2.0b): Description and a box model test. *Geoscientific Model Development*, *7*, 1137–1157.

Kalashnikova, O. V., & Sokolik, I. N. (2002). Importance of shapes and compositions of wind-blown dust particles for remote sensing at solar wavelengths. *Geophysical Research Letters*, *29*(10), 1398. https://doi.org/10.1029/2002GL014947

Kanaani, H., Hargreaves, M., Ristovski, Z., & Morawska, L. (2007). Performance assessment of UVAPS: Influence of fungal spore age and air exposure. *Journal of Aerosol Science*, *38*(1), 83–96.

Kandler, K., & Schütz, L. (2007). Climatology of the average water-soluble volume fraction of atmospheric aerosol. *Atmospheric Research*, *83*(1), 77–92.

Kandler, K., Schütz, L., Jäckel, S., Lieke, K., Emmel, C., Müller-Ebert, D., et al. (2011). Ground-based off-line aerosol measurements at Praia, Cape Verde, during the Saharan Mineral Dust Experiment: Microphysical properties and mineralogy. *Tellus B*, *63*(4), 459–474.

Kanji, Z. A., Ladino, L. A., Wex, H., Boose, Y., Burkert-Kohn, M., Cziczo, D. J., & Krämer, M. (2017). Overview of ice nucleating particles. *Meteorological Monographs*, *58*, 1–1.

Katrinak, K. A., Rez, P., Perkes, P. R., & Buseck, P. R. (1993). Fractal geometry of carbonaceous aggregates from an urban aerosol. *Environmental Science & Technology*, *27*(3), 539–547.

Katz, U., & Kocmond, W. (1973). An investigation of the size-supersaturation relationship of soluble condensation nuclei. *Journal of the Atmospheric Sciences*, *30*(1), 160–165.

Kaufmann, R. (1986). Laser-microprobe mass spectroscopy (LAMMA) of particulate matter. In K. R. Spurny (Ed.), *Physical and chemical characterization of individual airborne particles* (pp. 233–237). Chichester, UK: Ellis & Horwood Ltd.

Khalizov, A. F., Xue, H., Wang, L., Zheng, J., & Zhang, R. (2009). Enhanced light absorption and scattering by carbon soot aerosol internally mixed with sulfuric acid. *The Journal of Physical Chemistry A*, *113*(6), 1066–1074.

Kim, D., Hopke, P., Massart, D., Kaufman, L., & Casuccio, G. (1987). Multivariate analysis of CCSEM auto emission data. *Science of the Total Environment*, *59*, 141–155.

Kirpes, R. M., Bondy, A. L., Bonanno, D., Moffet, R. C., Wang, B., Laskin, A., et al. (2018). Secondary sulfate is internally mixed with sea spray aerosol and organic aerosol in the winter arctic. *Atmospheric Chemistry and Physics*, *18*(6), 3937–3949.

Klaus, N. (1986). *Aerosol analysis by secondary-ion mass spectrometry*. Chichester: Ellis Horwood Limited.

Kleeman, M. J., & Cass, G. R. (2001). A 3D Eulerian source-oriented model for an externally mixed aerosol. *Environmental Science & Technology*, *35*(24), 4834–4848.

Knopf, D. A., & Alpert, P. A. (2013). A water activity based model of heterogeneous ice nucleation kinetics for freezing of water and aqueous solution droplets. *Faraday Discussions*, *165*, 513–534.

Knopf, D. A., Alpert, P. A., & Wang, B. (2018). The role of organic aerosol in atmospheric ice nucleation: A review. *ACS Earth and Space Chemistry*, *2*(3), 168–202.

Koch, D. (2001). Transport and direct radiative forcing of carbonaceous and sulfate aerosols in the GISS GCM. *Journal of Geophysical Research*, *106*, 20,311–20,332.

Koch, D., Schulz, M., Kinne, S., McNaughton, C., Spackman, J., Balkanski, Y., et al. (2009). Evaluation of black carbon estimations in global aerosol models. *Atmospheric Chemistry and Physics*, *9*(22), 9001–9026.

Köhler, H. (1936). The nucleus in and the growth of hygroscopic droplets. *Transactions of the Faraday Society*, *32*, 1152.

Kwon, D., Or, V. W., Sovers, M. J., Tang, M., Kleiber, P. D., Grassian, V. H., & Young, M. A. (2018). Optical property measurements and single particle analysis of secondary organic aerosol produced from the aqueous-phase reaction of ammonium sulfate with methylglyoxal. *ACS Earth and Space Chemistry*, *2*(4), 356–365.

Lack, D. A., Langridge, J. M., Bahreini, R., Cappa, C. D., Middlebrook, A. M., & Schwarz, J. P. (2012). Brown carbon and internal mixing in biomass burning particles. *Proceedings of the National Academy of Sciences*, *109*(37), 14,802–14,807.

Lack, D. A., Moosmüller, H., McMeeking, G. R., Chakrabarty, R. K., & Baumgardner, D. (2014). Characterizing elemental, equivalent black, and refractory black carbon aerosol particles: A review of techniques, their limitations and uncertainties. *Analytical and Bioanalytical Chemistry*, *406*(1), 99–122.

Lake, D. A., Tolocka, M. P., Johnston, M. V., & Wexler, A. S. (2004). The character of single particle sulfate in Baltimore. *Atmospheric Environment*, *38*(31), 5311–5320.

Lance, S., Raatikainen, T., Onasch, T. B., Worsnop, D. R., Yu, X.-Y., Alexander, M., et al. (2013). Aerosol mixing state, hygroscopic growth and cloud activation efficiency during mirage 2006. *Atmospheric Chemistry and Physics*, *13*(9), 5049–5062.

Larner, E. (1964). Electron microscopy of sodium chloride aerosol particles. United Kingdom Atomic Energy Authority.
Laskin, A., Gilles, M. K., Knopf, D. A., Wang, B., & China, S. (2016). Progress in the analysis of complex atmospheric particles. *Annual Review of Analytical Chemistry*, *9*, 117–143.
Laskin, J., Laskin, A., & Nizkorodov, S. A. (2013). New mass spectrometry techniques for studying physical chemistry of atmospheric heterogeneous processes. *International Reviews in Physical Chemistry*, *32*(1), 128–170.
Laskin, A., Laskin, J., & Nizkorodov, S. A. (2015). Chemistry of atmospheric brown carbon. *Chemical Reviews*, *115*(10), 4335–4382.
Laskin, J., Laskin, A., & Nizkorodov, S. A. (2018). Mass spectrometry analysis in atmospheric chemistry. *Analytical Chemistry*, *90*, 166–189.
Laskin, A., Wietsma, T. W., Krueger, B. J., & Grassian, V. H. (2005). Heterogeneous chemistry of individual mineral dust particles with nitric acid: A combined CCSEM/EDX, ESEM, and ICP-MS study. *Journal of Geophysical Research*, *110*, D10208. https://doi.org/10.1029/2004JD005206
Laskina, O., Morris, H. S., Grandquist, J. R., Estillore, A. D., Stone, E. A., Grassian, V. H., & Tivanski, A. V. (2015). Substrate-deposited sea spray aerosol particles: Influence of analytical method, substrate, and storage conditions on particle size, phase, and morphology. *Environmental Science & Technology*, *49*(22), 13,447–13,453.
Laskina, O., Young, M. A., Kleiber, P. D., & Grassian, V. H. (2013). Infrared extinction spectroscopy and micro-Raman spectroscopy of select components of mineral dust mixed with organic compounds. *Journal of Geophysical Research: Atmospheres*, *118*, 6593–6606. https://doi.org/10.1002/jgrd.50494
Lathem, T., Beyersdorf, A., Thornhill, K., Winstead, E., Cubison, M., Hecobian, A., et al. (2013). Analysis of CCN activity of Arctic aerosol and Canadian biomass burning during summer 2008. *Atmospheric Chemistry and Physics*, *13*(5), 2735–2756.
Lauer, A., Hendricks, J., Ackermann, I., Schell, B., Hass, H., & Metzger, S. (2005). Simulating aerosol microphysics with the ECHAM/MADE GCM—Part I: Model description and comparison with observations. *Atmospheric Chemistry and Physics*, *5*(12), 3251–3276.
Leck, C., & Svensson, E. (2015). Importance of aerosol composition and mixing state for cloud droplet activation over the arctic pack ice in summer. *Atmospheric Chemistry and Physics*, *15*(5), 2545–2568.
Lee, S. H., & Allen, H. C. (2012). Analytical measurements of atmospheric urban aerosol. *Analytical Chemistry*, *84*, 1196–1201.
Lee, H.-H., Chen, S.-H., Kleeman, M. J., Zhang, H., DeNero, S. P., & Joe, D. K. (2016). Implementation of warm-cloud processes in a source-oriented WRF/Chem model to study the effect of aerosol mixing state on fog formation in the Central Valley of California. *Atmospheric Chemistry and Physics*, *16*, 8353–8374.
Lee, H. D., Estillore, A. D., Morris, H. S., Ray, K. K., Alejandro, A., Grassian, V. H., & Tivanski, A. V. (2017a). Direct surface tension measurements of individual sub-micrometer particles using atomic force microscopy. *The Journal of Physical Chemistry A*, *121*(43), 8296–8305.
Lee, H. D., Ray, K. K., & Tivanski, A. V. (2017b). Solid, semisolid, and liquid phase states of individual submicrometer particles directly probed using atomic force microscopy. *Analytical Chemistry*, *89*(23), 12,720–12,726.
Lehmpuhl, D. W., Ramirez-Aguilar, K. A., Michel, A. E., Rowlen, K. L., & Birks, J. W. (1999). Physical and chemical characterization of atmospheric aerosols by atomic force microscopy. *Analytical Chemistry*, *71*(2), 379–383.
Lesins, G., Chylek, P., & Lohmann, U. (2002). A study of internal and external mixing scenarios and its effect on aerosol optical properties and direct radiative forcing. *Journal of Geophysical Research*, *107*(D10), 4094.
Li, J., Pósfai, M., Hobbs, P. V., & Buseck, P. R. (2003). Individual aerosol particles from biomass burning in southern Africa: 2, compositions and aging of inorganic particles. *Journal of Geophysical Research*, *108*(D13), 8484. https://doi.org/10.1029/2002JD002310
Li, W., Shao, L., Zhang, D., Ro, C.-U., Hu, M., Bi, X., et al. (2016). A review of single aerosol particle studies in the atmosphere of East Asia: Morphology, mixing state, source, and heterogeneous reactions. *Journal of Cleaner Production*, *112*, 1330–1349.
Liu, S., Aiken, A. C., Gorkowski, K., Dubey, M. K., Cappa, C. D., Williams, L. R., et al. (2015). Enhanced light absorption by mixed source black and brown carbon particles in UK winter. *Nature Communications*, *6*, 8435.
Liu, X., Easter, R. C., Ghan, S. J., Zaveri, R., Rasch, P., Shi, X., et al. (2012). Toward a minimal representation of aerosols in climate models: Description and evaluation in the Community Atmosphere Model CAM5. *Geoscientific Model Development*, *5*(3), 709.
Liu, X., Ma, P-L., Wang, H., Tilmes, S., Singh, B., Easter, R., et al. (2016). Description and evaluation of a new four-mode version of the modal aerosol module (MAM4) within version 5.3 of the Community Atmosphere Model. *Geoscientific Model Development*, *9*, 505–522.
Liu, D.-Y., Rutherford, D., Kinsey, M., & Prather, K. A. (1997). Real-time monitoring of pyrotechnically derived aerosol particles in the troposphere. *Analytical Chemistry*, *69*(10), 1808–1814.
Liu, Y., Yang, Z., Desyaterik, Y., Gassman, P. L., Wang, H., & Laskin, A. (2008). Hygroscopic behavior of substrate-deposited particles studied by micro-FT-IR spectroscopy and complementary methods of particle analysis. *Analytical Chemistry*, *80*(3), 633–642.
Loh, N., Hampton, C. Y., Martin, A. V., Starodub, D., Sierra, R. G., Barty, A., et al. (2012). Fractal morphology, imaging and mass spectrometry of single aerosol particles in flight. *Nature*, *486*(7404), 513.
Lohmann, U., Feichter, J., Chuang, C. C., & Penner, J. E. (1999). Prediction of the number of cloud droplets in the ECHAM GCM. *Journal of Geophysical Research*, *104*, 9169–9198.
Losey, D. J., Parker, R. G., & Freedman, M. A. (2016). pH dependence of liquid–liquid phase separation in organic aerosol. *The Journal of Physical Chemistry Letters*, *7*(19), 3861–3865.
Lu, J., & Bowman, F. (2010). A detailed aerosol mixing state model for investigating interactions between mixing state, semivolatile partitioning, and coagulation. *Atmospheric Chemistry and Physics*, *10*(8), 4033–4046.
Ma, Y., Li, S., Zheng, J., Khalizov, A., Wang, X., Wang, Z., & Zhou, Y. (2017). Size-resolved measurements of mixing state and cloud-nucleating ability of aerosols in Nanjing, China. *Journal of Geophysical Research: Atmospheres*, *122*, 9430–9450. https://doi.org/10.1002/2017JD026583
Ma, N., Zhao, C., Müller, T., Cheng, Y., Liu, P., Deng, Z., et al. (2012). A new method to determine the mixing state of light absorbing carbonaceous using the measured aerosol optical properties and number size distributions. *Atmospheric Chemistry and Physics*, *12*(5), 2381–2397.
Mamane, Y., & De Pena, R. G. (1978). A quantitative method for the detection of individual submicrometer size sulfate particles.
Maria, S. F., Russell, L. M., Turpin, B. J., & Porcja, R. J. (2002). FTIR, measurements of functional groups and organic mass in aerosol samples over the Caribbean. *Atmospheric Environment*, *36*(33), 5185–5196.
Maria, S., Russell, L., Turpin, B., Porcja, R., Campos, T., Weber, R., & Huebert, B. (2003). Source signatures of carbon monoxide and organic functional groups in Asian Pacific Regional Aerosol Characterization Experiment (ACE-Asia) submicron aerosol types. *Journal of Geophysical Research*, *108*(D23), 8637. https://doi.org/10.1029/2003JD003703
Martinez, I. S., Peterson, M. D., Ebben, C. J., Hayes, P. L., Artaxo, P., Martin, S. T., & Geiger, F. M. (2011). On molecular chirality within naturally occurring secondary organic aerosol particles from the central Amazon Basin. *Physical Chemistry Chemical Physics*, *13*(26), 12,114–12,122.

Maskey, S., Chong, K. Y., Seo, A., Park, M., Lee, K., & Park, K. (2017). Cloud condensation nuclei activation of internally mixed black carbon particles. *Aerosol and Air Quality Research*, *17*(4), 867–877.

Matsui, H., Koike, M., Kondo, Y., Fast, J. D., & Takigawa, M. (2014). Development of an aerosol microphysical module: Aerosol Two-dimensional bin module for foRmation and Aging Simulation (ATRAS). *Atmospheric Chemistry and Physics*, *14*(18), 10,315–10,331.

Matsui, H., Koike, M., Kondo, Y., Moteki, N., Fast, J. D., & Zaveri, R. A. (2013). Development and validation of a black carbon mixing state resolved three-dimensional model: Aging processes and radiative impact. *Journal of Geophysical Research: Atmospheres*, *118*, 2304–2326. https://doi.org/10.1029/2012JD018446

May, N. W., Axson, J. L., Watson, A., Pratt, K. A., & Ault, A. P. (2016). Lake spray aerosol generation: A method for producing representative particles from freshwater wave breaking. *Atmospheric Measurement Techniques*, *9*(9), 4311–4325.

May, N. W., Gunsch, M. J., Olson, N., Bondy, A. L., Kirpes, R. M., Bertman, S., et al. (2018b). Unexpected contributions of sea spray and lake spray aerosol to inland particulate matter. *Environmental Science & Technology Letters*, *2*, 1075–1086.

May, N. W., Olson, N. E., Panas, M., Axson, J. L., Tirella, P. S., Kirpes, R. M., et al. (2018a). Aerosol emissions from great lakes harmful algal blooms. *Environmental Science & Technology*, *52*, 397–405.

McFiggans, G., Artaxo, P., Baltensperger, U., Coe, H., Facchini, M., Feingold, G., et al. (2006). The effect of physical and chemical aerosol properties on warm cloud droplet activation. *Atmospheric Chemistry and Physics*, *6*(9), 2593–2649.

McGraw, R. (1997). Description of aerosol dynamics by the quadrature method of moments. *Aerosol Science and Technology*, *27*, 255–265.

McGraw, R., Leng, L., Zhu, W., Riemer, N., & West, M. (2008). Aerosol dynamics using the quadrature method of moments: Comparing several quadrature schemes with particle-resolved simulation. *Journal of Physics: Conference Series*, *125*(012), 020.

McGraw, R., & Wright, D. L. (2003). Chemically resolved aerosol dynamics for internal mixtures by the quadrature method of moments. *Journal of Aerosol Science*, *34*(2), 189–209.

McKeown, P., Johnston, M., & Murphy, D. (1991). On-line single-particle analysis by laser desorption mass spectrometry. *Analytical Chemistry*, *63*(18), 2069–2073.

McNeill, V. F. (2017). Atmospheric aerosols: Clouds, chemistry, and climate. *Annual Review of Chemical and Biomolecular Engineering*, *8*, 427–444.

Merikallio, S., Lindqvist, H., Nousiainen, T., & Kahnert, M. (2011). Modelling light scattering by mineral dust using spheroids: Assessment of applicability. *Atmospheric Chemistry and Physics*, *11*(11), 5347–5363.

Meskhidze, N., Xu, J., Gantt, B., Zhang, Y., Nenes, A., Ghan, S. J., et al. (2011). Global distribution and climate forcing of marine organic aerosol: 1. model improvements and evaluation. *Atmospheric Chemistry and Physics*, *11*(22), 11,689–11,705.

Middlebrook, A. M., Murphy, D. M., Lee, S.-H., Thomson, D. S., Prather, K. A., Wenzel, R. J., et al. (2003). A comparison of particle mass spectrometers during the 1999 Atlanta Supersite Project. *Journal of Geophysical Research*, *108*(D7), 8424. https://doi.org/10.1029/2001JD000660

Mie, G. (1908). Beiträge zur Optik trüber Medien, speziell kolloidaler Metallösungen. *Annalen der physik*, *330*(3), 377–445.

Mikhailov, E., Vlasenko, S., Krämer, L., & Niessner, R. (2001). Interaction of soot aerosol particles with water droplets: Influence of surface hydrophilicity. *Journal of Aerosol Science*, *32*(6), 697–711.

Mishchenko, M. I., Travis, L. D., & Mackowski, D. W. (1996). T-matrix computations of light scattering by nonspherical particles: A review. *Journal of Quantitative Spectroscopy and Radiative Transfer*, *55*(5), 535–575.

Mitchem, L., Buajarern, J., Ward, A. D., & Reid, J. P. (2006). A strategy for characterizing the mixing state of immiscible aerosol components and the formation of multiphase aerosol particles through coagulation. *The Journal of Physical Chemistry B*, *110*(28), 13,700–13,703.

Moffet, R. C., Henn, T., Laskin, A., & Gilles, M. K. (2010). Automated chemical analysis of internally mixed aerosol particles using X-ray spectromicroscopy at the carbon K-edge. *Analytical Chemistry*, *82*(19), 7906–7914.

Moffet, R. C., O'Brien, R. E., Alpert, P. A., Kelly, S. T., Pham, D. Q., Gilles, M. K., et al. (2016). Morphology and mixing of black carbon particles collected in central California during the CARES field study. *Atmospheric Chemistry and Physics*, *16*(22), 14,515–14,525.

Moffet, R., & Prather, K. (2005). Simultaneous measurements of optical properties, size and chemical composition on single aerosol particles, *Abstracts of Papers of the American Chemical Society* (Vol. 229, pp. U111–U111). Washington, DC: American Chemical Society.

Moffet, R. C., & Prather, K. A. (2009). In-situ measurements of the mixing state and optical properties of soot with implications for radiative forcing estimates. *Proceedings of the National Academy of Sciences*, *106*(29), 11,872–11,877.

Moffet, R. C., Qin, X., Rebotier, T., Furutani, H., & Prather, K. A. (2008). Chemically segregated optical and microphysical properties of ambient aerosols measured in a single-particle mass spectrometer. *Journal of Geophysical Research*, *113*, D12213. https://doi.org/10.1029/2007JD009393

Moffet, R. C., Rödel, T., Kelly, S. T., Yu, X.-Y., Carroll, G., Fast, J., et al. (2013). Spectro-microscopic measurements of carbonaceous aerosol aging in Central California. *Atmospheric Chemistry and Physics*, *13*(20), 10,445–10,459.

Moise, T., Flores, J. M., & Rudich, Y. (2015). Optical properties of secondary organic aerosols and their changes by chemical processes. *Chemical Reviews*, *115*(10), 4400–4439.

Moore, R., Bahreini, R., Brock, C., Froyd, K., Cozic, J., Holloway, J., et al. (2011). Hygroscopicity and composition of Alaskan Arctic CCN during April 2008. *Atmospheric Chemistry and Physics*, *11*, 11,807–11,825.

Morrical, B., Fergenson, D., & Prather, K. (1998). Coupling two-step laser desorption/ionization with aerosol time-of-flight mass spectrometry for the analysis of individual organic particles. *Journal of the American Society for Mass Spectrometry*, *9*(10), 1068–1073.

Morris, H. S., Estillore, A. D., Laskina, O., Grassian, V. H., & Tivanski, A. V. (2016). Quantifying the hygroscopic growth of individual submicrometer particles with atomic force microscopy. *Analytical Chemistry*, *88*(7), 3647–3654.

Morris, R., Koo, B., & Yarwood, G. (2005). Evaluation of multisectional and two-section particulate matter photochemical grid models in the western United States. *Journal of the Air & Waste Management Association*, *55*(11), 1683–1693.

Moteki, N., Kondo, Y., Miyazaki, Y., Takegawa, N., Komazaki, Y., Kurata, G., et al. (2007). Evolution of mixing state of black carbon particles: Aircraft measurements over the western Pacific in March 2004. *Geophysical Research Letters*, *34*, L11803. https://doi.org/10.1029/2006GL028943

Murphy, D. M. (2007). The design of single particle laser mass spectrometers. *Mass Spectrometry Reviews*, *26*(2), 150–165.

Murphy, D., Anderson, J., Quinn, P., McInnes, L., Brechtel, F., Kreidenweis, S., et al. (1998a). Influence of sea-salt on aerosol radiative properties in the Southern Ocean marine boundary layer. *Nature*, *392*(6671), 62.

Murphy, D., Cziczo, D., Froyd, K., Hudson, P., Matthew, B., Middlebrook, A., et al. (2006). Single-particle mass spectrometry of tropospheric aerosol particles. *Journal of Geophysical Research*, *111*, D23S32. https://doi.org/10.1029/2006JD007340

Murphy, B. N., Donahue, N., Robinson, A., & Pandis, S. (2014). A naming convention for atmospheric organic aerosol. *Atmospheric Chemistry and Physics*, *14*(11), 5825–5839.

Murphy, D., & Thomson, D. (1997). Chemical composition of single aerosol particles at Idaho Hill: Negative ion measurements. *Journal of Geophysical Research*, *102*(D5), 6353–6368.

Murphy, D., Thomson, D., & Mahoney, M. (1998b). In situ measurements of organics, meteoritic material, mercury, and other elements in aerosols at 5 to 19 kilometers. *Science*, *282*(5394), 1664–1669.

Murphy, D., Thomson, D., Middlebrook, A., & Schein, M. (1998c). In situ single-particle characterization at Cape Grim. *Journal of Geophysical Research*, *103*(D13), 16,485–16,491.

Murray, B., O'sullivan, D., Atkinson, J., & Webb, M. (2012). Ice nucleation by particles immersed in supercooled cloud droplets. *Chemical Society Reviews*, *41*(19), 6519–6554.

Myers, R. L., & Fite, W. L. (1975). Electrical detection of airborne particulates using surface ionization techniques. *Environmental Science & Technology*, *9*(4), 334–336.

Naumann, K.-H. (2003). COSIMA—A computer program simulating the dynamics of fractal aerosols. *Journal of Aerosol Science*, *34*(10), 1371–1397.

Nenes, A., Ghan, S., Abdul-Razzak, H., Chuang, P. Y., & Seinfeld, J. H. (2001). Kinetic limitations on cloud droplet formation and impact on cloud albedo. *Tellus B: Chemical and Physical Meteorology*, *53*(2), 133–149.

Niedermeier, D., Hartmann, S., Clauss, T., Wex, H., Kiselev, A., Sullivan, R. C., et al. (2011). Experimental study of the role of physicochemical surface processing on the IN ability of mineral dust particles. *Atmospheric Chemistry and Physics*, *11*(21), 11,131–11,144.

Noble, C. A., & Prather, K. A. (2000). Real-time single particle mass spectrometry: A historical review of a quarter century of the chemical analysis of aerosols. *Mass Spectrometry Reviews*, *19*(4), 248–274.

Nordmeyer, T., & Prather, K. (1994). Real-time measurement capabilities using aerosol time-of-flight mass spectrometry. *Analytical Chemistry*, *66*(20), 3540–3542.

O'Brien, R. E., Wang, B., Laskin, A., Riemer, N., West, M., Zhang, Q., et al. (2015). Chemical imaging of ambient aerosol particles: Observational constraints on mixing state parameterization. *Journal of Geophysical Research: Atmospheres*, *120*, 9591–9605. https://doi.org/10.1002/2015JD023480

Oakes, M., Weber, R., Lai, B., Russell, A., & Ingall, E. (2012). Characterization of iron speciation in urban and rural single particles using XANES spectroscopy and micro X-ray fluorescence measurements: Investigating the relationship between speciation and fractional iron solubility. *Atmospheric Chemistry and Physics*, *12*(2), 745–756.

Ofner, J., Deckert-Gaudig, T., Kamilli, K. A., Held, A., Lohninger, H., Deckert, V., & Lendl, B. (2016). Tip-enhanced Raman spectroscopy of atmospherically relevant aerosol nanoparticles. *Analytical Chemistry*, *88*(19), 9766–9772.

Okada, K. (1985). Number-size distribution and formation process of submicrometer sulfate-containing particles in the urban atmosphere of Nagoya. *Atmospheric Environment*, *19*(5), 743–757.

Onasch, T., Trimborn, A., Fortner, E., Jayne, J., Kok, G., Williams, L., et al. (2012). Soot particle aerosol mass spectrometer: Development, validation, and initial application. *Aerosol Science and Technology*, *46*(7), 804–817.

Or, V. W., Estillore, A. D., Tivanski, A. V., & Grassian, V. H. (2018). Lab on a tip: Atomic force microscopy–photothermal infrared spectroscopy of atmospherically relevant organic/inorganic aerosol particles in the nanometer to micrometer size range. *Analyst*, *143*, 2765–2774.

Oshima, N., Koike, M., Zhang, Y., & Kondo, Y. (2009). Aging of black carbon in outflow from anthropogenic sources using a mixing state resolved model: 2. Aerosol optical properties and cloud condensation nuclei activities. *Journal of Geophysical Research*, *114*, D18202. https://doi.org/10.1029/2008JD011681

Ovadnevaite, J., Zuend, A., Laaksonen, A., Sanchez, K. J., Roberts, G., Ceburnis, D., et al. (2017). Surface tension prevails over solute effect in organic-influenced cloud droplet activation. *Nature*, *546*(7660), 637.

Parungo, F., Ackerman, E., Caldwell, W., & Weickmann, H. (1979). Individual particle analysis of Antarctic aerosols. *Tellus*, *31*(6), 521–529.

Parungo, F., Ackerman, E., Proulx, H., & Pueschel, R. (1978). Nucleation properties of fly ash in a coal-fired power-plant plume. *Atmospheric Environment*, *12*(4), 929–935.

Patterson, J. P., Collins, D. B., Michaud, J. M., Axson, J. L., Sultana, C. M., Moser, T., et al. (2016). Sea spray aerosol structure and composition using cryogenic transmission electron microscopy. *ACS Central Science*, *2*(1), 40–47.

Penner, J. E., Dong, X., & Chen, Y. (2004). Observational evidence of a change in radiative forcing due to the indirect aerosol effect. *Nature*, *427*(6971), 231.

Perring, A., Schwarz, J., Baumgardner, D., Hernandez, M., Spracklen, D., Heald, C., et al. (2015). Airborne observations of regional variation in fluorescent aerosol across the United States. *Journal of Geophysical Research: Atmospheres*, *120*, 1153–1170. https://doi.org/10.1002/2014JD022495

Petters, M. D., & Kreidenweis, S. M. (2007). A single parameter representation of hygroscopic growth and cloud condensation nucleus activity. *Atmospheric Chemistry and Physics*, *7*, 1961–1971.

Petters, S. S., & Petters, M. D. (2016). Surfactant effect on cloud condensation nuclei for two-component internally mixed aerosols. *Journal of Geophysical Research: Atmospheres*, *121*, 1878–1895. https://doi.org/10.1002/2015JD024090

Petzold, A., Schloesser, H., Sheridan, P. J., Arnott, W. P., Ogren, J. A., & Virkkula, A. (2005). Evaluation of multiangle absorption photometry for measuring aerosol light absorption. *Aerosol Science and Technology*, *39*(1), 40–51.

Phillips, V. T., DeMott, P. J., & Andronache, C. (2008). An empirical parameterization of heterogeneous ice nucleation for multiple chemical species of aerosol. *Journal of the Atmospheric Sciences*, *65*(9), 2757–2783.

Pöhlker, C., Wiedemann, K. T., Sinha, B., Shiraiwa, M., Gunthe, S. S., Smith, M., et al. (2012). Biogenic potassium salt particles as seeds for secondary organic aerosol in the Amazon. *Science*, *337*(6098), 1075–1078.

Pope, C. A. III, & Dockery, D. W. (2006). Health effects of fine particulate air pollution: Lines that connect. *Journal of the air & waste management association*, *56*(6), 709–742.

Popoola, L. T., Adebanjo, S. A., & Adeoye, B. K. (2018). Assessment of atmospheric particulate matter and heavy metals: A critical review. *International Journal of Environmental Science and Technology*, *15*, 935–948.

Pöschl, U., Martin, S., Sinha, B., Chen, Q., Gunthe, S., Huffman, J., et al. (2010). Rainforest aerosols as biogenic nuclei of clouds and precipitation in the Amazon. *Science*, *329*(5998), 1513–1516.

Pósfai, M., Anderson, J. R., Buseck, P. R., Shattuck, T. W., & Tindale, N. W. (1994). Constituents of a remote Pacific marine aerosol: A TEM study. *Atmospheric Environment*, *28*(10), 1747–1756.

Pósfai, M., Anderson, J. R., Buseck, P. R., & Sievering, H. (1999). Soot and sulfate aerosol particles in the remote marine troposphere. *Journal of Geophysical Research*, *104*(D17), 21,685–21,693. https://doi.org/10.1029/1999JD900208

Pósfai, M., Simonics, R., Li, J., Hobbs, P. V., & Buseck, P. R. (2003). Individual aerosol particles from biomass burning in southern Africa: 1. compositions and size distributions of carbonaceous particles. *Journal of Geophysical Research*, *108*(D13), 8484. https://doi.org/10.1029/2002JD002310

Pósfai, M., Xu, H., Anderson, J. R., & Buseck, P. R. (1998). Wet and dry sizes of atmospheric aerosol particles: An AFM-TEM study. *Geophysical Research Letters*, *25*(11), 1907–1910.

Power, R. M., & Reid, J. P. (2014). Probing the micro-rheological properties of aerosol particles using optical tweezers. *Reports on Progress in Physics*, *77*(7), 074601.
Powers, K. W., Palazuelos, M., Moudgil, B. M., & Roberts, S. M. (2007). Characterization of the size, shape, and state of dispersion of nanoparticles for toxicological studies. *Nanotoxicology*, *1*(1), 42–51.
Prather, K. A., Bertram, T. H., Grassian, V. H., Deane, G. B., Stokes, M. D., DeMott, P. J., et al. (2013). Bringing the ocean into the laboratory to probe the chemical complexity of sea spray aerosol. *Proceedings of the National Academy of Sciences*, *110*(19), 7550–7555.
Prather, K. A., Hatch, C. D., & Grassian, V. H. (2008). Analysis of atmospheric aerosols. *Annual Review of Analytical Chemistry*, *1*, 485–514.
Prather, K. A., Nordmeyer, T., & Salt, K. (1994). Real-time characterization of individual aerosol particles using time-of-flight mass spectrometry. *Analytical Chemistry*, *66*(9), 1403–1407.
Pratt, K. A., DeMott, P. J., French, J. R., Wang, Z., Westphal, D. L., Heymsfield, A. J., et al. (2009c). In situ detection of biological particles in cloud ice-crystals. *Nature Geoscience*, *2*(6), 398.
Pratt, K. A., Hatch, L. E., & Prather, K. A. (2009b). Seasonal volatility dependence of ambient particle phase amines. *Environmental Science & Technology*, *43*(14), 5276–5281.
Pratt, K. A., Mayer, J. E., Holecek, J. C., Moffet, R. C., Sanchez, R. O., Rebotier, T. P., et al. (2009a). Development and characterization of an aircraft aerosol time-of-flight mass spectrometer. *Analytical Chemistry*, *81*(5), 1792–1800.
Pratt, K. A., & Prather, K. A. (2009). Real-time, single-particle volatility, size, and chemical composition measurements of aged urban aerosols. *Environmental Science & Technology*, *43*(21), 8276–8282. https://doi.org/10.1021/es902002t
Pratt, K. A., & Prather, K. A. (2010). Aircraft measurements of vertical profiles of aerosol mixing states. *Journal of Geophysical Research*, *115*, D11305. https://doi.org/10.1029/2009jd013150
Pratt, K. A., & Prather, K. A. (2012a). Mass spectrometry of atmospheric aerosols—Recent developments and applications. Part I: Off-line mass spectrometry techniques. *Mass spectrometry reviews*, *31*(1), 1–16.
Pratt, K. A., & Prather, K. A. (2012b). Mass spectrometry of atmospheric aerosols—Recent developments and applications. Part II: On-line mass spectrometry techniques. *Mass spectrometry reviews*, *31*(1), 17–48.
Pye, H. O., Murphy, B. N., Xu, L., Ng, N. L., Carlton, A. G., Guo, H., et al. (2017). On the implications of aerosol liquid water and phase separation for organic aerosol mass. *Atmospheric Chemistry and Physics*, *17*(1), 343–369.
Qin, X., & Prather, K. A. (2006). Impact of biomass emissions on particle chemistry during the California Regional Particulate Air Quality Study. *International Journal of Mass Spectrometry*, *258*(1-3), 142–150.
Qin, X., Pratt, K. A., Shields, L. G., Toner, S. M., & Prather, K. A. (2012). Seasonal comparisons of single-particle chemical mixing state in Riverside, CA. *Atmospheric environment*, *59*, 587–596.
Quinn, P., & Coffman, D. (1998). Local closure during the first aerosol Characterization Experiment (ACE 1): Aerosol mass concentration and scattering and backscattering coefficients. *Journal of Geophysical Research*, *103*(D13), 16,575–16,596.
Quinn, P. K., Collins, D. B., Grassian, V. H., Prather, K. A., & Bates, T. S. (2015). Chemistry and related properties of freshly emitted sea spray aerosol. *Chemical Reviews*, *115*(10), 4383–4399.
Ravishankara, A., Rudich, Y., & Wuebbles, D. (2015). Physical chemistry of climate metrics. *Chemical Reviews*, *115*(10), 3682–3703.
Rebotier, T. P., & Prather, K. A. (2007). Aerosol time-of-flight mass spectrometry data analysis: A benchmark of clustering algorithms. *Analytica chimica acta*, *585*(1), 38–54.
Reid, J. P., Bertram, A. K., Topping, D. O., Laskin, A., Martin, S. T., Petters, M. D., et al. (2018). The viscosity of atmospherically relevant organic particles. *Nature Communications*, *9*(1), 956.
Reinard, M. S., Adou, K., Martini, J. M., & Johnston, M. V. (2007). Source characterization and identification by real-time single particle mass spectrometry. *Atmospheric Environment*, *41*(40), 9397–9409.
Riemer, N., Vogel, H., & Vogel, B. (2004). Soot aging time scales in polluted regions during day and night. *Atmospheric Chemistry and Physics*, *4*(7), 1885–1893.
Riemer, N., Vogel, H., Vogel, B., & Fiedler, F. (2003). Modeling aerosols on the mesoscale-$\gamma$: Treatment of soot aerosol and its radiative effects. *Journal of Geophysical Research*, *108*(D19), 14608082. https://doi.org/10.1029/2003jd003448
Riemer, N., & West, M. (2013). Quantifying aerosol mixing state with entropy and diversity measures. *Atmospheric Chemistry and Physics*, *13*(22), 11,423–11,439.
Riemer, N., West, M., Zaveri, R. A., & Easter, R. C. (2009). Simulating the evolution of soot mixing state with a particle-resolved aerosol model. *Journal of Geophysical Research*, *114*, D09202. https://doi.org/10.1029/2008JD011073
Riemer, N., West, M., Zaveri, R., & Easter, R. (2010). Estimating black carbon aging time-scales with a particle-resolved aerosol model. *Journal of Aerosol Science*, *41*(1), 143–158.
Rindelaub, J. D., Craig, R. L., Nandy, L., Bondy, A. L., Dutcher, C. S., Shepson, P. B., & Ault, A. P. (2016). Direct measurement of pH in individual particles via Raman microspectroscopy and variation in acidity with relative humidity. *The Journal of Physical Chemistry A*, *120*(6), 911–917.
Roberts, G., & Nenes, A. (2005). A continuous-flow streamwise thermal-gradient CCN chamber for atmospheric measurements. *Aerosol Science and Technology*, *39*(3), 206–221.
Rose, D., Gunthe, S., Su, H., Garland, R., Yang, H., Berghof, M., et al. (2011). Cloud condensation nuclei in polluted air and biomass burning smoke near the mega-city Guangzhou, China—Part 2: Size-resolved aerosol chemical composition, diurnal cycles, and externally mixed weakly CCN-active soot particles. *Atmospheric Chemistry and Physics*, *11*(6), 2817–2836.
Rudich, Y., Donahue, N. M., & Mentel, T. F. (2007). Aging of organic aerosol: Bridging the gap between laboratory and field studies. *Annual Review of Physical Chemistry*, *58*, 321–352.
Ruehl, C. R., Davies, J. F., & Wilson, K. R. (2016). An interfacial mechanism for cloud droplet formation on organic aerosols. *Science*, *351*(6280), 1447–1450.
Russell, L. M., Maria, S. F., & Myneni, S. C. (2002). Mapping organic coatings on atmospheric particles. *Geophysical Research Letters*, *29*(16), 1779. https://doi.org/10.1029/2002GL014874
Ryu, J., & Ro, C.-U. (2009). Attenuated total reflectance FT-IR imaging and quantitative energy dispersive-electron probe X-ray microanalysis techniques for single particle analysis of atmospheric aerosol particles. *Analytical Chemistry*, *81*(16), 6695–6707.
Saleh, R., Adams, P. J., Donahue, N. M., & Robinson, A. L. (2016). The interplay between assumed morphology and the direct radiative effect of light-absorbing organic aerosol. *Geophysical Research Letters*, *43*, 8735–8743. https://doi.org/10.1002/2016GL069786
Samad, E. H., Khammash, M., Petzold, L., & Gillespie, D. (2005). Stochastic modeling of gene regulatory networks. *International Journal of Robust and Nonlinear Control*, *15*(15), 691–711.
Sander, M., West, R. H., Celnik, M. S., & Kraft, M. (2009). A detailed model for the sintering of polydispersed nanoparticle agglomerates. *Aerosol Science and Technology*, *43*(10), 978–989.

Scarnato, B., Vahidinia, S., Richard, D., & Kirchstetter, T. (2013). Effects of internal mixing and aggregate morphology on optical properties of black carbon using a discrete dipole approximation model. *Atmospheric Chemistry and Physics*, *13*(10), 5089–5101.
Schaefer, V. J. (1949). The formation of ice crystals in the laboratory and the atmosphere. *Chemical Reviews*, *44*, 291–320.
Schill, S. R., Collins, D. B., Lee, C., Morris, H. S., Novak, G. A., Prather, K. A., et al. (2015). The impact of aerosol particle mixing state on the hygroscopicity of sea spray aerosol. *ACS Central Science*, *1*(3), 132–141.
Schill, G. P., & Tolbert, M. A. (2014). Heterogeneous ice nucleation on simulated sea-spray aerosol using Raman microscopy. *The Journal of Physical Chemistry C*, *118*(50), 29,234–29,241.
Schnaiter, M., Linke, C., Möhler, O., Naumann, K.-H., Saathoff, H., Wagner, R., et al. (2005). Absorption amplification of black carbon internally mixed with secondary organic aerosol. *Journal of Geophysical Research*, *110*, D19204. https://doi.org/10.1029/2005JD006046
Schult, I., Feichter, J., & Cooke, W. F. (1997). Effect of black carbon and sulfate aerosols on the global radiation budget. *Journal of Geophysical Research*, *102*(D25), 30,107–30,117.
Schwarz, J., Gao, R., Spackman, J., Watts, L., Thomson, D., Fahey, D., et al. (2008). Measurement of the mixing state, mass, and optical size of individual black carbon particles in urban and biomass burning emissions. *Geophysical Research Letters*, *35*, L13810. https://doi.org/10.1029/2008GL033968
Sedlacek, A. J., Lewis, E. R., Kleinman, L., Xu, J., & Zhang, Q. (2012). Determination of and evidence for non-core-shell structure of particles containing black carbon using the Single-Particle Soot Photometer (SP2). *Geophysical Research Letters*, *39*, L06802. https://doi.org/10.1029/2012GL050905
Sedlacek, A. J., Lewis, E. R., Onasch, T. B., Lambe, A. T., & Davidovits, P. (2015). Investigation of refractory black carbon-containing particle morphologies using the single-particle soot photometer (SP2). *Aerosol Science and Technology*, *49*(10), 872–885.
Seinfeld, J. H., & Pandis, S. (2016). *Atmospheri chemistry and physics*. Hoboken, NJ: Wiley.
Semeniuk, T. A., Wise, M. E., Martin, S. T., Russell, L. M., & Buseck, P. R. (2007). Hygroscopic behavior of aerosol particles from biomass fires using environmental transmission electron microscopy. *Journal of Atmospheric Chemistry*, *56*(3), 259–273.
Shen, H., Peters, T. M., Casuccio, G. S., Lersch, T. L., West, R. R., Kumar, A., et al. (2016). Elevated concentrations of lead in particulate matter on the neighborhood-scale in Delhi, India as determined by single particle analysis. *Environmental Science & Technology*, *50*(10), 4961–4970.
Shields, L. G., Suess, D. T., & Prather, K. A. (2007). Determination of single particle mass spectral signatures from heavy-duty diesel vehicle emissions for PM2.5 source apportionment. *Atmospheric Environment*, *41*(18), 3841–3852.
Shiraiwa, M., Kondo, Y., Iwamoto, T., & Kita, K. (2010b). Amplification of light absorption of black carbon by organic coating. *Aerosol Science and Technology*, *44*(1), 46–54.
Shiraiwa, M., Pfrang, C., Koop, T., & Pöschl, U. (2012). Kinetic multi-layer model of gas-particle interactions in aerosols and clouds (KM-GAP): Linking condensation, evaporation and chemical reactions of organics, oxidants and water. *Atmospheric Chemistry and Physics*, *12*(5), 2777–2794.
Shiraiwa, M., Pfrang, C., & Pöschl, U. (2010a). Kinetic multi-layer model of aerosol surface and bulk chemistry (KM-SUB): The influence of interfacial transport and bulk diffusion on the oxidation of oleic acid by ozone. *Atmospheric Chemistry and Physics*, *10*(8), 3673–3691.
Shrivastava, M., Cappa, C. D., Fan, J., Goldstein, A. H., Guenther, A. B., Jimenez, J. L., et al. (2017). Recent advances in understanding secondary organic aerosol: Implications for global climate forcing. *Reviews of Geophysics*, *55*, 509–559. https://doi.org/10.1002/2016RG000540
Shulman, M. L., Jacobson, M. C., Carlson, R. J., Synovec, R. E., & Young, T. E. (1996). Dissolution behavior and surface tension effects of organic compounds in nucleating cloud droplets. *Geophysical Research Letters*, *23*(3), 277–280.
Silva, P. J., Carlin, R. A., & Prather, K. A. (2000). Single particle analysis of suspended soil dust from Southern California. *Atmospheric Environment*, *34*(11), 1811–1820.
Silva, P. J., Liu, D.-Y., Noble, C. A., & Prather, K. A. (1999). Size and chemical characterization of individual particles resulting from biomass burning of local Southern California species. *Environmental Science & Technology*, *33*(18), 3068–3076.
Sinha, M., Giffin, C., Norris, D., Estes, T., Vilker, V., & Friedlander, S. (1982). Particle analysis by mass spectrometry. *Journal of Colloid and Interface Science*, *87*(1), 140–153.
Sivaprakasam, V., Hart, M. B., & Eversole, J. D. (2017). Surface enhanced Raman spectroscopy of individual suspended aerosol particles. *The Journal of Physical Chemistry C*, *121*(40), 22,326–22,334.
Sloane, C. S. (1983). Optical properties of aerosols–comparison of measurements with model calculations. *Atmospheric Environment*, *17*(2), 409–416.
Sobanska, S., Falgayrac, G., Rimetz-Planchon, J., Perdrix, E., Brémard, C., & Barbillat, J. (2014). Resolving the internal structure of individual atmospheric aerosol particle by the combination of Atomic Force Microscopy, ESEM–EDX, Raman and ToF-SIMS imaging. *Microchemical Journal*, *114*, 89–98.
Sobanska, S., Hwang, H., Choël, M., Jung, H.-J., Eom, H.-J., Kim, H., et al. (2012). Investigation of the chemical mixing state of individual Asian dust particles by the combined use of electron probe X-ray microanalysis and Raman microspectrometry. *Analytical Chemistry*, *84*(7), 3145–3154.
Sodeman, D. A., Toner, S. M., & Prather, K. A. (2005). Determination of single particle mass spectral signatures from light-duty vehicle emissions. *Environmental Science & Technology*, *39*(12), 4569–4580.
Solmon, F., Giorgi, F., & Liousse, C. (2006). Aerosol modelling for regional climate studies: Application to anthropogenic particles and evaluation over a European/African domain. *Tellus B: Chemical and Physical Meteorology*, *58*(1), 51–72.
Song, X.-H., Faber, N. K. M., Hopke, P. K., Suess, D. T., Prather, K. A., Schauer, J. J., & Cass, G. R. (2001). Source apportionment of gasoline and diesel by multivariate calibration based on single particle mass spectral data. *Analytica Chimica Acta*, *446*(1-2), 327–341.
Song, X.-H., Hadjiiski, L., Hopke, P. K., Ashbaugh, L. L., Carvacho, O., Casuccio, G. S., & Schlaegle, S. (1999b). Source apportionment of soil samples by the combination of two neural networks based on computer-controlled scanning electron microscopy. *Journal of the Air & Waste Management Association*, *49*(7), 773–783.
Song, X.-H., Hopke, P. K., Fergenson, D. P., & Prather, K. A. (1999a). Classification of single particles analyzed by ATOFMS using an artificial neural network, ART-2A. *Analytical Chemistry*, *71*(4), 860–865.
Song, M., Marcolli, C., Krieger, U. K., Lienhard, D. M., & Peter, T. (2013). Morphologies of mixed organic/inorganic/aqueous aerosol droplets. *Faraday Discussions*, *165*, 289–316.
Song, J., & Peng, P. (2009). Surface characterization of aerosol particles in Guangzhou, China: A study by XPS. *Aerosol Science and Technology*, *43*(12), 1230–1242.
Song, Y.-C., Ryu, J., Malek, M. A., Jung, H.-J., & Ro, C.-U. (2010). Chemical speciation of individual airborne particles by the combined use of quantitative energy-dispersive electron probe X-ray microanalysis and attenuated total reflection Fourier transform-infrared imaging techniques. *Analytical Chemistry*, *82*(19), 7987–7998.

Sorensen, C. (2011). The mobility of fractal aggregates: A review. *Aerosol Science and Technology*, *45*(7), 765–779.
Spencer, M., Holecek, J., Corrigan, C., Ramanathan, V., & Prather, K. (2008). Size-resolved chemical composition of aerosol particles during a monsoonal transition period over the Indian Ocean. *Journal of Geophysical Research*, *113*, D16305. https://doi.org/10.1029/2007JD008657
Spracklen, D., Pringle, K., Carslaw, K., Chipperfield, M., & Mann, G. (2005). A global off-line model of size-resolved aerosol microphysics: I. Model development and prediction of aerosol properties. *Atmospheric Chemistry and Physics*, *5*(8), 2227–2252.
Stier, P., Feichter, J., Kinne, S., Kloster, S., Vignati, E., Wilson, J., et al. (2005). The aerosol-climate model ECHAM5-HAM. *Atmospheric Chemistry and Physics*, *5*(4), 1125–1156.
Stier, P., Seinfeld, J. H., Kinne, S., & Boucher, O. (2007). Aerosol absorption and radiative forcing. *Atmospheric Chemistry and Physics*, *7*(19), 5237–5261.
Strong, S., Koberle, R., de Ruyter van Steveninck, R., & Bialek, W. (1998). Entropy and information in neural spike trains. *Physical Review Letters*, *80*(1), 197–200. https://doi.org/10.1103/PhysRevLett.80.197
Su, H., Rose, D., Cheng, Y., Gunthe, S., Massling, A., Stock, M., et al. (2010). Hygroscopicity distribution concept for measurement data analysis and modeling of aerosol particle mixing state with regard to hygroscopic growth and CCN activation. *Atmospheric Chemistry and Physics*, *10*(15), 7489–7503.
Suess, D. T., & Prather, K. A. (1999). Mass spectrometry of aerosols. *Chemical Reviews*, *99*(10), 3007–3036.
Sullivan, R. C., Gorkowski, K., & Jahn, L. (2018). Characterization of individual Aerosol Particles. In J. A. Faust, & J. E. House, (Eds.), *Physical Chemistry of Gas-Liquid Interfaces 2018* (pp. 353–402). Cambridge, MA: Elsevier.
Sullivan, R., Guazzotti, S., Sodeman, D., & Prather, K. (2007a). Direct observations of the atmospheric processing of Asian mineral dust. *Atmospheric Chemistry and Physics*, *7*(5), 1213–1236.
Sullivan, R. C., Guazzotti, S. A., Sodeman, D. A., Tang, Y., Carmichael, G. R., & Prather, K. A. (2007b). Mineral dust is a sink for chlorine in the marine boundary layer. *Atmospheric Environment*, *41*(34), 7166–7179.
Sullivan, R., Moore, M., Petters, M., Kreidenweis, S., Roberts, G., & Prather, K. (2009). Effect of chemical mixing state on the hygroscopicity and cloud nucleation properties of calcium mineral dust particles. *Atmospheric Chemistry and Physics*, *9*(10), 3303–3316.
Sullivan, R., Petters, M., DeMott, P., Kreidenweis, S., Wex, H., Niedermeier, D., et al. (2010). Irreversible loss of ice nucleation active sites in mineral dust particles caused by sulphuric acid condensation. *Atmospheric Chemistry and Physics*, *10*(23), 11,471–11,487.
Sullivan, R. C., & Prather, K. A. (2005). Recent advances in our understanding of atmospheric chemistry and climate made possible by on-line aerosol analysis instrumentation. *Analytical Chemistry*, *77*(12), 3861–3886.
Sullivan, R. C., & Prather, K. A. (2007). Investigations of the diurnal cycle and mixing state of oxalic acid in individual particles in Asian aerosol outflow. *Environmental Science & Technology*, *41*(23), 8062–8069.
Swietlicki, E., Hansson, H.-C., Hämeri, K., Svenningsson, B., Massling, A., McFiggans, G., et al. (2008). Hygroscopic properties of submicrometer atmospheric aerosol particles measured with H-TDMA instruments in various environments—A review. *Tellus B*, *60*(3), 432–469.
Takahama, S., Gilardoni, S., Russell, L., & Kilcoyne, A. (2007). Classification of multiple types of organic carbon composition in atmospheric particles by scanning transmission X-ray microscopy analysis. *Atmospheric Environment*, *41*(40), 9435–9451.
Tang, C. Y., Huang, Z., & Allen, H. C. (2010). Interfacial water structure and effects of Mg2+ and Ca2+ binding to the COOH headgroup of a palmitic acid monolayer studied by sum frequency spectroscopy. *The Journal of Physical Chemistry B*, *115*(1), 34–40.
Taylor, J., Allan, J., Liu, D., Flynn, M., Weber, R., Zhang, X., et al. (2015). Assessment of the sensitivity of core/shell parameters derived using the single-particle soot photometer to density and refractive index. *Atmospheric Measurement Techniques*, *8*(4), 1701.
Tegen, I., & Miller, R. (1998). A general circulation model study on the interannual variability of soil dust aerosol. *Journal of Geophysical Research*, *103*(D20), 25,975–25,995.
Tervahattu, H., Juhanoja, J., & Kupiainen, K. (2002). Identification of an organic coating on marine aerosol particles by ToF-SIMS. *Journal of Geophysical Research*, *107*(D16), 4319.
Toner, S. M., Shields, L. G., Sodeman, D. A., & Prather, K. A. (2008). Using mass spectral source signatures to apportion exhaust particles from gasoline and diesel powered vehicles in a freeway study using UF-ATOFMS. *Atmospheric Environment*, *42*(3), 568–581.
Toner, S. M., Sodeman, D. A., & Prather, K. A. (2006). Single particle characterization of ultrafine and accumulation mode particles from heavy duty diesel vehicles using aerosol time-of-flight mass spectrometry. *Environmental Science & Technology*, *40*(12), 3912–3921.
Topping, D., McFiggans, G., Kiss, G., Varga, Z., Facchini, M., Decesari, S., & Mircea, M. (2007). Surface tensions of multi-component mixed inorganic/organic aqueous systems of atmospheric significance: Measurements, model predictions and importance for cloud activation predictions. *Atmospheric Chemistry and Physics*, *7*(9), 2371–2398.
Toprak, E., & Schnaiter, M. (2013). Fluorescent biological aerosol particles measured with the Waveband Integrated Bioaerosol Sensor WIBS-4: Laboratory tests combined with a one year field study. *Atmospheric Chemistry and Physics*, *13*(1), 225.
Um, J., McFarquhar, G., Hong, Y., Lee, S., Jung, C., Lawson, R., & Mo, Q. (2015). Dimensions and aspect ratios of natural ice crystals. *Atmospheric Chemistry and Physics*, *15*, 3933–3956.
Usher, C. R., Michel, A. E., & Grassian, V. H. (2003). Reactions on mineral dust. *Chemical Reviews*, *103*(12), 4883–4940.
Utsunomiya, S., Jensen, K. A., Keeler, G. J., & Ewing, R. C. (2004). Direct identification of trace metals in fine and ultrafine particles in the detroit urban atmosphere. *Environmental Science & Technology*, *38*(8), 2289–2297.
Vander Wal, R. L., Bryg, V. M., & Hays, M. D. (2011). XPS, analysis of combustion aerosols for chemical composition, surface chemistry, and carbon chemical state. *Analytical Chemistry*, *83*(6), 1924–1930.
Veghte, D. P., Altaf, M. B., & Freedman, M. A. (2013). Size dependence of the structure of organic aerosol. *Journal of the American Chemical Society*, *135*(43), 16,046–16,049.
Veghte, D. P., Bittner, D. R., & Freedman, M. A. (2014). Cryo-transmission electron microscopy imaging of the morphology of submicrometer aerosol containing organic acids and ammonium sulfate. *Analytical Chemistry*, *86*(5), 2436–2442.
Verbueken, A., Bruynseels, F., & Van Grieken, R. (1985). Laser microprobe mass analysis: A review of applications in the life sciences. *Biological Mass Spectrometry*, *12*(9), 438–463.
Vester, B. P., Ebert, M., Barnert, E. B., Schneider, J., Kandler, K., Schütz, L., & Weinbruch, S. (2007). Composition and mixing state of the urban background aerosol in the Rhein-Main area (Germany). *Atmospheric Environment*, *41*(29), 6102–6115.
Vestin, A., Rissler, J., Swietlicki, E., Frank, G., & Andreae, M. (2007). Cloud-nucleating properties of the Amazonian biomass burning aerosol: Cloud condensation nuclei measurements and modeling. *Journal of Geophysical Research*, *112*, D14201. https://doi.org/10.1029/2006JD8104
Vignati, E., Wilson, J., & Stier, P. (2004). M7: An efficient size-resolved aerosol microphysics module for large-scale aerosol transport models. *Journal of Geophysical Research*, *109*, D22202. https://doi.org/10.1029/2003JD004485

Virkkula, A., Ahlquist, N. C., Covert, D. S., Arnott, W. P., Sheridan, P. J., Quinn, P. K., & Coffman, D. J. (2005). Modification, calibration and a field test of an instrument for measuring light absorption by particles. *Aerosol Science and Technology*, *39*(1), 68–83.

Vogel, B., Vogel, H., Bäumer, D., Bangert, M., Lundgren, K., Rinke, R., & Stanelle, T. (2009). The comprehensive model system COSMO-ART–Radiative impact of aerosol on the state of the atmosphere on the regional scale. *Atmospheric Chemistry and Physics*, *9*(22), 8661–8680.

Von Schneidemesser, E., Monks, P. S., Allan, J. D., Bruhwiler, L., Forster, P., Fowler, D., et al. (2015). Chemistry and the linkages between air quality and climate change. *Chemical Reviews*, *115*(10), 3856–3897.

von Smoluchowski, M. (1916a). Drei Vorträge über Diffusion, Brownsche Molekularbewegung und Koagulation von Kolloidteilchen. *Physikalische Zeitschrift*, *17*, 557–571–585–599.

von Smoluchowski, M. (1916b). Versuch einer mathematischen Theorie der Koagulationskinetik kolloider Lösungen, Z. *Physical Chemistry*, *92*, 129–168.

Wang, J., Cubison, M., Aiken, A., Jimenez, J., & Collins, D. (2010). The importance of aerosol mixing state and size-resolved composition on CCN concentration and the variation of the importance with atmospheric aging of aerosols. *Atmospheric Chemistry and Physics*, *10*(15), 7267–7283.

Wang, J., & Martin, S. T. (2007). Satellite characterization of urban aerosols: Importance of including hygroscopicity and mixing state in the retrieval algorithms. *Journal of Geophysical Research*, *112*, D17203. https://doi.org/10.1029/2006JD008078

Wang, S., Zordan, C. A., & Johnston, M. V. (2006). Chemical characterization of individual, airborne sub-10-nm particles and molecules. *Analytical Chemistry*, *78*(6), 1750–1754.

Wegener, A. (1911). Thermodynamik der Atmosphäre, JA Barth.

Wehner, B., Berghof, M., Cheng, Y., Achtert, P., Birmili, W., Nowak, A., et al. (2009). Mixing state of nonvolatile aerosol particle fractions and comparison with light absorption in the polluted Beijing region. *Journal of Geophysical Research*, *114*, D00G17. https://doi.org/10.1029/2008JD010923

Wells, C., Morgan, N., Kraft, M., & Wagner, W. (2006). A new method for calculating the diameters of partially-sintered nanoparticles and its effect on simulated particle properties. *Chemical Engineering Science*, *61*, 158–166.

Wentzel, M., Gorzawski, H., Naumann, K.-H., Saathoff, H., & Weinbruch, S. (2003). Transmission electron microscopical and aerosol dynamical characterization of soot aerosols. *Journal of Aerosol Science*, *34*(10), 1347–1370.

Wex, H., McFiggans, G., Henning, S., & Stratmann, F. (2010). Influence of the external mixing state of atmospheric aerosol on derived CCN number concentrations. *Geophysical Research Letters*, *37*, L10805. https://doi.org/10.1029/2010GL043337

Whitby, E. R., & McMurry, P. H. (1997). Modal aerosol dynamics modeling. *Aerosol Science and Technology*, *27*(6), 673–688.

Whiteaker, J. R., & Prather, K. A. (2003). Hydroxymethanesulfonate as a tracer for fog processing of individual aerosol particles. *Atmospheric Environment*, *37*(8), 1033–1043.

Whiteaker, J. R., Suess, D. T., & Prather, K. A. (2002). Effects of meteorological conditions on aerosol composition and mixing state in Bakersfield, CA. *Environmental Science & Technology*, *36*(11), 2345–2353.

Whittaker, R. H. (1972). Evolution and measurement of species diversity. *Taxon*, *21*(2/3), 213–251.

Wieser, P., & Wurster, R. (1986). Application of laser-microprobe mass analysis to particle collections. In K. R. Spurny (Ed.), *Physical and chemical characterization of individual airborne particles* (pp. 251–270). Chichester, UK: Ellis Horwood Ltd.

Willis, M. D., Healy, R. M., Riemer, N., West, M., Wang, J. M., Jeong, C.-H., et al. (2016). Quantification of black carbon mixing state from traffic: Implications for aerosol optical properties. *Atmospheric Chemistry and Physics*, *16*, 4693–4706.

Wilson, J., Cuvelier, C., & Raes, F. (2001). A modeling study of global mixed aerosol fields. *Journal of Geophysical Research*, *106*(D24), 34,081–34,108.

Winkler, P. (1973). The growth of atmospheric aerosol particles as a function of the relative humidity—II. An improved concept of mixed nuclei. *Journal of Aerosol Science*, *4*(5), 373–387.

Wise, M. E., Baustian, K. J., Koop, T., Freedman, M. A., Jensen, E. J., & Tolbert, M. A. (2012). Depositional ice nucleation onto crystalline hydrated NaCl particles: A new mechanism for ice formation in the troposphere. *Atmospheric Chemistry and Physics*, *12*(2), 1121–1134.

Wise, M. E., Baustian, K. J., & Tolbert, M. A. (2010). Internally mixed sulfate and organic particles as potential ice nuclei in the tropical tropopause region. *Proceedings of the National Academy of Sciences*, *107*(15), 6693–6698.

Wise, M. E., Biskos, G., Martin, S. T., Russell, L. M., & Buseck, P. R. (2005). Phase transitions of single salt particles studied using a transmission electron microscope with an environmental cell. *Aerosol Science and Technology*, *39*(9), 849–856.

Wise, M. E., Semeniuk, T. A., Bruintjes, R., Martin, S. T., Russell, L. M., & Buseck, P. R. (2007). Hygroscopic behavior of NaCl-bearing natural aerosol particles using environmental transmission electron microscopy. *Journal of Geophysical Research*, *112*, D10224. https://doi.org/10.1029/2006jd007678

Wright, D. L., McGraw, R., & Rosner, D. E. (2001). Bivariate extension of the quadrature method of moments for modeling simultaneous coagulation and sintering of particle populations. *Journal of Colloid and Interface Science*, *236*(2), 242–251.

Wright, T. P., & Petters, M. D. (2013). The role of time in heterogeneous freezing nucleation. *Journal of Geophysical Research: Atmospheres*, *118*, 3731–3743. https://doi.org/10.1002/jgrd.50365

Wu, Y., Cheng, T., Zheng, L., & Chen, H. (2016). Models for the optical simulations of fractal aggregated soot particles thinly coated with non-absorbing aerosols. *Journal of Quantitative Spectroscopy and Radiative Transfer*, *182*, 1–11.

Wu, C., Wu, D., & Yu, J. Z. (2018). Quantifying black carbon light absorption enhancement with a novel statistical approach. *Atmospheric Chemistry and Physics*, *18*(1), 289–309.

Xu, M., Spinney, R., & Allen, H. C. (2009). Water structure at the air- aqueous interface of divalent cation and nitrate solutions. *The Journal of Physical Chemistry B*, *113*(13), 4102–4110.

Xu, P., Xu, J., He, M., Song, L., Chen, D., Guo, G., & Dai, H. (2016). Morphology and chemical characteristics of micro-and nano-particles in the haze in Beijing studied by XPS and TEM/EDX. *Science of the Total Environment*, *565*, 827–832.

Yan, J., Wang, X., Gong, P., Wang, C., & Cong, Z. (2018). Review of brown carbon aerosols: Recent progress and perspectives. *Science of the Total Environment*, *634*, 1475–1485.

Ye, Q., Gu, P., Li, H. Z., Robinson, E. S., Lipsky, E. M., Kaltsonoudis, C., et al. (2018). Spatial variability of sources and mixing state of atmospheric particles in a metropolitan area. *Environmental Science & Technology*, *52*, 6807–6815.

You, Y., Renbaum-Wolff, L., Carreras-Sospedra, M., Hanna, S. J., Hiranuma, N., Kamal, S., et al. (2012). Images reveal that atmospheric particles can undergo liquid–liquid phase separations. *Proceedings of the National Academy of Sciences*, *109*(33), 13,188–13,193.

Zaveri, R. A., Barnard, J. C., Easter, R. C., Riemer, N., & West, M. (2010). Particle-resolved simulation of aerosol size, composition, mixing state, and the associated optical and cloud condensation nuclei activation properties in an evolving urban plume. *Journal of Geophysical Research*, *115*, D17210. https://doi.org/10.1029/2009JD013616

Zaveri, R. A., Easter, R. C., Fast, J. D., & Peters, L. K. (2008). Model for Simulating Aerosol Interactions and Chemistry (MOSAIC). *Journal of Geophysical Research*, *113*, D13204. https://doi.org/10.1029/2007JD008782

Zelenyuk, A., & Imre, D. (2005). Single particle laser ablation time-of-flight mass spectrometer: An introduction to SPLAT. *Aerosol Science and Technology*, *39*(6), 554–568.

Zelenyuk, A., Imre, D., Nam, E. J., Han, Y., & Mueller, K. (2008b). ClusterSculptor: Software for expert-steered classification of single particle mass spectra. *International Journal of Mass Spectrometry*, *275*(1-3), 1–10.

Zelenyuk, A., Yang, J., Choi, E., & Imre, D. (2009). SPLAT, II: An aircraft compatible, ultra-sensitive, high precision instrument for in-situ characterization of the size and composition of fine and ultrafine particles. *Aerosol Science and Technology*, *43*(5), 411–424. https://doi.org/10.1080/02786820802709243

Zelenyuk, A., Yang, J., Song, C., Zaveri, R. A., & Imre, D. (2008a). A new real-time method for determining particles' sphericity and density: Application to secondary organic aerosol formed by ozonolysis of $\alpha$-pinene. *Environmental Science & Technology*, *42*(21), 8033–8038.

Zhang, R., Khalizov, A. F., Pagels, J., Zhang, D., Xue, H., & McMurry, P. H. (2008). Variability in morphology, hygroscopicity, and optical properties of soot aerosols during atmospheric processing. *Proceedings of the National Academy of Sciences*, *105*(30), 10,291–10,296.

Zhu, S., Sartelet, K. N., Healy, R. M., & Wenger, J. C. (2016b). Simulation of particle diversity and mixing state over Greater Paris: A model–measurement inter-comparison. *Faraday Discussions*, *189*, 547–566.

Zhu, S., Sartelet, K. N., & Seigneur, C. (2015). A size-composition resolved aerosol model for simulating the dynamics of externally mixed particles: SCRAM (v 1.0). *Geoscientific Model Development*, *8*(6), 1595.

Zhu, S., Sartelet, K., Zhang, Y., & Nenes, A. (2016a). Three-dimensional modeling of the mixing state of particles over Greater Paris. *Journal of Geophysical Research: Atmospheres*, *121*, 5930–5947. https://doi.org/10.1002/2015jd024241